



**HAL**  
open science

## Catalytic selective oxidation of light alkanes

Li Zhang

► **To cite this version:**

Li Zhang. Catalytic selective oxidation of light alkanes. Chemical engineering. Centrale Lille Institut, 2021. English. NNT: 2021CLIL0014 . tel-03710301

**HAL Id: tel-03710301**

**<https://theses.hal.science/tel-03710301v1>**

Submitted on 30 Jun 2022

**HAL** is a multi-disciplinary open access archive for the deposit and dissemination of scientific research documents, whether they are published or not. The documents may come from teaching and research institutions in France or abroad, or from public or private research centers.

L'archive ouverte pluridisciplinaire **HAL**, est destinée au dépôt et à la diffusion de documents scientifiques de niveau recherche, publiés ou non, émanant des établissements d'enseignement et de recherche français ou étrangers, des laboratoires publics ou privés.

CENTRALE LILLE

**THÈSE**

Présentée en vue

d'obtenir le grade de

**DOCTEUR**

En

Spécialité : Molécules et Matière Condensée

Par

**Li ZHANG**

DOCTORAT DÉLIVRÉ PAR CENTRALE LILLE

---

**CATALYTIC SELECTIVE OXIDATION OF LIGHT ALKANES**

---

**VALORISATION D'ALCANES LÉGERS PAR VOIE CATALYTIQUE**

---

Soutenue le 12 Octobre 2021 devant le jury d'examen :

*Président :* **M. Sébastien PAUL**, Professeur, Centrale Lille

*Directeur :* **M. Benjamin KATRYNIOK**, Maître de Conférences, Centrale Lille

*Co-directeur :* **M. Franck DUMEIGNIL**, Professeur, Université de Lille

*Rapporteurs :* **M. Jean-Marc MILLET**, Directeur de Recherche CNRS, IRCELYON

**Mme Nadine ESSAYEM**, Directeur de Recherche CNRS, IRCELYON

*Examineurs :* **M. Joris THYBAUT**, Professeur, University of Gent (BE)

Thèse préparée dans le Laboratoire UCCS

Ecole Doctorale SMRE 104

### **Acknowledgements**

I am very grateful to the CSC-GEC (China Scholarship Council – Groupe des Écoles Centrales) PhD scholarship programs for giving me the opportunity to experience French life, culture and science, and for giving me financial support.

I would like to express my heartfelt thanks to my supervisors Dr. Benjamin Katryniok and Prof. Franck Dumeignil. I am grateful for the valuable guidance and advice given to me during my three years of PhD study in UCCS, both in terms of scientific discussions and professional skills that have benefited me deeply during my study. This thesis has been completed under the careful guidance of my supervisors. I was impressed by their scientific approach and attitude.

Special thanks to Prof. Sébastien Paul, for his extensive information and background in the subject and technology, which has given me invaluable advice and assistance during the research work and the writing of this thesis. Deep gratitude is expressed to Dr. Axel Löfberg for his kind guidance on technical aspects during the catalytic tests.

I would also like to thank the jury members of my thesis, Prof. Jean-Marc Millet, Dr. Nadine Essayem and Prof. Joris Thybaut, for the reading and the examination of this manuscript.

I would like to thank my colleagues and friends at UCCS for the help they have given me during three years of research and life, and for providing a relaxed, friendly and harmonious working atmosphere. Their presence has been an invaluable asset to me.

Finally, I would like to express my gratitude to my family. I am grateful to my parents for their encouragement and support, which gave me the courage to give up my stable job and change my old life. I am also grateful to my boyfriend, Dichao Shi, for his understanding and help, which enabled me to complete my study in France.

**Contents**

Nomenclature .....	1
Résumé .....	2
Abstract .....	5
General introduction.....	8
Chapter 1 Bibliographical study.....	13
1.1 Development of selective oxidation of <i>isobutane</i> .....	13
1.1.1 Utilization and conversion of light alkanes.....	13
1.1.2 Significance of selective oxidation of <i>isobutane</i> .....	15
1.1.2.1 Manufacturing processes of methacrylic acid and methyl methacrylate .....	15
1.1.2.2 Selective oxidation of <i>isobutane</i> to methacrylic acid and methacrolein .....	20
1.2 Keggin-type heteropolycompounds catalysts.....	22
1.2.1 Keggin structure .....	23
1.2.2 Heteropolycompounds-based catalysts for oxidizing <i>isobutane</i> to MAA and MAC .....	26
1.2.3 Supported heteropolycompounds .....	28
1.2.4 Mixed metal oxides .....	29
1.3 Catalytic reactor technologies for selective oxidation .....	31
1.3.1 Co-feeding of oxygen and <i>isobutane</i> in continuous fixed-bed reactor.....	32
1.3.2 Alternating feed operation of a reactor .....	35
1.3.3 Continuous regeneration on Circulating Fluidized-Bed Reactor (CFBR) .....	37
1.3.4 Two-Zone Fluidized-Bed reactor (TZFBR).....	38
1.4 Conclusion and research strategy .....	41
References .....	43
Chapter 2 Experimental.....	52
2.1 Characterization techniques .....	52
2.1.1 Optical microscope.....	52
2.1.2 Thermogravimetric analysis.....	52

2.1.3 X-ray Diffraction.....	53
2.1.4 IR Raman spectroscopy.....	53
2.1.5 Nitrogen adsorption/desorption.....	54
2.1.6 Temperature-Programmed Reduction .....	54
2.1.7 Temperature-Programmed Desorption of ammonia .....	55
2.1.8 X-ray Photoelectron Spectroscopy.....	55
2.2 Catalysts syntheses.....	56
2.2.1 Vanadium-substituted phosphomolybdic acids precursors .....	56
2.2.2 Preparation of the supported catalysts.....	57
2.3 Experimental set-ups and catalytic performance evaluation.....	58
2.3.1 Fixed-bed reactor.....	58
2.3.1.1 Description of the experimental set-up and operation conditions.....	58
2.3.1.2 Catalytic performances measurements .....	62
2.3.2 Periodic reactor .....	63
2.3.2.1 Description of the experimental set-up and operation conditions.....	63
2.3.2.2 Catalytic performances measurements.....	67
2.3.3 Two zones fluidized-bed reactor .....	69
2.3.3.1 Description of the experimental set-up and operation conditions.....	69
2.3.3.2 Catalytic performances measurements.....	74
References .....	75
Chapter 3 Catalytic selective oxidation of IBAN to MAA and MAC in a fixed-bed reactor ..	77
3.1 Introduction .....	77
3.2 Physicochemical properties of the catalysts.....	77
3.2.1 Macrostructure of the catalysts .....	77
3.2.2 Thermal decomposition of the fresh catalysts – TGA.....	80
3.2.3 Crystal phases analysis of the samples - XRD.....	81
3.2.4 BET specific surface area and pore volume of the catalysts.....	83
3.2.5 Structural features of the catalysts - Raman spectroscopy.....	84

3.2.6 Reducibility measurements - TPR.....	85
3.3 Catalytic evaluation in selective oxidation of <i>isobutane</i> in a fixed-bed reactor.....	89
3.3.1 Effect of the support.....	89
3.3.2 Effect of the active phase .....	90
3.3.3 Effect of active phase amount .....	95
3.3.4 Effect of the weight hourly space velocity (WHSV) .....	99
3.4 Conclusions .....	100
References .....	102
Chapter 4 Catalytic selective oxidation of IBAN to MAA and MAC in a periodic reactor ..	105
4.1 Introduction .....	105
4.2 Catalytic evaluation in selective oxidation of <i>isobutane</i> in a periodic reactor.....	106
4.2.1 Effect of reaction temperature.....	106
4.2.2 Effect of the cycling time .....	110
4.3 Physicochemical properties of the catalysts used in periodic conditions.....	115
4.3.1 Crystal phases and structural features analysis by XRD and Raman.....	115
4.3.2 BET specific surface area and pore volume of the catalysts.....	116
4.3.3 Surface analysis by XPS .....	116
4.4 Conclusions .....	119
References .....	121
Chapter 5 Catalytic selective oxidation of IBAN to MAA and MAC in a TZFBR .....	124
5.1 Introduction .....	124
5.2 Physicochemical properties of the catalysts.....	124
5.2.1 Microstructure of the catalysts .....	124
5.2.2 Crystal phases analysis of the samples by XRD .....	125
5.2.3 Structural features of the catalysts observed by IR-Raman spectroscopy .....	125
5.2.4 Surface analysis by XPS .....	126
5.2.5 Size distribution of the catalysts.....	127
5.3 Catalytic performance evaluation for the selective oxidation of <i>isobutane</i> in a TZFBR	

## Content

---

.....	128
5.3.1 Hydrodynamic study and catalytic tests.....	128
5.3.2 Effect of oxygen/ <i>isobutane</i> molar ratio.....	131
5.3.3 Effect of the reaction temperature.....	133
5.4 Conclusions.....	134
References.....	136
Chapter 6 General conclusions and perspectives.....	138
6.1 General conclusions.....	138
6.2 Perspectives.....	141
References.....	144

**Nomenclature**

IBAN	<i>isobutane</i>
MAC	methacrolein
MAA	methacrylic acid
HPA	heteropolyacid
POM	polyoxometalate
HPC	heteropolycompound
MMA	methyl methacrylate
PMMA	poly-methyl-methacrylate
ACH	acetone cyanohydrin
HCN	hydrogen cyanide
ODH	oxidative dehydrogenation
ACA	acrylic acid
AA	acetic acid
ACT	acetone
ATH	acetaldehyde
CsV <sub>1</sub>	Cs <sub>2</sub> H <sub>2</sub> PMo <sub>11</sub> VO <sub>40</sub>
CsV <sub>2</sub>	Cs <sub>2.5</sub> H <sub>2.5</sub> PMo <sub>10</sub> V <sub>2</sub> O <sub>40</sub>
RbV <sub>1</sub>	Rb <sub>2</sub> H <sub>2</sub> PMo <sub>11</sub> VO <sub>40</sub>
RbV <sub>2</sub>	Rb <sub>2.5</sub> H <sub>2.5</sub> PMo <sub>10</sub> V <sub>2</sub> O <sub>40</sub>
TGA	Thermogravimetric Analyzer
XRD	X-Ray Diffraction
BET	N <sub>2</sub> physisorption
TPR	Temperature programmed reduction
NH <sub>3</sub> -TPD	Temperature-programmed desorption of ammonia
XPS	X-ray photoelectron spectroscopy
MS	Mass spectrometer
TZFBFR	Two-Zone Fluidized-Bed Reactor
CFBR	Circulating Fluidized-Bed Reactor
MVK	Mars and Van Krevelen
$U_{mf}$	minimum fluidization velocity
$\Delta P$	pressure drop
$U$	gas velocity
$\alpha$	fluidization quality

### Résumé

L'oxydation catalytique sélective est l'un des principaux domaines de la production pétrochimique. Environ un quart des produits chimiques organiques sont synthétisés par des procédés d'oxydation catalytique en phase gazeuse ou liquide. Au cours des dernières décennies, la possibilité de développer de nouveaux procédés à faible impact environnemental et à faible coût a augmenté l'intérêt pour la conversion des alcanes légers par oxydation en composés oxygénés tels que l'acide acrylique, l'acide méthacrylique, l'acide acétique, l'acroléine, etc. – tous des produits chimiques ou des monomères importants dans l'industrie pétrochimique. Cependant, la conversion oxydative des alcanes légers est une tâche beaucoup plus complexe que la conversion oxydative des alcènes correspondants, nécessitant le développement de nouvelles voies chimiques en raison de leur grande inertie chimique.

L'acide méthacrylique (MAA) est un produit chimique intermédiaire utilisé pour la production de poly-méthacrylate de méthyle (PMMA) qui est largement utilisé en industrie polymère (PLEXIGLASS®), médecine et chimie fine. Les principaux procédés commerciaux de production de MMA sont la voie acétone-cyanohydrine (ACH) et la voie des hydrocarbures légers, à partir d'éthylène, de propane, de propylène, de propyne, d'isobutène ou d'*isobutane*. La première est de loin la plus importante. La réaction de l'acétone et du cyanure d'hydrogène (HCN) donne du MMA. Cependant, les intermédiaires produits (cyanure d'hydrogène et cyanohydrine d'acétone) sont toxiques et constituent une source de danger pour l'environnement. La nécessité d'un procédé alternatif apparaît donc comme évidente.

L'oxydation sélective de l'*isobutane* (IBAN) en méthacroléine (MAC) et en acide méthacrylique est ainsi d'un grand intérêt pour l'industrie chimique. Les avantages de cette réaction proviennent non seulement de son faible coût en matière première et de la simplicité du procédé, mais aussi de l'absence de réactifs toxiques et de la réduction des déchets. Cependant, si l'on considère l'oxydation sélective de l'*isobutane*, au moins deux questions doivent être abordées : *i*) comment activer la liaison C-H très stable pour initier la conversion avec l'énergie la plus faible possible et *ii*) comment contrôler la réaction d'oxydation pour obtenir sélectivement le produit souhaité.

Ces facteurs ne sont pas seulement liés aux propriétés chimiques de l'alimentation et du

produit, mais aussi au catalyseur utilisé. Les catalyseurs bifonctionnels ayant des propriétés acides et redox sont nécessaires pour activer la liaison C-H, et les propriétés redox ont évidemment une forte influence sur la réaction d'insertion de l'oxygène avec l'oxygène du réseau  $O^{2-}$ , qui est connue pour être sélective pour les produits souhaités. Les composés hétéropoly anioniques (HPAs) sont des catalyseurs acides bien connus, qui peuvent également présenter des propriétés redox. Les HPAs consistent en métaux de transition, des éléments du groupe principal, ainsi qu'un certain nombre de protons et/ou de molécules d'eau. La société Rohm & Haas a été la première, en 1981, à revendiquer l'oxydation en une étape de l'*isobutane* en MAC et MAA à base d'oxydes Mo/P/Sb, dont les compositions sont proches de celles des hétéropolyacides de type Keggin. Ensuite, plusieurs études successives ont montré que les hétéropolyacides de type Keggin (sous forme d'acide partiellement neutralisé pour en augmenter la stabilité) présentent les meilleures performances catalytiques pour l'activation de l'*isobutane*. Cela est dû à leurs propriétés d'acidité et d'oxydoréduction fortes et modifiables.

Les principaux inconvénients des catalyseurs à base de HPA sont leur faible stabilité sous flux (durée de vie trop courte dans les réacteurs commerciaux), ainsi que leur faible surface spécifique. Pour pallier ces inconvénients, il est possible de synthétiser des catalyseurs supportés. Le supportage des HPAs de type Keggin permet non seulement de disperser mais aussi de stabiliser la phase active, améliorant ainsi les performances du catalyseur. L'activité catalytique et la sélectivité du produit sont sensibles à la nature du support et à la dispersion de la phase active. Notamment, les matériaux mésoporeux présentent de nombreux avantages en tant que supports de catalyseurs en raison de leurs propriétés texturales uniques telles qu'une surface spécifique élevée, un grand volume de pores et une distribution uniforme de la taille des pores.

Dans ce travail, des hétéropolyacides de type Keggin contenant du rubidium ou du césium comme contre-cations, ont été préparés et supportés sur silice commerciale. Plus précisément, les phases actives  $Cs_2H_2PMo_{11}VO_{40}$  ( $CsV_1$ ),  $Cs_{2.5}H_{2.5}PMo_{10}V_2O_{40}$  ( $CsV_2$ ),  $Rb_2H_2PMo_{11}VO_{40}$  ( $RbV_1$ ) et  $Rb_{2.5}H_{2.5}PMo_{10}V_2O_{40}$  ( $RbV_2$ ) ont été supportées sur CARiACT  $SiO_2$ , avec différentes teneurs en poids (10-50 %). Il a été démontré que la stabilité thermique et la réductibilité des HPA ont été améliorées grâce au support. Les propriétés texturales, les caractéristiques structurales, les propriétés d'acidité et d'oxydoréduction et la stabilité des catalyseurs ont été

étudiées à l'aide de diverses techniques afin d'établir des corrélations entre les propriétés physico-chimiques des échantillons et leurs performances catalytiques. Les résultats obtenus dans la réaction d'oxydation catalytique de l'*isobutane* en MAA et MAC ont montré que la densité de sites acides joue un rôle crucial pour la performance catalytique.

En plus du développement du catalyseur, l'utilisation de nouvelles configurations de réacteurs a été étudiée pour diminuer la formation de produits de suroxydation. En ce qui concerne le mécanisme de Mars-van-Krevelen, les réactions d'oxydation catalytique se déroulent en deux étapes : *i*) oxydation du réactif qui réduit en même temps le catalyseur et *ii*) la réoxydation du catalyseur par un oxydant (généralement O<sub>2</sub>). En général, les deux étapes se déroulent simultanément dans un réacteur, ce qui entraîne également un contact direct entre l'oxydant et le réactif, ce qui peut conduire à des réactions de suroxydation réduisant ainsi le rendement des produits souhaités.

En plus du réacteur à lit fixe, l'oxydation de l'*isobutane* en MAC et MAA a également été appliquée dans deux autres types de réacteurs : le réacteur de type pulsé et le lit fluidisé à deux zones (TZFBR). Ces réacteurs découplent les étapes d'oxydation du réactif et de ré-oxydation du catalyseur selon le mécanisme redox de Mars-Van-Krevelen. Dans un réacteur pulsé, la séparation temporelle de la réduction et de la réoxydation du catalyseur et le contrôle de la concentration en oxygène dans la phase gazeuse peuvent être réalisés par des impulsions alternées d'alcane et d'oxygène. Dans ce travail, l'influence de divers paramètres de réaction, tels que le rapport molaire oxygène/*isobutane*, la température de réaction et le temps de cycle ont également été étudiés dans les deux réacteurs. De manière surprenante, dans aucun de ces réacteurs, une performance comparable à celle du réacteur à lit fixe n'a été atteinte.

**Abstract**

Over the past few decades, selective oxidation of *isobutane* (IBAN) to methacrolein (MAC) and methacrylic acid (MAA) has received great interests both in the chemical industry and in fundamental research. The advantages of this reaction originate not only from its low raw-materials' cost and reduced process complexity, but also from limiting the use of toxic reactants and the reduction of wastes. Successive studies and reports have shown that heteropolycompounds with Keggin structures (under the form of a partially neutralized acid to increase their stability) present the best catalytic behavior for *isobutane* conversion. This is due to their strong and tunable acidity and redox properties. In this work, Keggin-type heteropolyacids (HPAs) containing rubidium or cesium as counter cations have been prepared. Keggin-type polyoxometalates (POMs) as heterogeneous catalyst perform surface-type reaction, however the low surface area and low thermal stability of the bulk heteropolycompounds (HPCs) limit their applications. Therefore, supported Keggin-type HPCs were investigated as catalysts. More precisely the active phase  $\text{Cs}_2\text{H}_2\text{PMo}_{11}\text{VO}_{40}$  ( $\text{CsV}_1$ ),  $\text{Cs}_{2.5}\text{H}_{2.5}\text{PMo}_{10}\text{V}_2\text{O}_{40}$  ( $\text{CsV}_2$ ),  $\text{Rb}_2\text{H}_2\text{PMo}_{11}\text{VO}_{40}$  ( $\text{RbV}_1$ ) and  $\text{Rb}_{2.5}\text{H}_{2.5}\text{PMo}_{10}\text{V}_2\text{O}_{40}$  ( $\text{RbV}_2$ ) were supported on a commercial CARiACT  $\text{SiO}_2$  carrier, with various loadings of 10-50 wt.% to obtain high specific surface area. It was evidenced that the thermal stability and reducibility of the Keggin type HPAs were improved by supporting the active phase on  $\text{SiO}_2$ . The textural properties, structural features, acidity and redox properties and the stability of the catalysts were studied using various techniques to establish correlations between the key properties of the samples and their catalytic performances. The results in catalytic performance of *isobutane* to MAA and MAC showed that a well-balanced surface acid site density is necessary to get an efficient catalyst for *isobutane* conversion and MAA + MAC selectivity.

Furthermore, the investigation of the catalytic performances not only focused on the improvement of catalyst properties, but also on using novel reactor configurations that can continuously provide uniform and controllable oxygen concentration to decrease the generation of overoxidation products. In addition to the fixed-bed reactor oxidation of *isobutane* to MAC and MAA was therefore also applied in two other reactor types: periodic reactor and two zone fluidized-bed. Such reactors decouple the reaction and oxidation steps of the HPC-based

catalysts, which follow the Mars and Van Krevelen redox mechanism. The influence of various reaction parameters, such as oxygen/*isobutane* molar ratio, reaction temperature and cycling time were studied. Surprisingly, in none of these reactors, a performance comparable to that of the fixed-bed reactor could be reached.

# **General introduction**

## General introduction

Selective catalytic oxidation is one of the main areas of petrochemical production. About a quarter of the major organic chemicals are synthesized by gas- or liquid-phase catalytic oxidation processes. In the recent decades, the possibility of developing new processes with low environmental impact and low cost has increased the interest in the conversion of light alkanes by oxidation into valuable oxygenated compounds or alkenes. Selective oxidation of light alkanes gives access to valuable oxygenated products such as acrylic acid [1,2], methacrylic acid [3], acetic acid, acrolein, *etc.* [3–5], which are important chemicals or monomers in the petrochemical industry [6]. However, the oxidative conversion of light alkanes is a much more complex technical task than the oxidative conversion of the corresponding alkenes, requiring the development of new chemical routes due to their high chemical inertness.

Methacrylic acid (MAA) is an intermediate chemical used for the production of polymethyl-methacrylate (PMMA) that is widely used in civil engineering, medicine and fine chemistry. The main MMA production commercial processes include the acetone-cyanohydrin (ACH) route and the light hydrocarbons route, from ethylene, propane, propylene, propyne, *isobutene*, or *isobutane*. The former is by far the dominant one. Reacting acetone and hydrogen cyanide (HCN) yields MMA. However, the produced intermediates (hydrogen cyanide, and acetone cyanohydrin) are toxic and the source of environmental hazard. Hence, the need for an alternative process appears as obvious.

Selective oxidation of *isobutane* (IBAN) to methacrolein (MAC) and methacrylic acid (MAA) has attracted considerable interest in the chemical industry and research laboratories over the last few decades. Actually, *isobutane* oxidation is a one-step route to form MAA that overcomes the environmental and production problems associated with the acetone cyanohydrin process, while being a simple process generating less by-products. Moreover, the alkane used as feedstock is highly abundant and cheap.

However, considering the selective oxidation of *isobutane*, at least two issues need to be addressed: *i*) activate the very stable C-H bond to initiate the conversion with the lowest possible energy and *ii*) control the oxidation reaction to selectively obtain the desired product.

These factors are not only related to the chemical properties of the feed and product, but

also to the catalyst used. Bifunctional catalysts with acidic and redox properties are necessary to activate the C-H bond [7–10], and redox properties have obviously a strong influence on the oxygen insertion reaction with lattice oxygen  $O^{2-}$ , which is known to be selective for desired products [7].

Heteropoly compounds (HPC) are well-known acid catalysts, which can also exhibit redox properties. HPC are a large class of nanoscale clusters containing transition metals, main group elements, as well as a certain number of protons and/or water molecules. Rohm & Haas Company was the first, in 1981, to claim the one-step oxidation of *isobutane* to MAC and MAA based on Mo/P/Sb oxides, of which the compositions are close to that of Keggin-type heteropoly acids [11]. Then, several patents appeared in the 1980s and 1990s claiming the possibility of carrying out the synthesis of MAA by the one-step oxidation of *isobutane* in the gas phase, over Keggin-type heteropolyacids as heterogeneous catalysts [12].

The main drawbacks of HPC-based catalysts are their poor stability under stream (too short lifetime in commercial reactors), and also their low specific surface area. To overcome these shortcomings, it is possible to synthesize supported catalysts. Supporting Keggin-type HPCs not only disperses but also stabilizes the active phase, hence improving the catalyst performance [13]. Catalytic activity and product selectivity are sensitive to the nature of the support and to the active phase dispersion. Notably, mesoporous materials have many advantages as catalyst supports due to their unique textural properties such as a high specific surface area, a large pore volume, and a uniform pore size distribution.

The optimization of catalytic performance in terms of reactant conversion, yield and desired product selectivity is not only related to the properties of the catalyst, the interaction between the reaction components and the active phase, but also to the development and implementation of a suitable reactor. With respect to the Mars and van Krevelen mechanism, catalytic oxidation reactions take place in two steps: *i*) Oxidation of the reactant which reduces the catalyst at the same time and *ii*) re-oxidation of the catalyst by an oxidant (generally  $O_2$ ). Generally, both steps take place simultaneously in a co-fed reactor, causing thus also the direct contact between the oxidant and the reactant, which can lead to side overoxidation reactions lowering the yield in desired products.

Based on the Mars and van Krevelen model, several reactor configurations for selective

oxidation reactions are proposed, in order to decouple the oxidation and reduction steps. In a periodic reactor, the temporal separation of catalyst reduction and reoxidation and the control of the oxygen concentration in the gas phase can be achieved by alternating pulses of alkane and oxygen. The temporal and spatial separation of redox processes is possible, as can be seen based on examples of applications of this type of reactor [14–17]. This kind the process solves the problem of the need of periodic regeneration of the catalyst. Also, fluidized reactors, such as a two-zone-fluidized bed reactor (TZFBR) are very efficient for heat transfer in such a way that the reactor may operate isothermally. The main idea of the TZFBR is that the reduction and reoxidation can take place in different zones of the same vessel, and that the reduction of the catalyst by the hydrocarbon and reoxidation by molecular oxygen can be spatially decoupled. In the last decades, TZFBR have been applied to different processes [18–20], such as the partial oxidation of propane to acrylic acid.

In this manuscript, the background to the research on the subject, the selection and preparation of new HPC-based supported catalysts and the evaluation of their catalytic performance in different kinds of reactors, are described.

Chapter 1 introduces the research field of selective oxidation and the prospects for light alkane applications. The structure and properties of heteropolyacid catalysts used for *isobutane* selective oxidation are also described. In addition, a technical study of the operating conditions and different types of reactors for selective catalytic oxidation is presented and the possibilities for innovation are discussed.

Chapter 2 lists the characterization methods as well as a detailed description of the synthesis of catalysts and of the chemical reagents used. In addition, the catalytic set-ups used for catalyst performance evaluation are described with their feed zone, reaction zone and analysis zone. The analytical methods used and calculations of the performance criteria such as conversion, selectivities, yields and carbon balance are also presented.

Chapter 3 investigates Keggin-type heteropolyacid catalysts on SiO<sub>2</sub> carrier containing rubidium or cesium as counter cations. The thermal stability, structural properties, acidity and reducibility of the catalysts are analyzed by characterization techniques. In addition, focus is put on the selective oxidation of IBAN for the production of MAC and MAA in a fixed-bed reactor under co-feed conditions with different loadings, different counter-cations and different

reaction temperatures.

Chapter 4 proposes the concept of a periodic operation for the selective oxidation of *isobutane*. Cesium-based Keggin-type HPA catalysts were investigated as oxygen carriers, and their catalytic activity were evaluated during the chemical cycling process. Data processing of the test results was carried out to obtain complete information during the test, which includes, in addition to the total conversion and selectivity, the instantaneous changes in each cycle.

Chapter 5 checks the mechanical stability of the solid catalysts during fluidization, the quality of fluidization and then the reactivity in a TZFBR using 40 wt.%  $\text{Cs}_2\text{H}_2\text{PMo}_{11}\text{VO}_{40}$  /  $\text{SiO}_2$  catalyst, while studying the feasibility of selective oxidation of *isobutane* to methacrylic acid and methacrolein in a TZFBR and evaluating the catalytic performance of the 40CsV<sub>1</sub> catalyst.

Finally, the dissertation is completed by a general conclusion and some perspectives.

# **Chapter 1**

## **Bibliographical study**

## Chapter 1 Bibliographical study

### 1.1 Development of selective oxidation of *isobutane*

#### 1.1.1 Utilization and conversion of light alkanes

Hydrocarbons are generally issued from fossil resources such as coal, oil and natural gas, which are nowadays still the main feedstocks being utilized in the chemical industry (Figure 1.1). In addition, natural gas extraction has become increasingly significant as compared to other fossil energies, as the supply of natural gas is expected to last longer than those of oil (roughly 200 years in the Middle East taking into account current known reserves and consumption) [1]. Therefore, the transformation of hydrocarbons constitutes an extremely important field of research. Selective oxidations are important chemical processes in the chemical industry. Many chemical products and fine chemistry intermediates are actually synthesized *via* a process that includes an oxidation step [2]. However, only a few chemical processes have been industrialized for the oxidative conversion of light alkanes, while they are widely available from natural gas and liquefied petroleum gas (Table 1.1). The main reason behind this fact is that oxidative conversion of light alkanes is a much more complex technological task than the conversion of corresponding olefins due to their poor chemical reactivity. On the other hand, since alkanes are cheaper raw materials than the corresponding olefins, available in abundance and of low toxicity compared to aromatics, more and more attention has been paid to the production of light olefins from hydrocarbons, where oxidative dehydrogenation reactions could be applied for the production of ethylene, propylene, *isobutene* or butadiene from the corresponding alkanes [3–7].

Selective oxidation of light alkanes can also give an access to valuable oxygenated products such as acrylic acid [8,9], methacrylic acid [10], acetic acid, acrolein, etc. [10–12], which are all important chemicals or monomers in the petrochemical industry [1]. The development of new catalysts for the selective oxidation of alkanes is therefore at the intersection between strong economic interests for optimizing the manufacture of chemical building blocks and the enduring scientific challenge to activate these very inert compounds for

functionalization [1]. Today, activation and selective conversion of light alkanes ( $C_1$ - $C_4$ ) are not only important research topics for the utilization of natural gas components, but also of practical significance to produce high value-added products, listed in Table 1.1 [1]. Therefore, the development of new efficient catalysts for the selective oxidation of light alkanes is still of scientific and industrial interest [13,14].

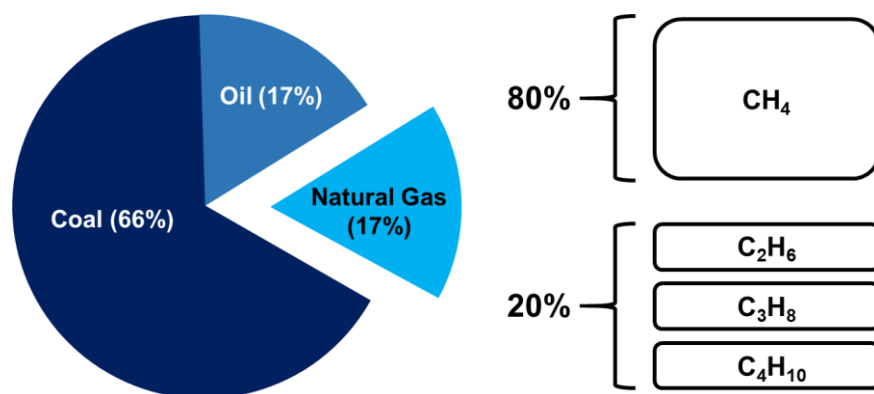


**Figure 1.1** Repartition of the fossil resources use as chemical feedstocks [1].

**Table 1.1** Processes under study or development for the oxidation of light alkanes ( $C_1$  -  $C_4$ ) [1,15].

Raw material	Product	Phase	Catalyst	Development stage
methane	methanol	gas	Metal oxides [1], Metal-organic framework [16,17]	pilot plan
methane	syngas	gas	Ni/MgO, Ni/CaO, Ni/CeO <sub>2</sub> [18], Ni/TiO <sub>2</sub> [19]	pilot plan
methane	ethylene	gas	Sr-La <sub>2</sub> O <sub>3</sub> , LaAl(Fe, Ni)O <sub>3</sub> [20]	pilot plan
methane	formaldehyde	gas	V <sub>2</sub> O <sub>5</sub> /SiO <sub>2</sub> , MoO <sub>3</sub> /SiO <sub>2</sub> , VO <sub>x</sub> /SBA-15 [21]	industrial
ethane	acetic acid	gas	MoVNbPd/TiO <sub>2</sub> [22]	industrial
ethane	ethylene	gas	Boron nitride (BN) [23,24]	research
ethane	acetaldehyde	gas	BPO <sub>4</sub> [25]	research
propane	acrylic acid	gas	MoVTeNb [26]	research
propane	acrylonitrile	gas	Alumina-supported Sb-V-O [27], Mo <sub>1.0</sub> V <sub>0.33</sub> Nb <sub>0.11</sub> Te <sub>0.22</sub> O <sub>n</sub> [28]	industrial
propane	propylene	gas	BNOH [29], VO <sub>x</sub> /CaO- $\gamma$ -Al <sub>2</sub> O <sub>3</sub> [30]	research
<i>n</i> -butane	acetic acid	liquid	Cobalt compound [31]	industrial
<i>n</i> -butane	maleic anhydride	gas	VPO [32]	industrial
<i>n</i> -butane	butadiene	gas	Mo <sub>12</sub> BiNi <sub>8</sub> Pb <sub>0.5</sub> Cr <sub>3</sub> K <sub>0.2</sub> O <sub>x</sub> [33]	industrial
<i>iso</i> -butane	methacrylic acid	gas	Keggin polyoxometalates [34]	research
<i>iso</i> -butane	<i>iso</i> -butene	gas	ZnZrO <sub>x</sub> [35]	research
<i>iso</i> -butane	<i>t</i> -butyl alcohol	liquid	<i>N</i> -hydroxyphthalimide (NHPI) and Co (II) salt [36]	research

## 1.1.2 Significance of selective oxidation of *isobutane*

### 1.1.2.1 Manufacturing processes of methacrylic acid and methyl methacrylate

Methacrylic acid (MAA) is an important chemical, which has two functional groups: a carbon-carbon double bond and a carboxylic acid group. It is used to prepare methyl methacrylate (MMA) for coatings, rubber, adhesive, resin, polymer material additives and functional polymer materials. MMA, is a specialty monomer used for the production of poly-methyl-methacrylate (PMMA) that is widely used in civil engineering, medicine and fine chemicals [37–40]. In 2018, the total available PMMA market was estimated at \$7 billion with an anticipated market size of \$11.65 billion in 2022, representing 17 % growth [41]. Demand for MMA will surpass 4.8 million metric tons by 2020 [37]. Academia and industry continue to develop technologies and modify current processes with novel materials, catalysts, and optimized operating conditions. The Web of Science Core Collection indexed over 11 000 manuscripts since 2014 that mention MAA or MMA [37]. China published most of these articles (25 %), followed by the USA (12 %), Japan (7 %), India (6 %), Korea (5 %), and Iran (4 %) [37]. A dozen of technologies are under development or practiced commercially for producing MMA, and MAA is often used as a precursor for other products, as shown in Table 1.2 and Figure 1.2 [37,42,43].

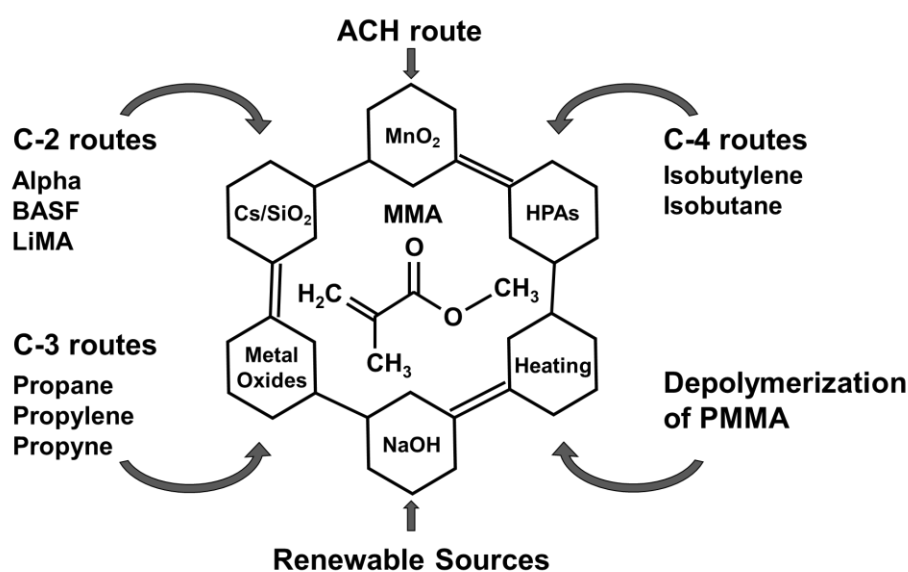


**Figure 1.2** Commercialized processes for MMA production and those under development [37].

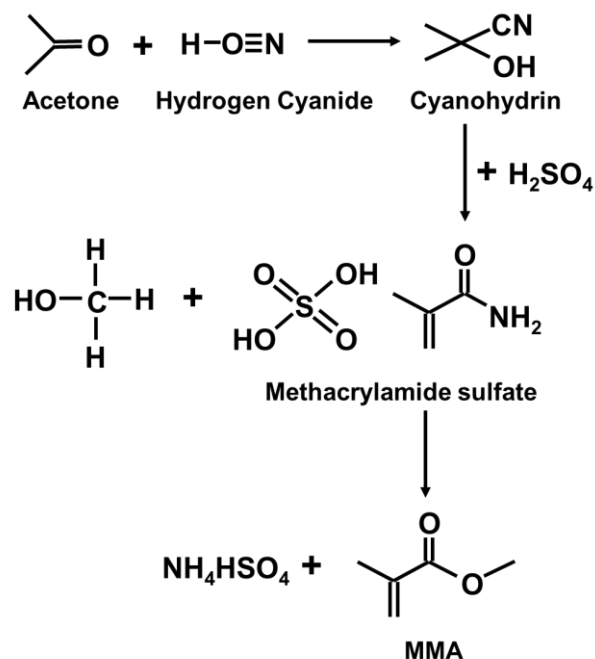
**Table 1.2** Summary of the processes used for the synthesis of MMA [43].

Process	Raw materials (without esterification)	Features	Producer
Commercial processes			
ACH (acetone cyanohydrin)	Acetone, HCN, H <sub>2</sub> SO <sub>4</sub>	Toxic reactant Coproduct disposal	Several companies
New ACH	Acetone, methylformate	Three catalytic steps No coproducts, no supply of HCN	Mitsubishi Gas
<i>Isobutene</i> oxidation	<i>Isobutene</i> or <i>t</i> -butyl alcohol, air	Two catalytic oxidations	Several in Japan
<i>Isobutene</i> ammoxidation	<i>Isobutene</i> , air, ammonia, H <sub>2</sub> SO <sub>4</sub>	Catalytic ammoxidation to meth acrylonitrile, and hydrolysis Coproduct disposal	Asahi Kasei
C <sub>2</sub> route	Ethylene, CO, H <sub>2</sub> , H <sub>2</sub> CO <sub>3</sub>	Carbonylation of ethylene to propionaldehyde, and catalytic condensation with formaldehyde	BASF
Alpha process	C <sub>2</sub> H <sub>4</sub> , CO, CH <sub>3</sub> OH, H <sub>2</sub> CO <sub>3</sub>	Catalytic carbonylation of ethylene to methyl propionate, and catalytic condensation with formaldehyde	Lucite
Processes under development or investigation			
Propyne process	C <sub>3</sub> H <sub>4</sub> , CO, CH <sub>3</sub> OH	Catalytic carbonylation of propyne One-step reaction, high yield The limit is the supply of propyne	Shell
<i>Isobutane</i> process	<i>i</i> -C <sub>4</sub> H <sub>10</sub> , air	One-step catalytic oxidation	Several companies

The main production routes for MMA include the acetone-cyanohydrin (ACH) process and the conversion of light hydrocarbons (ethylene, propane, propylene, propyne, *isobutene*, and *isobutane*).

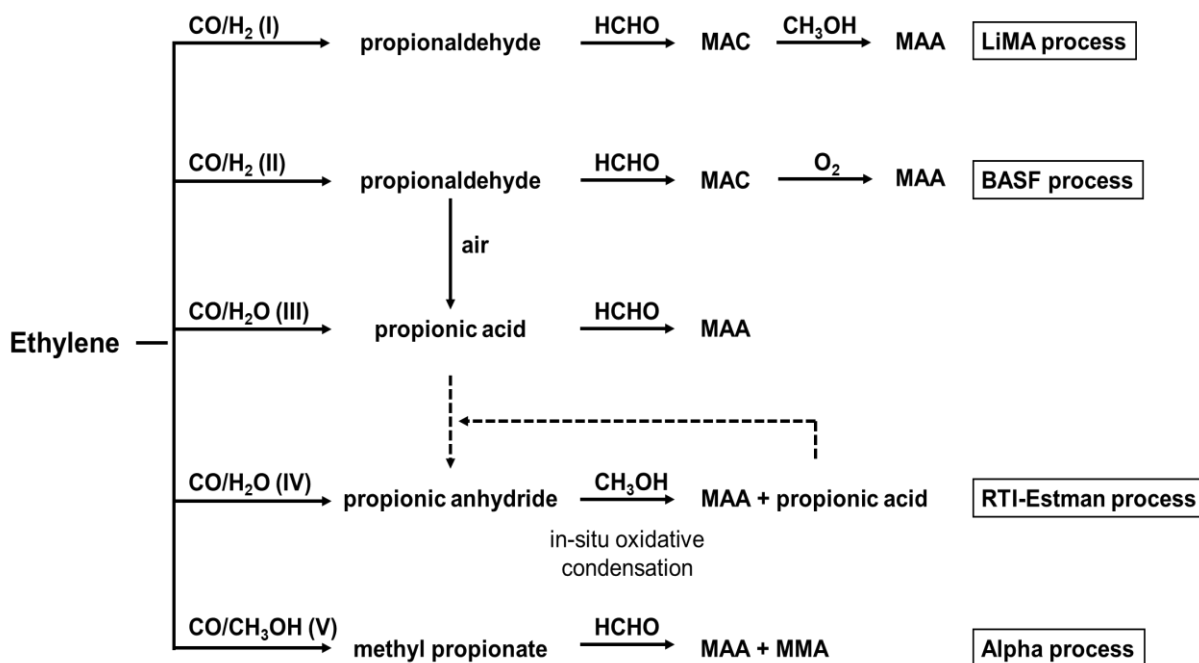
The ACH process was first industrially produced by Rohm & Haas Co. in 1933 [44]. Acetone and hydrogen cyanide (HCN) react to form acetone cyanohydrin; this intermediate then reacts with excess of concentrated sulfuric acid to methacrylamide sulfate. The latter is treated with an excess of aqueous methanol, whereby the amide is hydrolyzed and esterified forming a mixture of MMA and NH<sub>4</sub>HSO<sub>4</sub> (Scheme 1.1) [37]. This process is the most widely used route in Europe and North America, however, the intermediates (hydrogen cyanide, and acetone cyanohydrin) are highly toxic and sources of environmental hazard. Moreover, the

disposal of large quantities of ammonium bisulfate requires additional processing units and investment [45]. Hence, the ACH technology is currently environmentally and economically unrentable for any new installation [46].



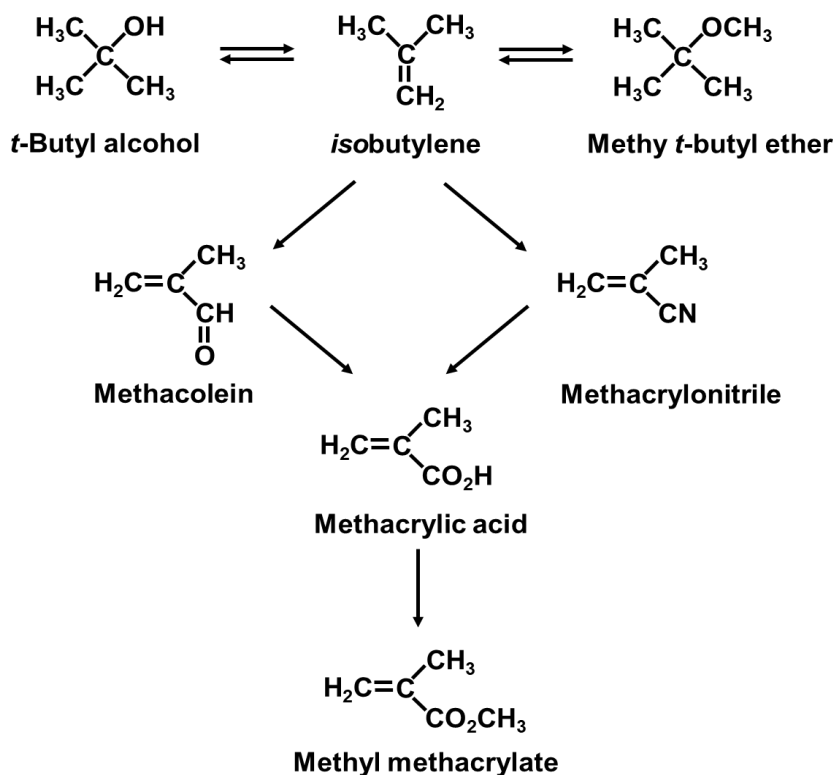
**Scheme 1.1** Common ACH approach to produce MMA [46].

There is therefore a strong drive to replace the ACH process in the chemical industry. In the United States, there is particular interest in a process that is based on fossil-based syngas. The C-2 routes shown in Scheme 1.2 is a commercially attractive technology for MMA manufacturing. Ethylene forms MAA and MMA *via* intermediates, including propanal, propionic acid or methyl propionate, which are condensed with formaldehyde to produce either MAA in Processes (I) (II) and (III), or a mixture of MAA and MMA in Processes (IV) and (V). Formaldehyde in Process (IV) is produced by partial oxidation of methanol, which also esterifies the resulting MAA to MMA [46]. “*BASF*” and “*Alpha*” are the two main commercial processes to produce MMA and MAA from C2 hydrocarbons.



Scheme 1.2 C-2 routes for MMA manufacture [46].

Synthesis of MAA through C-3 routes, with propane, propylene and propyne as a raw material, require adding a carbon atom to form the four-carbon methacrylate backbone. Propane is mainly used as a fuel for energy production but, to a lesser extent, it is also used as a raw material in the chemical industry, mainly for the production of ethylene and propylene [47]. The carbonylation of propane to *isobutyraldehyde* remains an option to produce MMA but, so far, propane as a feedstock has had little success [37]. On the other hand, with propylene as a raw material, the synthesis of *isobutyric acid* by propene carbonylation followed by oxidative dehydrogenation (ODH) yielding methacrylic acid (MAA), which is then esterified by methanol to methylmethacrylate was reported [48]. Propylene carbonylation produces both *n*-butyric and *isobutyric acids*, and MAA requires high *isobutyric acid* selectivity and full conversion, which strongly increases the cost of the process [2]. Shell oil company developed propyne-based technology with MMA yield of 99 % in a single step reaction [49]. This technology now belongs to INEOS. The methoxy carbonylation reaction includes propyne, carbon monoxide and methanol and a group VII metal catalyst systems like palladium acetate, organic phosphine and a protonic acid. Like the ethylene process, the catalyst lifetime is short and the process yields are low [37].



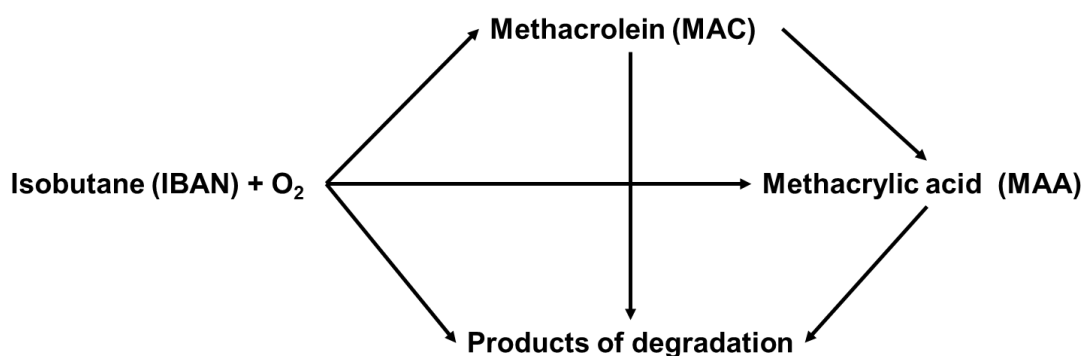
**Scheme 1.3** C-4 routes to MAA/MMA [50].

Variants of the C-4 oxidation process have been commercialized by several companies. Nippon Shokubai Kagaku Kogyo company (in 1982), Mitsubishi Rayon company (in 1983), Japan Methacrylic Monomer company (in 1984), followed by Asahi (in 1998) and Thai (in 1999) built several plants to oxidize *isobutene* to MAA and MMA [50]. In the first step MAC forms from either *isobutene* or *tert-butyl alcohol*; the catalysts are based on complex mixed-metal oxides of molybdenum, bismuth, and iron. In the second step, the selective oxidation of methacrolein to methacrylic acid is most often performed over a phosphomolybdic acid-based catalyst (Scheme 1.3) [50]. From the process point of view, oxidizing *isobutylene* to MAA suffers from short catalyst lifetime and higher separation costs.

Synthesis of MMA through esterification of MAA is an alternative route. Light hydrocarbons, such as  $\text{C}_2$ ,  $\text{C}_3$  and  $\text{C}_4$  hydrocarbons, were widely developed as feedstocks for MAA. Nevertheless, industrial application was restricted by the environmental issues, harsh reaction conditions, the expensive reactants, the low yields, the waste removal and the relatively high number of reaction steps [51].

### 1.1.2.2 Selective oxidation of *isobutane* to methacrylic acid and methacrolein

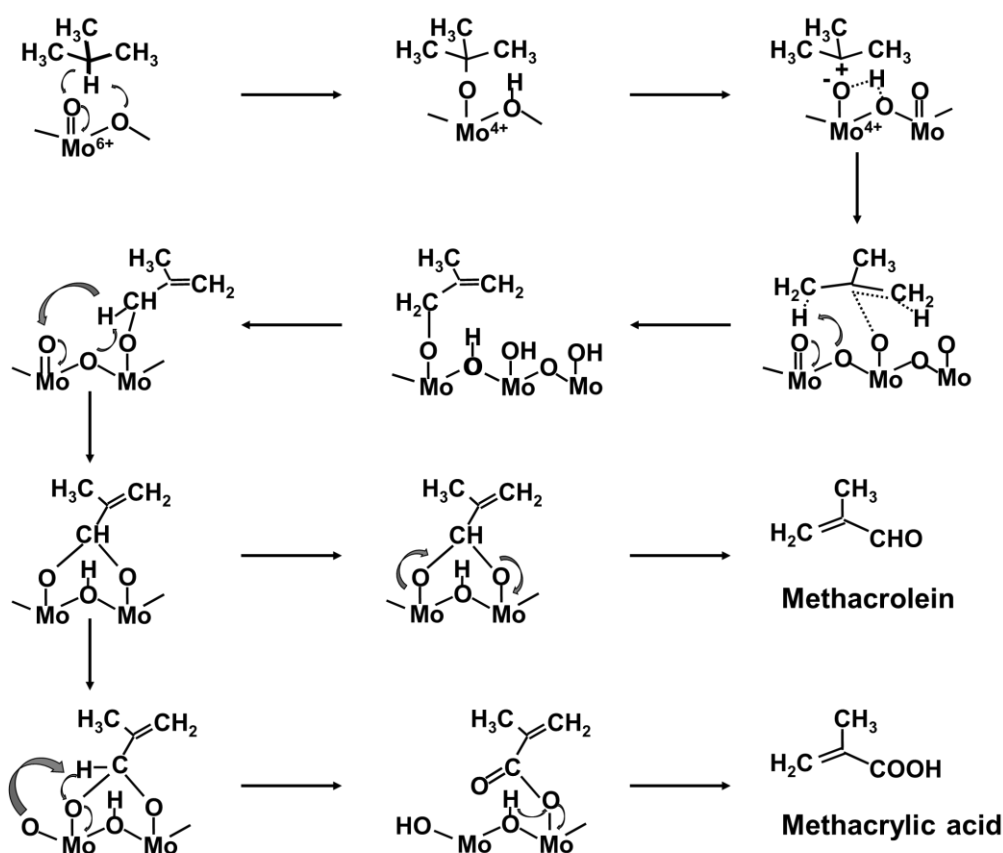
In addition to natural gas, a large amount of C4 isomers are produced as by-products in the petroleum refining industry. At the same time, because of the chemical inertness of alkanes, most of them are only valorized as fuels, which undoubtedly causes a great waste of resources and a strong environmental impact. From an economic point of view, the cheap *isobutane* as a raw material for the synthesis of high value-added polymer, such as PMMA, would actually bring high economic benefits [51]. Therefore, the *isobutane* oxidation method, which would provide a one-step route to form methacrylic acid, has driven much attention because of the easiness of the process and the decreased generation of byproducts [51,52], as shown in Scheme 1.4. Moreover, it is inexpensive and would have a lower environmental impact than other fossil feedstocks-based routes and optimally converts to MAA in a single step [53–56]. Rohm & Haas Company was the first, in 1981, to claim the one-step oxidation of *isobutane* to methacrolein and methacrylic acid based on Mo/P/Sb oxides, but the catalyst composition is close to that of heteropoly acids with Keggin structures [57]. Then, several patents have appeared in the 1980s and 1990s claiming the possibility of carrying out the synthesis of methacrylic acid by the one-step oxidation of *isobutane* in the gas phase, over Keggin-type HPAs as heterogeneous catalysts [58].



**Scheme 1.4** Formal reaction scheme for the oxidation of *isobutane* to MAA [34].

As far as the reaction mechanism is concerned, the particular activity/selectivity characteristics of heteropolycompounds (HPCs) for the synthesis of methacrylic acid from *isobutane* are related to the combination of high proton acidity, fast electron transfer and electron delocalization ability [59]. In the first step, the catalyst dehydrogenates the reactant to

form a C=C double bond. *Isobutane* can be activated by the catalyst at the tertiary carbon by oxidative activation of the weakest C-H bond: two electrons are transferred to the catalyst, which is consequently reduced. In the following steps, the adjacent methyl group is partially oxidized to a carboxyl group (allylic oxidation). The rate-limiting step appears to be the reaction of *isobutane* on the oxidized surface of the catalyst [34]. Busca et al. [59,60] proposed a common intermediate over  $K_1(NH_4)_2PMo_{12}O_{40}$  catalyst for the parallel formation of methacrolein and methacrylic acid: a dioxyalkylidene species, shown in Scheme 1.5. The latter can evolve either to methacrolein, through dissociation of a C-O bond, or to a carboxylate species, via oxidation on Mo-O. In particular, the possibility of improving the conversion rate of *isobutane* and the selectivity of methacrylic acid by developing polyoxometalates containing specific cations has attracted great attention. However, the major obstacle to further development of this process is the catalyst, which, on the one hand, is active and selective, and on the other, is structurally stable, both of which can withstand the necessary reaction conditions [55].



**Scheme 1.5** Proposed reaction mechanism for the oxidation of *isobutane* on a HPC catalyst [59].

## 1.2 Keggin-type heteropolycompounds catalysts

Regardless of the alkane, two problems occur with their selective oxidation. The first is to activate the C-H bonds at as low energy as possible to initiate transformation, and the other one is how to use oxidation reactions to generate selectively the target compound. Many factors affect these reactions, and all of them are related to the catalysts employed. Bifunctional catalysts with acidic and redox properties are necessary to activate the C-H bond [61–64]. Redox properties also have an effect on the oxygen insertion reactions, which generate the oxidized products. Therefore, bifunctional catalysts simultaneously possessing acid and redox properties are necessary, which brings heteropoly anion-based catalysts into the game. Heteropoly acids were first commercially used in Japan as homogeneous catalysts for the hydration of propylene for the manufacture of 2-propanol in 1972 [1]. During the 1980s, large-scale studies on the use of heteropoly acids or their salts as catalysts emerged (Figure 1.3). Because of the unique bifunctional redox and acidic properties of heteropolycompounds, their performance as catalysts for the partial oxidation of organic compounds has attracted much attention in the last four decades.

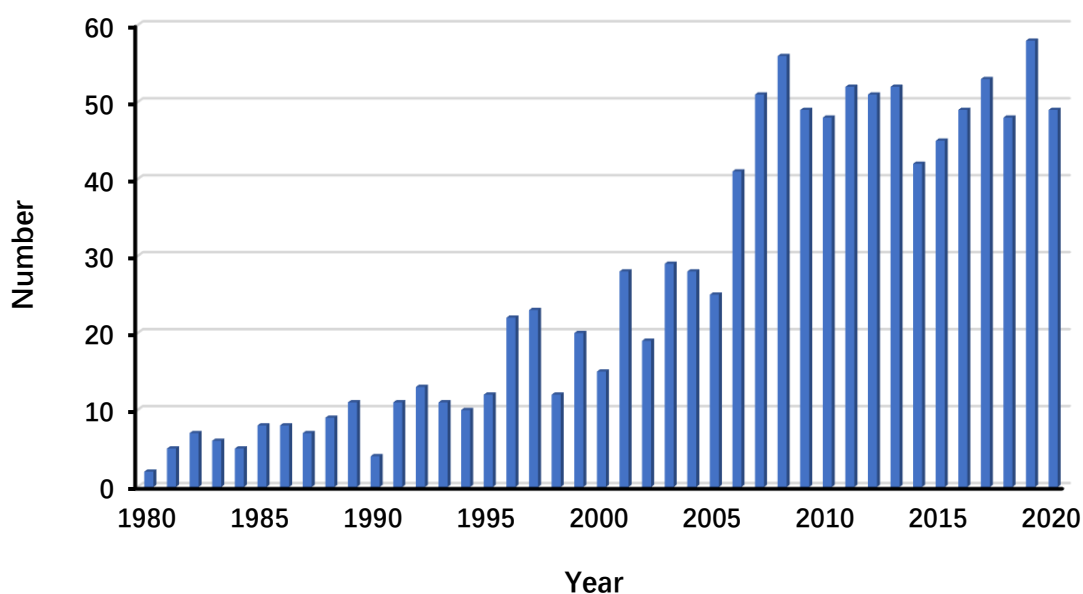


**Figure 1.3** Number of articles using heteropoly acid as catalysts per year (statistical data from Scinapse) with the keywords “*Heteropoly Acid*” and “*Catalyst*”.

### 1.2.1 Keggin structure

Polyoxometalates, also known as heteropolyacids, are nanoscale inorganic metal-oxygen clusters formed by oxygen bonding of pretransition metals (Mo, W, V, Nb, Ta, *etc.*) [65]. In 1934, Keggin used X-ray powder diffraction technology to determine the famous Keggin structure model for the first time [66,67]. After that, Dawson, Anderson, Waugh, Silverton and Lindqvist and other structures were determined successively. Among them, the importance of the Keggin structure was first suggested in 1959 in a Sohio patent for the oxidation of methacrolein [68], and then, the Keggin heteropolyacids were widely studied as one of the most convenient structures for catalytic applications. The complex structure of these compounds can be divided into two levels of organization [69]. The primary structure is the Keggin polyanion, consisting in the atomic arrangement of the heteropolyanion itself, the general formula is  $[XM_{12}O_{40}]^{n-}$  ( $X = P, Si, Ge, As, \dots$ ,  $M = Mo, W$ ),  $X$  is the central atom, and a central  $XO_4$  tetrahedron is linked by the corners with 12  $MO_6$  octahedra, while  $M$  is the coordination atom. Each of the three octahedron is connected to form a trihedral  $M_3O_{13}$  assembly, and the octahedra within a same group are linked by the edges. In heteropoly acids (acid form) in the solid state, protons play an essential role in the structure of the crystal, by linking the neighboring heteropolyanions. The secondary structure can be depicted as a tridimensional arrangement between the heteropolyanions, the cations and the crystallization water. The observed complex molecular organization is maintained by electrostatic forces or weak Van-der-Waals or hydrogen bonds [70]. Hence, it is flexible to different extents depending on the counter cation and the structure of the polyanion, and is the basis of bulk-type catalysis of solid HPA catalysts. The tertiary structure is the secondary structure assembled into solid particles describing the physical characteristics of the material, such as particle size, surface area, and pore structure, playing an important role in heterogeneous catalysis. Using Keggin-type heteropolyanion as an illustration, the primary, secondary, and tertiary structures of HPC are depicted in Figure 1.4.

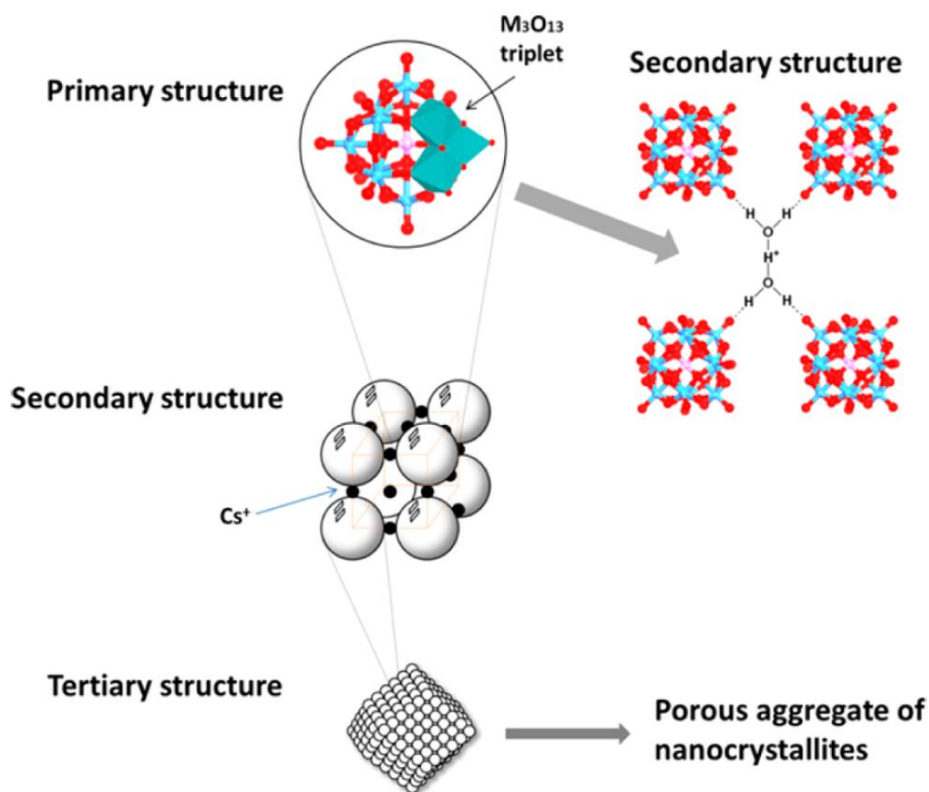


**Figure 1.4** Hierarchical structure of heteropolyacids (HPAs) in the solid state [61].

Based on the above composition and structural characteristics, Keggin heteropolyacids usually exhibit two properties: Brønsted acidity and redox properties [66]. The strong Brønsted acidity is related to its highly symmetrical spatial structure. Due to symmetry, cage structure and nanometer size, the negative charge is highly delocalized in the Keggin anion, so that the charge density on the surface is low, the binding ability to proton is weak, and the activity of proton is quite large [70–72]. The coordination atoms in Keggin heteropolyacids are generally in their highest oxidation state. So, they can be used as multi-electron acceptors with certain oxidation properties. Notably Mo-based heteropolyacids (HPA) accept easily electrons and formation of reduced heteropolymolybdate anions, due to the blue color, named as “*heteropoly blue*”. A general feature of heteropolymolybdates is their high reducibility. Electrochemical investigations by Okuhara *et al.* [73] on Keggin-type heteropolyanions in aqueous or non-aqueous solutions have revealed sequences of reversible one- or two-electron reduction steps, which yield deeply colored mixed-valence species “*heteropoly blues*”. Nevertheless, the initial anion structure is kept after the heteropoly acid is reduced to “*heteropoly blue*”. Heteropolyacid

can be re-oxidized to recover their initial oxidation state, hence showing a reversible redox property [66].

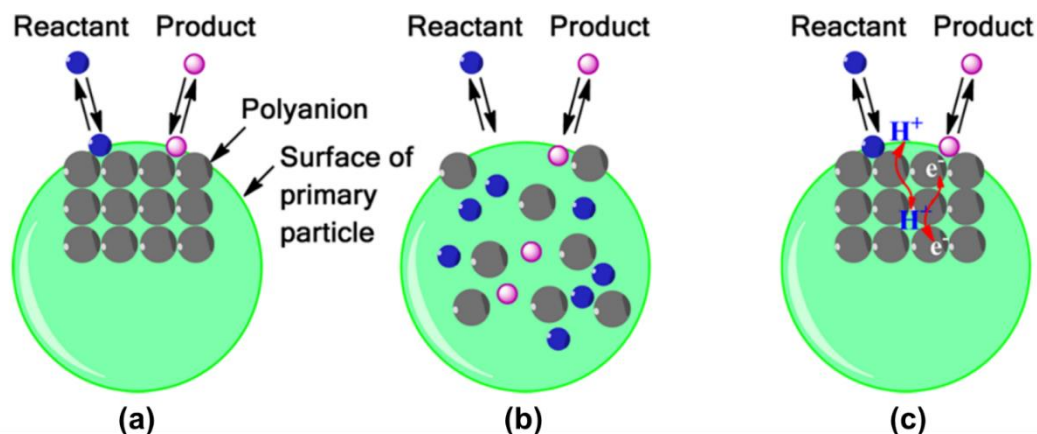


**Figure 1.5** Three types of catalysis by heteropolycompounds: (a) surface-type, (b) bulk type I (or pseudoliquid) and (c) bulk type II [1].

Solid heteropolycompounds belong to a discrete ionic structure that consists of fairly mobile structural units, heteropoly anions and counter-cations. Such structures are often preserved during substitution or oxidation/reduction and exhibit extremely high proton mobility also related as a "pseudoliquid phase". In addition, many HPCs have high solubility in polar solvents and quite high thermal stability in solid states [1]. Pseudoliquid-phase catalysis (bulk type I catalysis) was reported in 1979, and bulk type II behavior in 1983 [73]. In fact, catalysis by solid HPCs can be performed in homogeneous and heterogeneous systems, that is, gas-solid and liquid-solid systems, there are three different classes of catalysis: (a) surface catalysis, (b) bulk type I (pseudoliquid catalysis), and (c) bulk type II catalysis, as shown in Figure 1.5 [1]. Surface-type catalysis is ordinary heterogeneous catalysis, whereby the reactions occur on the solid surface, the outer surface and pore walls, and the catalytic surface area determine the reaction rate. The model (a) catalysis is two-dimensional field, while the catalytic reaction field represented by models (b) and (c) is three-dimensional. In the pseudoliquid phase, these catalysts appear as solids, but behave as liquids. The reactant molecules are absorbed between the polyanions (not "in" a polyanion) in the ionic crystal by replacing water of crystallization or expanding the lattice. The polyanion structure itself remains usually intact. For acid-

catalyzed reactions, the reaction rate is then directly related to the total number of acidic groups in the solid body. Bulk type II catalysis was discovered for oxidation reactions at high temperatures. The whole solid bulk participates in the reduction-oxidation cycle owing to the rapid migration into the bulk of redox carriers such as protons and electrons. The rate is proportional to the volume of catalyst. Solid HPAs containing cations of low ionic radii to charge ratio, such as  $H^+$ ,  $Na^+$ ,  $Cu^{2+}$ , *etc.* (classified into group A salts [74]) readily absorb small polar molecules and tend to exhibit pseudoliquid behavior and are soluble in water. The salts of large cations such as Cs and  $NH_4$  salts (classified as group B salts) usually show only surface-type catalysis [61]. The thermal stability of most group B salts is relatively high, which is also important in heterogeneous catalysis [73].

### 1.2.2 Heteropolycompounds-based catalysts for oxidizing *isobutane* to MAA and MAC

The basic Keggin-structure, phosphomolybdic acid ( $H_3PMo_{12}O_{40}$ ) performs well when oxidizing MAC to MAA, but poorly when oxidizing *isobutane*, due to its poor stability and low specific surface area. Correspondingly, substitution with cesium, vanadium, ammonium and other ions into  $H_3PMo_{12}O_{40}$  was studied to improve the performance (Table 1.3), in order to adjust acidity and redox properties. Indeed, vanadium plays a key role both for dehydrogenation and selective oxidation in all the steps of the reaction networks. Inserting vanadium into the Keggin primary structure to replace molybdenum reduces the  $Mo^{6+}$  to  $Mo^{5+}$  owing to vanadium migration from the primary structure to the secondary one. Vanadium improves the catalyst performance by lower oxidative decomposition of MAA and MAC in *isobutane* conversion [37]. Meanwhile, the high activity of acidic cesium salt of heteropolyacid with  $Cs^+$  instead of proton is related to its large specific surface area increasing thus the spatial density of active sites. Since the selective oxidation of hydrocarbons is a surface reaction, larger specific surface areas improve the *isobutane* conversion. Keggin-structures containing Cs and  $NH_4^+$  uniquely modulate their specific surface area and acidity, connecting their properties to their catalytic activity. These properties as well as their oxidizing ability are controllable over a wide range which is of use in catalyst design [75]. Ammonia is released from the Keggin-structure at high temperature modifying the acid properties and partially reducing the transition metals. The

reduced state improves selectivity to valuable products [37]. A detailed study on the introduction of ammonium and vanadium ions into HPAs to replace protons and molybdenum in phosphomolybdate acid, respectively, has been done by Sultan *et al.* and Jing *et al.* [54,76]. So far, Keggin-type HPCs are still the most effective catalysts to oxidize *isobutane* to MAA in a single step [77–80]. However, yield in MAA+MAC are still very low (<10 %).

**Table 1.3** Selectivity of MAA and MAC with insertion of Cs<sup>+</sup> and NH<sub>4</sub><sup>+</sup> and V<sup>5+</sup> into H<sub>3</sub>PMo<sub>12</sub>O<sub>40</sub> catalyst.

Catalysts	Conversion <sup>a</sup> , %	Selectivity, %			Yields, % (MAA+ MAC)	Feed composition, IBAN/O <sub>2</sub> /H <sub>2</sub> O/inert, mol.%	Ref.
		MAA	MAC	CO <sub>x</sub>			
H <sub>3</sub> PMo <sub>12</sub> O <sub>40</sub>	5	3	7	82	0.5	17.0/33.0/-/50.0	[81]
H <sub>4</sub> PMo <sub>11</sub> VO <sub>40</sub>	5	30	36	34	-	17.0/33.0/-/50.0	[82]
H <sub>5</sub> PMo <sub>10</sub> V <sub>2</sub> O <sub>40</sub>	5	34	28	36	-	17.0/33.0/-/50.0	[82]
CsH <sub>2</sub> PMo <sub>12</sub> O <sub>40</sub>	6	23	17	50	2.4	17.0/33.0/-/50.0	[83]
Cs <sub>2</sub> HPMo <sub>12</sub> O <sub>40</sub>	11	34	10	50	4.8	17.0/33.0/-/50.0	[82]
Cs <sub>3</sub> PMo <sub>12</sub> O <sub>40</sub>	8	0	10	67	0.8	17.0/33.0/-/50.0	[83]
Cs <sub>3</sub> HPMo <sub>11</sub> VO <sub>40</sub>	1.2	32	16	23	0.6	27.0/13.5/10.0/49.5	[76]
Cs <sub>1.6</sub> H <sub>2.4</sub> P <sub>1.7</sub> Mo <sub>11</sub> V <sub>1.1</sub> O <sub>40</sub>	10.6	38	8	15	4.8	26.0/12.0/12.0/50.0	[84]
Cs <sub>0.5</sub> (NH <sub>4</sub> ) <sub>2.5</sub> HPMo <sub>11</sub> VO <sub>40</sub>	4.1	41	29	17	2.9	27.0/13.5/10.0/49.5	[76]
Cs <sub>1.15</sub> (NH <sub>4</sub> ) <sub>1.85</sub> HPMo <sub>11</sub> VO <sub>40</sub>	6	45	15	-	-	26.0/13.0/12.0/49.0	[54]
Cs <sub>1.5</sub> (NH <sub>4</sub> ) <sub>1.5</sub> HPMo <sub>11</sub> VO <sub>40</sub>	5.8	45	22	19	3.9	27.0/13.5/10.0/49.5	[76]
Cs <sub>1.7</sub> (NH <sub>4</sub> ) <sub>1.3</sub> HPMo <sub>11</sub> VO <sub>40</sub>	9.6	44	14	26	5.5	27.0/13.5/10.0/49.5	[76]
Cs <sub>1.75</sub> (NH <sub>4</sub> ) <sub>1.25</sub> HPMo <sub>11</sub> VO <sub>40</sub>	10.3	32	8	-	-	26.0/13.0/12.0/49.0	[54]
Cs <sub>2.4</sub> (NH <sub>4</sub> ) <sub>0.6</sub> HPMo <sub>11</sub> VO <sub>40</sub>	2.1	10	16	-	-	26.0/13.0/12.0/49.0	[54]
Cs <sub>2.5</sub> (NH <sub>4</sub> ) <sub>0.5</sub> HPMo <sub>11</sub> VO <sub>40</sub>	9.9	19	10	53	2.9	27.0/13.5/10.0/49.5	[76]

<sup>a</sup> Reaction temperature: 340 °C, atmospheric pressure.

Cs<sup>+</sup> as a counter-ion in the presence of V in Cs<sub>x</sub>H<sub>1-x</sub>VO [PMo<sub>12</sub>O<sub>40</sub>] achieved high MAA and MAC selectivities. Liu-Cai *et al.* [85] have shown that the oxidative activity decreases as the Cs<sup>+</sup> amount increases (*x* from 0 to 0.5) in the samples. Then increased for cesium greater than 0.5 and reached a maximum for *x* = 0.75. The selectivity to MAA and MAC together increases progressively with *x* in the 0 ≤ *x* ≤ 0.75 range and then falls down when *x* = 1. A high reactivity (*ca.* 52 mmol/h/g) and cumulated selectivity to MAA and MAC (76 %) were obtained with the Cs<sub>0.75</sub>H<sub>0.25</sub>VO[PMo<sub>12</sub>O<sub>40</sub>] catalyst. This suggests that the presence of Cs<sup>+</sup> cations make these samples more hydrophobic. In fact, the samples with more Cs<sup>+</sup> counterions should have

a tendency to expel polar molecules, such as MAA and MAC, and to make desorption of them more readily from the catalyst surface, thus leading to higher selectivity. When all the  $H^+$  are replaced by  $Cs^+$  ( $x = 1$  or  $x > 0.75$ ), the catalyst has no more Brønsted acid sites in its initial structure and is totally inactive, confirming a key role of acidity in both catalytic activity and selectivity.

### 1.2.3 Supported heteropolycompounds

However, heteropolycompound-based catalysts suffer from some issues: poor stability under stream and also low specific surface area and, hence, low activity. To overcome these shortcomings, it is possible to synthesize supported catalysts. In the literature, several supports have been mentioned for catalytic applications, for example: silica [86–93], alumina [94,95], carbon [95,96], zeolites [97], titania [98,99] and zirconia [100,101]. Catalytic activity and product selectivity are sensitive to support and active phase dispersion. Notably, mesoporous materials have many advantages as catalyst supports due to their unique textural properties such as high specific surface area, large pore volume, and uniform pore size distribution [102].

Kim *et al.* [102] synthesized nitrogen-containing mesoporous carbon (N-MC) with high specific surface area and large pore volume, while further modifying the support in order to obtain a positively charged surface, so as to provide sites for the immobilization of  $[PMo_{10}V_2O_{40}]^{5-}$  species. In the vapor-phase oxidation of methacrolein, the  $PMo_{10}V_2/N-MC$  catalyst showed a higher conversion (80 %) of methacrolein and a higher yield (65 %) for methacrylic acid than the unsupported  $H_5PMo_{10}V_2O_{40}$  catalyst (25 % and 20 %, respectively). Similarly, Kim and their group [103] also synthesized mesostructured silica as a support. The surface modified silica (SM-MCF) was synthesized from self-assembled aggregates of organic template and inorganic silica, then, modified by grafting 3-aminopropyl-triethoxysilane (APTES) to get the positive charge and thus to provide sites for the immobilization of  $H_3PMo_{12}O_{40}$ . The  $H_3PMo_{12}O_{40}/SM-MCF$  silica catalyst showed a higher ethanol conversion (45-50 %) than the bulk  $H_3PMo_{12}O_{40}$  catalyst (10-15 %). Kanno *et al.* [104] studied various unsupported and supported  $H_4PMo_{11}VO_{40}$  catalysts for methacrolein oxidation. While  $SiO_2$ -supported  $H_4PMo_{11}VO_{40}$  showed low selectivity to methacrylic acid,  $H_4PMo_{11}VO_{40}$  supported

on NH<sub>3</sub>-modified SiO<sub>2</sub>, exhibited both high selectivity (90 %) and high activity for the formation of methacrylic acid. The activity of H<sub>4</sub>PMo<sub>11</sub>VO<sub>40</sub>/NH<sub>3</sub>-modified SiO<sub>2</sub> was more than five times higher than that of the corresponding unsupported catalysts.

For the selective catalytic oxidation of *isobutane* to MAA and MAC, the catalytic activities of supported HPCs presented in the literature are summarized in Table 1.4. Jing *et al.* [86] impregnated (NH<sub>4</sub>)<sub>3</sub>HPMo<sub>11</sub>VO<sub>40</sub> (APMV) over commercial SiO<sub>2</sub>, SBA-15, ZrO<sub>2</sub>-grafted SBA-15, and Cs<sub>3</sub>PMo<sub>12</sub>O<sub>40</sub> (CPM). The conversion of *isobutane* and yield of MAC and MAA over non-supported APMV catalysts were 2.5 % and 1.4 %, but increased to 11 % and 3.1 % over a SiO<sub>2</sub>-supported catalyst, and further to 15 % and 8 % over a CPM-supported catalyst under the same operating conditions. Similar results were also obtained by Cai *et al.* [105], who supported 40 wt.% of APMV on CeO<sub>2</sub>, WO<sub>3</sub>/ZrO<sub>2</sub> and molecular sieves. It was found that the CPM support had the best chemical compatibility with the active phase, leading to a better stabilization ability of the active phase APMV. Consequently, CPM-supported APMV catalyst presented the best catalytic activity (11 % conversion of *isobutane*, 5.4 % yield of MAA and MAC).

**Table 1.4** Catalytic performance in the oxidation of *isobutane* over supported HPCs catalysts.

Catalysts	Reaction T., °C	Conversion, %	Selectivity %			Yields, % (MAA+MAC)	Ref.
			MAA	MAC	CO <sub>x</sub>		
(NH <sub>4</sub> ) <sub>3</sub> HPMo <sub>11</sub> VO <sub>40</sub> /SBA-15	340	5	10	18	42	30	[86]
(NH <sub>4</sub> ) <sub>3</sub> HPMo <sub>11</sub> VO <sub>40</sub> /ZrO <sub>2</sub> /SBA-15	340	7	2	10	64	0.7	[86]
(NH <sub>4</sub> ) <sub>3</sub> HPMo <sub>11</sub> VO <sub>40</sub> /SiO <sub>2</sub>	340	11	13	15	43	3	[86]
H <sub>3</sub> PMo <sub>12</sub> O <sub>40</sub> /SiO <sub>2</sub>	350	7	40	9	39	3.4	[89]
(NH <sub>4</sub> ) <sub>3</sub> HPMo <sub>11</sub> VO <sub>40</sub> /Molecular sieve	340	8	0.6	0.9	80	0.1	[105]
(NH <sub>4</sub> ) <sub>3</sub> HPMo <sub>11</sub> VO <sub>40</sub> /CeO <sub>2</sub>	340	8	0.3	0	99	0.02	[105]
(NH <sub>4</sub> ) <sub>3</sub> HPMo <sub>11</sub> VO <sub>40</sub> /WO <sub>3</sub> /ZrO <sub>2</sub>	340	7	0.9	4	85	0.3	[105]
(NH <sub>4</sub> ) <sub>3</sub> HPMo <sub>11</sub> VO <sub>40</sub> /Cs <sub>2.5</sub> H <sub>0.5</sub> PMo <sub>12</sub> O <sub>40</sub>	340	9	35	6	38	4.6	[105]
(NH <sub>4</sub> ) <sub>3</sub> HPMo <sub>11</sub> VO <sub>40</sub> /Cs <sub>3</sub> PMo <sub>12</sub> O <sub>40</sub>	340	11	43	5	42	5.4	[105]
(NH <sub>4</sub> ) <sub>3</sub> HPMo <sub>11</sub> VO <sub>40</sub> /Cs <sub>3</sub> HPMo <sub>11</sub> VO <sub>40</sub>	340	10	35	5	47	4	[105]
(NH <sub>4</sub> ) <sub>3</sub> HPMo <sub>11</sub> VO <sub>40</sub> /Cs <sub>4</sub> PMo <sub>11</sub> VO <sub>40</sub>	340	8	32	7	37	3.1	[105]
(NH <sub>4</sub> ) <sub>3</sub> HPMo <sub>11</sub> VO <sub>40</sub> /Cs <sub>3</sub> PMo <sub>12</sub> O <sub>40</sub>	340	15	42	10	31	8	[86]
H <sub>4</sub> PVMO <sub>11</sub> O <sub>40</sub> /Cs <sub>3</sub> HPVMO <sub>11</sub> O <sub>40</sub>	340	5	42	17	32	3	[106]
H <sub>4</sub> PVMO <sub>11</sub> O <sub>40</sub> /Cs <sub>3</sub> PMo <sub>12</sub> O <sub>40</sub>	340	11	24	7	54	3.4	[106]

#### 1.2.4 Mixed metal oxides

Mixed metal oxides catalysts have also been used as effective catalysts in the selective formation of MAC and MAA from *isobutane*. Due to the importance of redox properties of

catalysts in selective oxidation of *isobutane* reaction, the V and Mo elements have always been combined together in the catalyst as the redox reaction occurs:  $V^{5+} + Mo^{5+} \rightarrow V^{4+} + Mo^{6+}$ . Guan *et al.* [80] prepared a series of Mo-V-O catalysts by varying the V/Mo molar ratio. It was found that the catalyst with the V/Mo ratio of 0.3 achieved the best MAC selectivity (40.4 %) at an *isobutane* conversion of 6.4 %.

Moreover, doping with other elements, such as Te, Sb, Ce and P, could also improve the catalytic activity and products distribution effectively over Mo-V-O metal oxides. The group of Guan also doped different amounts of Te on the  $MoV_{0.3}$  (V/Mo ratio of 0.3) catalyst [107]. The Te/Mo ratio presented a clear effect on catalytic activity: The conversion of *isobutane* increased with increasing the Te/Mo ratio ( $Te/Mo \leq 0.25$ ), while it decreased by further increasing the Te content. Ultimately, the  $MoV_{0.3}Te_{0.25}$  catalyst showed a 44.2 % MAC selectivity at an *isobutane* conversion of 15.6 %, which is higher than that without adding Te. Sb was identified as another element that can increase the selectivity of MAC and conversion of *isobutane*. The maximum conversion (20 %) and MAC selectivity (39 %) were obtained over  $MoV_{0.3}Te_{0.23}Sb_{0.5}$  (Sb/Mo ratio of 0.5) catalyst at 470 °C [108]. The catalytic activity can also be improved by inserting Ce into Mo-V-Te oxide. 53 % total selectivity of MAC and MAA was obtained at 20 % of *isobutane* conversion over  $MoV_{0.3}Te_{0.23}Ce_{0.2}$  (Ce/Mo ratio of 0.2) catalyst at 420 °C [109]. The good catalytic performance upon adding Ce may be explained by the redox cycle of Ce and Mo ( $Ce^{3+} + Mo^{6+} \rightarrow Ce^{4+} + Mo^{5+}$ ), and also by improved mobility of lattice oxygen in the catalyst due to the strong capability of Ce for storing oxygen.

Adding phosphorous to metal oxide was also surveyed by Guan *et al.* [110] on the selective oxidation of *isobutane*. 48 % of selectivity to MAC and MAA was achieved at 10 % of *isobutane* conversion over  $MoV_{0.3}Te_{0.23}P_{0.3}$  (P/Mo ratio of 0.3) catalyst at 440 °C, which was higher than that without adding P (35 % selectivity to MAC+MAA, 10 % *isobutane* conversion). Similarly, 51 % of MAC and MAA selectivity with 10 % of *isobutane* conversion were obtained over  $MoV_{0.3}Te_{0.23}Sb_{0.1}P_{0.3}$  (P/Mo ratio of 0.3) catalyst, which was higher than that without adding P (43 % selectivity to MAC+MAA, 6 % *isobutane* conversion).

Usually, mixed metal oxides do not have a special structure like HPCs, which exhibit the

Keggin structure. They rather exhibit mixed crystalline phases or amorphous phases. As far as catalytic products are concerned, mixed metal catalysts are more favorable for the yield of MAC and low quantities of MAA. As far as the preparation technique is concerned, mixed metal oxides are generally obtained by a high-temperature thermal treatment. Therefore, the prepared catalysts could exhibit good thermal stability. This is definitely an advantage compared with the HPC catalysts. Nevertheless, the selectivity to MAA on metal oxides catalysts is very low or even undetectable, which is a major disadvantage compared to HPC catalysts.

### 1.3 Catalytic reactor technologies for selective oxidation

The basis of selective oxidation is the redox mechanism proposed in 1954 by Mars and van Krevelen [111]. They studied how the catalyst evolved during the oxidation of naphthalene by a reducible oxide,  $V_2O_5$ , and showed that lattice oxygens participate to the reaction and are responsible for selectivity. To be efficient in transforming reactant to product, the surface of an oxide catalyst must endeavor reduction by reactant and reoxidation by co-fed oxygen or by means of diffusion of  $O^{2-}$  oxide ion from the bulk to the surface, according to the redox mechanism [63]. The kinetic study carried out by Paul *et al.* [34] found that the Mars and Van Krevelen (MVK) kinetics model can be applied to the oxidation of *isobutane* in the presence of oxygen over a HPA catalyst. In the MVK model, the hydrocarbon reacts with the lattice oxygen to form the products and, then, the reduced sites of the catalyst are re-oxidized by gas phase oxygen [112], as shown in Figure 1.6. Correspondingly, the lattice oxygen from the catalyst plays an important role in the product yield. On the contrary, the interaction of the hydrocarbon (such as propane, *isobutane*...) with weakly adsorbed oxygen from the gas phase is detrimental, and leads to deep oxidation and formation of  $CO_x$  [113].

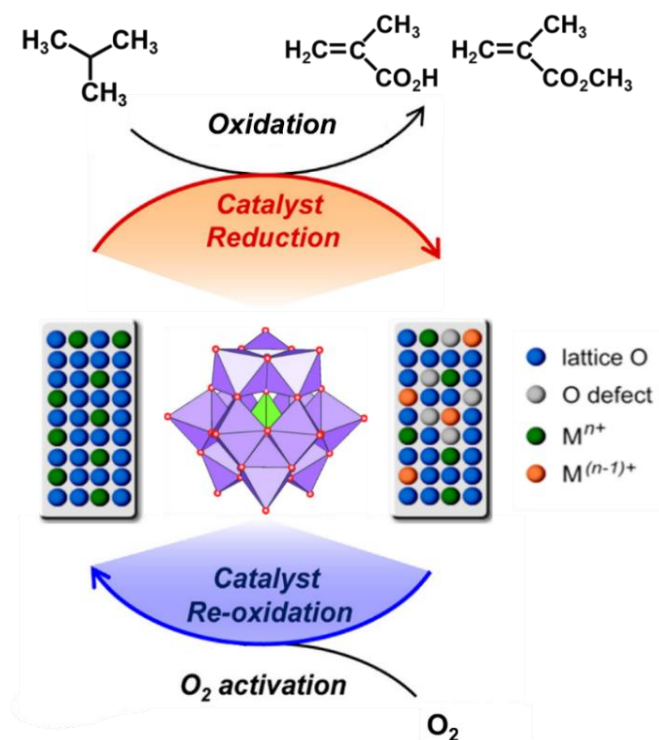


**Figure 1.6** A Mars-van Krevelen redox cycle involving the reduction of lattice O-atoms in catalysts and re-oxidation of reduced centers *via*  $\text{O}_2$  activation steps [114].

Products' selectivities depend on the different systems to be considered [115]: reactor, catalyst particle, or active element of the catalyst surface. This means that not only the catalyst determines the efficiency of a process, but also the reactor configuration and the operating conditions. Therefore, several types of reactor configurations have been proposed for selective oxidation reactions, such as continuous fixed-bed reactors [51,54], periodic reactors [113,116], Two-Zone Fluidized-Bed Reactor (TZFBR) [117,118], and Circulating Fluidized-Bed Reactor (CFBR) [119,120] and so on.

### 1.3.1 Co-feeding of oxygen and *isobutane* in continuous fixed-bed reactor

Fixed-bed reactors (Figure 1.7) come in all sizes, but we can generally group them as laboratory-scale, pilot plant-scale, or commercial-scale. We operate laboratory-scale fixed-bed reactors when developing a new process, investigating a new solid-supported catalyst, qualifying for commercial use a different catalyst, and supporting an existing commercial process [122]. Also, catalytic fixed-bed reactors find widespread use in chemical industries since their scale-up procedure is relatively easy. Fixed-bed reactors are the simplest type of

reactor to design, and consist of solid catalyst particles being loaded and packed into the bed [121]. A fixed or packed bed is an assembly of randomly arranged particles that are bathed by the reactant, which flows in random manner around the pellets [123]. In most cases, these catalysts are operated in a continuous feed mode, in which the hydrocarbon is fed together with oxygen or air through a packed catalyst bed. Several processes like desulfurization of diesel fuel [124] and Fischer-Tropsch synthesis [125] in petrochemistry, ammonia synthesis [126] in inorganic industry, selective oxidation of hydrocarbon compounds [85,127,128] in organic industry, are performed in a continuous fixed-bed reactor.

In general, the continuous fixed-bed reactors used for gas-solid selective oxidation reactions are multi-tubular, which makes them easy to design. They present many unique advantages such as residence time control, well controlled hydrodynamic and reduced losses of solid catalysts due to attrition [113]. The reaction conditions such as feed composition, reaction temperature and contact time are the main factors which affect the catalytic performances.

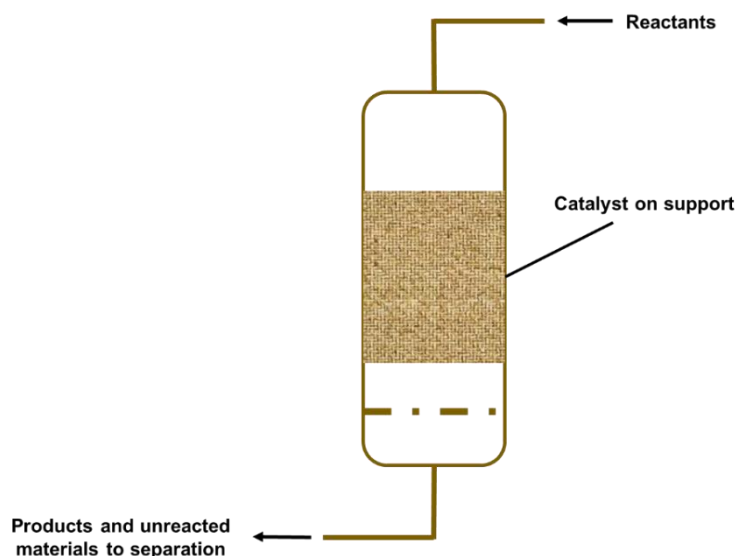


**Figure 1.7** Diagram of fixed-bed reactor [121].

The presence of steam in the feed composition of *isobutane* selective oxidation to MAA and MAC favors the surface reconstruction of the Keggin structure, the stabilization of the active catalyst structure depends on the presence of  $n\text{H}_2\text{O}$  in the secondary structure [63]. Safety

is an important aspect of the selective oxidation process, which is shown in the triangular diagram with respect to the flammability region at room temperature (Figure 1.8). Various companies [43,55,129] use *isobutane*-rich conditions: with *isobutane*-to-dioxygen molar ratios between 2 and 0.8. A lot of studies indicated that MAC and MAA selectivities were higher for dioxygen molar ratios larger than 2 [37].

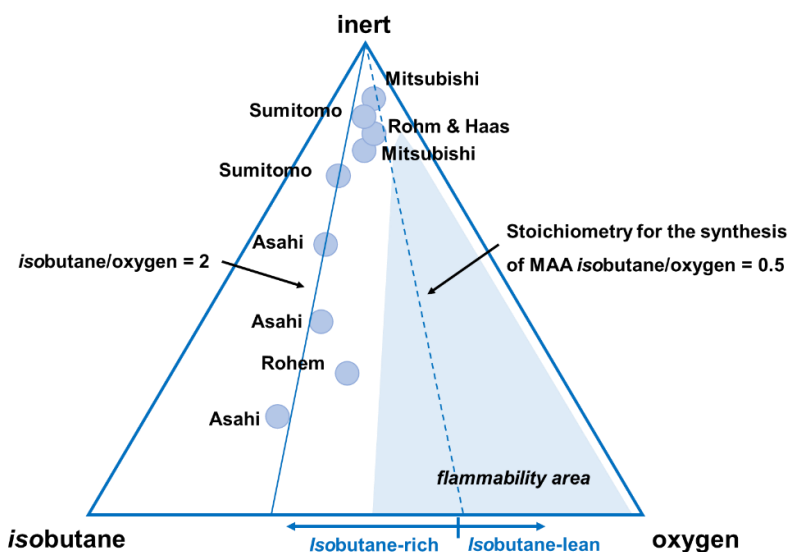


**Figure 1.8** Ternary diagram of composition *isobutane*/oxygen/*inert*, showing the flammability area for mixtures at room temperature, and the feed composition claimed by several industrial companies [1].

One of the main constraints of fixed-bed technologies is the poor heat transfer. Usually, in these situations, the catalyst has to be diluted with an inert component in order to minimize the development of hot spots. In addition, catalyst regeneration and replacement are not convenient in continuous fixed-bed reactor, and catalyst replacement requires interruption of the production [113]. Therefore, the yield and selectivity of the products of selective catalytic oxidation are limited.



Song *et al.* [133] compared a continuous feed of *isobutene* with a periodic flow mode, in which the catalyst was first treated with air at the reaction temperature, followed by reaction of *isobutene* in nitrogen or argon in the absence of oxygen. For BiMoO<sub>x</sub> catalysts, in the continuous feed mode, relatively low selectivity to methacrolein was observed and significant amounts of byproduct CO<sub>2</sub> were formed. In contrast, in the periodic mode, almost 80 % selectivity to methacrolein was observed, especially for the initial reaction period. With a more complex multicomponent catalyst, BiMo<sub>12</sub>Fe<sub>2</sub>NiCo<sub>7</sub>MgSb<sub>0.9</sub>Ti<sub>0.1</sub>Te<sub>0.02</sub>Cs<sub>0.4</sub>O<sub>x</sub>, methacrolein yield was enhanced and the selectivity to methacrolein was *ca.* 96 % at all the investigated reaction temperatures (360 - 390 °C), and neither carbon nor carbon-containing product depositions were observed during the periodic mode. G. Emig *et al.* [134], simulated the separation of the redox-process in selective oxidation of *n*-butane to maleic anhydride by using the pulse-technique. They found that the long duration of catalyst reoxidation reduced the space-time-yield to uneconomic level. To obtain improved selectivity using a short regeneration period it is in contrast necessary to apply a high regeneration-temperature. After detailed exploration of various parameters on the redox-process a yield of 78 % was achieved at 310 °C. Zhao *et al.* [116], investigated the selective oxidation of propane by lattice oxygen of vanadium-phosphorus oxide catalysts, with a pulse reactor in which the oxidation of propane and the re-oxidation of the catalyst were implemented alternately in the presence of water vapor. The principal products were acrylic acid (ACA) and acetic acid (AA) with a maximum total selectivity (ACA+AA) of 56.4 % (34.1 % + 23.3 %) at a propane conversion of 12 %. Although, small amounts of C1 and C2 hydrocarbons could also be found, in a fixed bed reactor, it was hard to obtain high selectivity at a high propane conversion due to the further degradation of acrylic acid and acetic acid. Hence, the catalytic performance was clearly improved in a pulse reactor. Dai *et al.* [135], investigated the partial oxidation of methane to synthesis gas on AFeO<sub>3</sub> (A = La, Nd, Eu) oxides by redox cyclic reaction in a pulse reactor. The experiments indicated that the AFeO<sub>3</sub> oxides provide mostly oxygen species, as the sole oxidant originated from lattice oxygen, which oxidized CH<sub>4</sub> to synthesis gas with high selectivity in the absence of gaseous oxygen. The two types of oxygen species were identified by experiments of continuous

reactions and pulses, and confirmed that methane was converted selectively to synthesis gas by lattice oxygen, exclusively, whereas the reoxidation of  $AFeO_3$  oxides was due to gaseous molecular oxygen. In other words, the pulse reactor avoids the complete oxidation of methane, thus improving the selectivity of the desired product, and the selectivity to CO at higher level (> 96 %).

As one can see, the temporal and spatial separations of the redox-process are possible, whereby the semi-regenerative reactor enables an improvement of the catalytic performance of the catalyst, mainly the selectivity to the main product. Compared to co-feed reactions where flammable regions exist, periodic reactions are much safer. However, the exothermic regeneration can cause hot spots in the reactor. During regeneration, an increase in temperature in the reactor can thus be observed. However, the relative non-continuous production and high capital costs are obvious disadvantages [118].

### **1.3.3 Continuous regeneration on Circulating Fluidized-Bed Reactor (CFBR)**

In late 1996, Dupont started up a new plant at Asturias in Spain to produce tetrahydrofuran using a new process based on maleic acid from *n*-butane [113]. This new process was the first commercial use of a circulating fluidized-bed reactor (CFBR) for the production of a specialty chemical, *i.e.*, butane conversion to maleic anhydride on a VPO catalyst [120]. In the CFBR, the catalyst is circulating from a reactor where the hydrocarbon reacts with the catalyst to the regenerator where it is re-oxidized with air before returning to the reactor, as shown in Figure 1.10. The CFBR technology can be considered when the catalyst operates according to the Mars-Van Krevelen mechanism. Catalyst reduction and re-oxidation are decoupled in time and in space, and reduction and re-oxidation take place in different vessels [119]. The CFBR notably allows the optimization of the reaction conditions independently since it uses two distinct reactors with characteristic residence times and temperatures in order to take into account the different kinetics of catalyst reduction and reoxidation to better control the degree of oxidation and regeneration of catalyst [113].

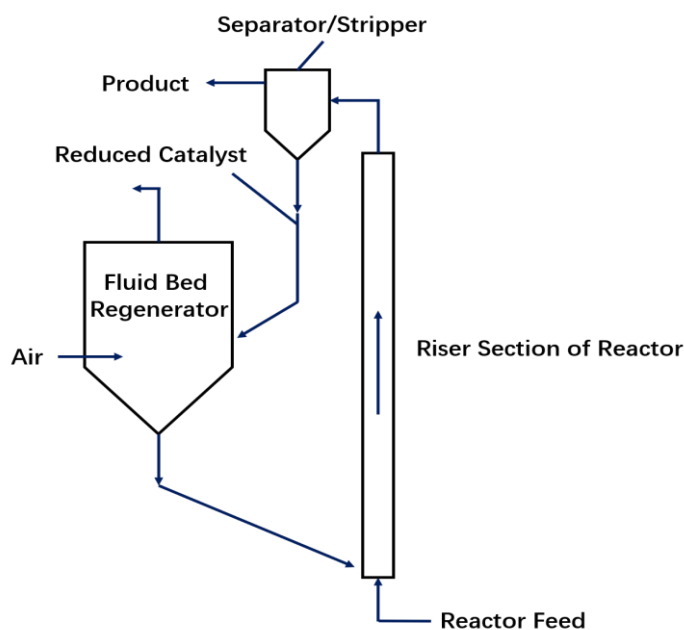


**Figure 1.10** Schematic diagram of a circulating fluidized-bed reactor [136].

Alkane selective oxidation, where the reduction of the catalyst by the hydrocarbon and reoxidation by molecular oxygen can be decoupled in time or in space, in the sense that circulating fluidized bed reactors can also provide a solution to reduce CO<sub>2</sub> emissions during selective oxidation. [119].

#### 1.3.4 Two-Zone Fluidized-Bed reactor (TZFBR)

As we have seen, the fixed-bed reactor has some unavoidable disadvantages for selective catalytic oxidation reactions. Periodic reactor can solve the problem of catalyst cycle regeneration, avoiding the over-oxidation of the product, and improve the selectivity to the target product. Even better, fluidized-bed reactors are more efficient heat transfer in such a way that the reactor may operate isothermally. Therefore, catalyst degradation associated to hot spots is avoided, meanwhile, the fluidized-bed reactor can also be used for catalyst regeneration and recycling in the reaction process [113]. However, CFBR also has its shortcoming, that is, the attrition of catalyst particles, the difficulty to operate and the high investment costs [118]. The main idea behind a Two-Zone Fluidized-Bed reactor (TZFBR) is that the reduction and reoxidation can take place in different zones, but in the same vessel. The reduction of the catalyst by the hydrocarbon and reoxidation by molecular oxygen can be decoupled in space, that is the two steps of the Mars and Van Krevelen mechanism. The solid catalyst is loaded in

the presence of oxygen in the re-oxidation zone, where the oxidizing agent is injected in the fluidized bed at the bottom of the reactor. In the upper part of the bed, where the reactant is injected in the middle of the bed *via* a nozzle, the catalyst comes in contact with the hydrocarbon. Thus, two zones can be distinguished, which reacts with lattice oxygen at the top zone and the catalysts recirculate with the oxidizing agent at the bottom zone [118]. However, while TZFBR has decreased investments compared to CFBR, the temperature is the same in both zones and therefore the contact time is more difficult to control independently in both zones, which to an extent also brings more factors to be considered for research.

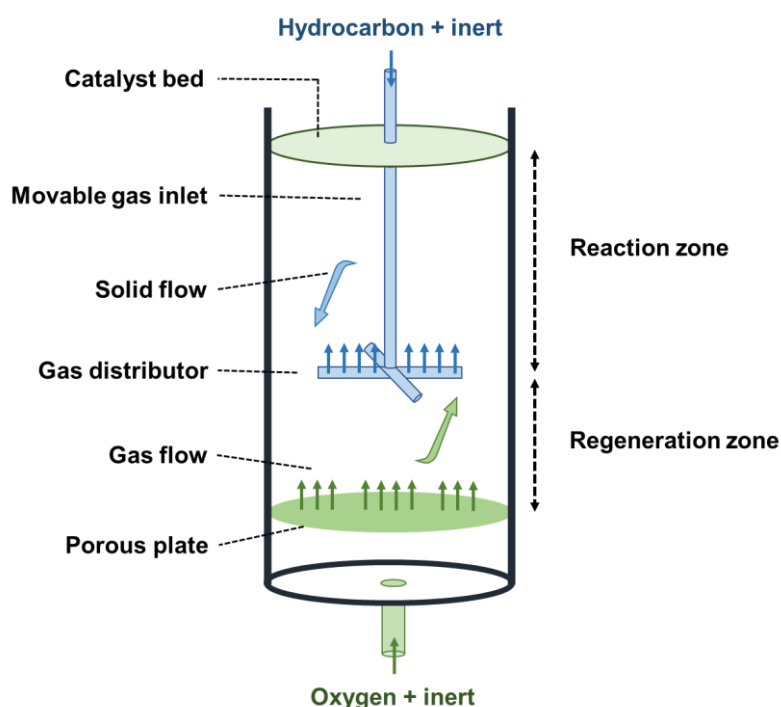


**Figure 1.11** Scheme of a Two Zone Fluidized-Bed Reactor (TZFBR) [137].

A TZFBR is represented schematically in Figure 1.11. Since hydrocarbon and oxygen are decoupled, the flammability concerns are less important (oxygen does not enter the upper zone when its conversion is high enough), and the degree of oxidation of the catalyst can be controlled better. Since non-selective reactions related to gas phase oxygen are not carried out, the desired product selectivity often improves [113,138].

TZFBR has been applied to different processes during the past decades. J. Soler *et al.* [139], studied the catalytic performance of a selective V-Mg-O catalyst in the oxidative

dehydrogenation of *n*-butane using different types of reactor: fixed-bed reactor, conventional fluidized-bed reactor and two-zone fluidized-bed reactor. The results indicated that the TZFBR outperforms the other two reactors, especially at high *n*-butane conversions. Thus, a selectivity to C4 olefins of 54 % at *n*-butane conversions of 60 % was achieved at 550 °C using an *in situ* redox fluidized-bed reactor, while selectivity to C4-olefins lower than 43 % were obtained on the other reactor types under the same reaction conditions. B. Katryniok *et al.* [118] used a TZFBR to carry out the glycerol dehydration to acrolein catalyzed by a Keggin-type catalyst containing 20 wt.% H<sub>3</sub>PW<sub>12</sub>O<sub>40</sub> on SiO<sub>2</sub>. The hydrodynamic behavior of the TZFBR shows good mixing, illustrated by the fluidization quality being superior to 80 % at a reaction temperature of 275 °C, at the same time, the deactivation of catalyst by coking was also avoided. The TZFBR design made it possible to simultaneously conduct the reaction of glycerol dehydration and the regeneration by oxygen of the coked catalyst. The feasibility of the continuous acrolein production from glycerol was therefore shown for the first time using this reactor technology. Mazloom *et al.* [117] employed a fluidized-bed reactor to investigate the partial oxidation of propane to acrylic acid over Mo<sub>1</sub>V<sub>0.3</sub>Te<sub>0.23</sub>Nb<sub>0.12</sub>O<sub>x</sub> catalyst, and the results were compared with classical fixed-bed reactor indicating that at constant temperature, the propane conversion obtained in the fixed-bed reactor was higher. In fact, in the fluidized-bed, some amount of propane passes through the bed in the bubble phase, resulting in poor contact with the catalyst and bad fluidization quality. The results indicated that at constant temperature propane conversion obtained in the fixed bed reactor was higher. However, the fluidized-bed recompensed it by higher acrylic acid selectivity. In addition, the oxygen ratio should be carefully adjusted to ensure that it can be completely consumed in the bottom zone, and back-mixing of gas, especially hydrocarbons transported with the bubbles, must be avoided [137]. This is not only relevant for the selectivity of the products, but is also crucial for safety issues.

As aforementioned, the advantages and disadvantages of the different reactors described are summarized in the Table 1.5 below.

**Table 1.5** Advantages and disadvantages of each reactor [118].

Reactors	Advantages	Disadvantages
Continuous fixed-bed reactors	Easy to design Lower loss of solid catalyst due to abrasion	Risk of explosive conditions Formation of side products
Periodic reactors	Separate catalyst reduction and regeneration to decrease by-products generation	Loss of productivity High capital costs
CFBR	Controllable processes for reduction and re-oxidation of catalysts	Attrition of catalyst particles High capital expenditure
TZFBR	Lower investment compared to CFBR	Difficult to control the reduction and re-oxidation processes of the catalyst independently

#### 1.4 Conclusion and research strategy

As aforementioned, selective oxidation of *isobutane* for the production of methyl methacrylate and methacrylic acid has attracted extensive research interest in the recent decades. Selective oxidation of *isobutane* to produce MAC and MAA requires C-H activation, oxidative dehydrogenation, and oxygen insertion. Therefore, the design and development of the catalytic system must focus on the optimization of the parameters influencing the steps of this mechanism. Given that vanadium is known to play a crucial role for both the dehydrogenation and selective oxidation steps of the reaction network, our strategy is focused on the development of a supported Keggin-type HPA catalyst for the selective oxidation of IBAN to MAC and MAA, where  $V^{5+}$  is inserted into  $H_3PMo_{12}O_{40}$  to form  $H_4PMo_{11}VO_{40}$  and  $H_5PMo_{10}V_2O_{40}$ . Moreover, the catalytic activity is strongly influenced by the presence of counter cations – such as  $Cs^+$  – which form an heteropoly salt presenting a high specific surface area. Cesium substitution, also increases the hydrophobicity, thus increasing the tendency to expel MAA and MAC, which are polar, resulting in better catalytic performance [85]. In addition, it has been reported that rubidium and cesium have similar physical and chemical properties [140], and partial exchange of protons by  $Rb^+$  also lead to solids with enhanced surface area [141]. To the best of our knowledge, Rb-substituted HPA catalysts were not used for the selective oxidation of *isobutane* to MAC and MAA. With respect to such findings, we decided to partially substitute  $H^+$  for  $Cs^+$  and  $Rb^+$  in  $H_{3+x}PMo_{12-x}V_xO_{40}$  ( $x = 1$  and  $2$ ) in order to

obtain the cesium, rubidium-vanado-molybdcic acid, respectively. Meanwhile, HPA supported catalysts exhibited improved thermal stability and increased active site dispersion. Hereby, silica is the most widely used carrier among all supports, it is non-toxic, inert, widely commercially available, and has a large specific surface area. The most important point is that it does not have negative impact on the acidity and structure of HPA [142–144].

Furthermore, in addition to the optimization of the catalyst, the reactor technology will also be studied. Part of the work is carried out in the classical fixed-bed reactor. However, selective oxidation of *isobutane* conforms to the Mars-van-Krevelen mechanism, that is, the reactive lattice oxygen in the catalyst reacts with the reactant *isobutane* to form oxygen vacancies, and the oxygen in the reactants flow adsorbs on the catalyst surface to form the process of consumption-replenishment. Therefore, the lattice oxygen from the catalyst plays an important role in the product yield. On the contrary, the interaction of *isobutane* with weakly adsorbed oxygen from the gas phase is detrimental, leading to deep oxidation and formation of  $\text{CO}_x$  [113]. Both processes can occur simultaneously in a classical fixed-bed reactor, operated in a continuous feed mode, and where IBAN is flowed together with oxygen through a packed catalyst bed. Compared with the continuous fixed-bed reactor, the periodic reactor and the TZFBR permit a better control of the gas phase composition and a constant catalyst regeneration through the separation of catalyst reduction and reoxidation in the MVK mechanism. However, to the best of our knowledge, these types of reactors have not been investigated so far in the selective oxidation of *isobutane* to MAA and MAC.

**References**

- [1] M. Sun, J. Zhang, P. Putaj, V. Caps, F. Lefebvre, J. Pelletier, J.M. Basset, *Chem. Rev.* 114 (2014) 981–1019.
- [2] F. Jing, Thesis, Université Lille1, (2012) 148.
- [3] F. Dury, E.M. Gaigneaux, P. Ruiz, *Appl. Catal. A Gen.* 242 (2003) 187–203.
- [4] K. Routray, K.R.S.K. Reddy, G. Deo, *Appl. Catal. A Gen.* 265 (2004) 103–113.
- [5] E.A. Mamedov, V. Cortés Corberán, *Appl. Catal. A, Gen.* 127 (1995) 1–40.
- [6] M. Baerns, O. Buyevskaya, *Catal. Today* 45 (1998) 13–22.
- [7] G. Liu, Z.J. Zhao, T. Wu, L. Zeng, J. Gong, *ACS Catal.* 6 (2016) 5207–5214.
- [8] W. Ueda, D. Vitry, T. Katou, *Catal. Today* 96 (2004) 235–240.
- [9] G. Landi, L. Lisi, J.C. Volta, *Chem. Commun.* 3 (2003) 492–493.
- [10] M. Misono, *Top. Catal.* 21 (2002) 89–96.
- [11] T. Kobayashi, *Catal. Today* 71 (2001) 69–76.
- [12] M. Ai, *J. Mol. Catal. A Chem.* 114 (1996) 3–13.
- [13] W. Chu, J. Luo, S. Paul, Y. Liu, A. Khodakov, E. Bordes, *Catal. Today* 298 (2017) 145–157.
- [14] V.S. Arutyunov, R.N. Magomedov, A.Y. Proshina, L.N. Strekova, *Chem. Eng. J.* 238 (2014) 9–16.
- [15] H. Arakawa, M. Aresta, J.N. Armor, M.A. Barteau, E.J. Beckman, A.T. Bell, J.E. Bercaw, C. Creutz, E. Dinjus, D.A. Dixon, K. Domen, D.L. DuBois, J. Eckert, E. Fujita, D.H. Gibson, W.A. Goddard, D.W. Goodman, J. Keller, G.J. Kubas, H.H. Kung, J.E. Lyons, L.E. Manzer, T.J. Marks, K. Morokuma, K.M. Nicholas, R. Periana, L. Que, J. Rostrup-Nielsen, W.M.H. Sachtler, L.D. Schmidt, A. Sen, G.A. Somorjai, P.C. Stair, B. Ray Stults, W. Tumas, *Chem. Rev.* 101 (2001) 953–996.
- [16] T. Ikuno, J. Zheng, A. Vjunov, M. Sanchez-Sanchez, M.A. Ortuño, D.R. Pahls, J.L. Fulton, D.M. Camaioni, Z. Li, D. Ray, B.L. Mehdi, N.D. Browning, O.K. Farha, J.T. Hupp, C.J. Cramer, L. Gagliardi, J.A. Lercher, *J. Am. Chem. Soc.* 139 (2017) 10294–10301.

- [17] J. Baek, B. Rungtaweevoranit, X. Pei, M. Park, S.C. Fakra, Y.S. Liu, R. Matheu, S.A. Alshmimri, S. Alshehri, C.A. Trickett, G.A. Somorjai, O.M. Yaghi, *J. Am. Chem. Soc.* 140 (2018) 18208–18216.
- [18] S. Tang, J. Lin, K.L. Tan, *Catal. Letters* 51 (1998) 169–175.
- [19] Q.G. Yan, W.Z. Weng, H.L. Wan, H. Toghiani, R.K. Toghiani, C.U. Pittman, *Appl. Catal. A Gen.* 239 (2003) 43–58.
- [20] Y. Gambo, A.A. Jalil, S. Triwahyono, A.A. Abdulrasheed, *J. Ind. Eng. Chem.* 59 (2018) 218–229.
- [21] V. Fornés, C. López, H.H. López, A. Martínez, *Appl. Catal. A Gen.* 249 (2003) 345–354.
- [22] S.I. Al-Mayman, M.A. Soliman, A.S. Al-Awadi, Y.S. Al-Zeghayer, *Appl. Petrochemical Res.* 8 (2018) 29–38.
- [23] Y. Zhou, J. Lin, L. Li, X. Pan, X. Sun, X. Wang, *J. Catal.* 365 (2018) 14–23.
- [24] L. Shi, B. Yan, D. Shao, F. Jiang, D. Wang, A.H. Lu, *Cuihua Xuebao/Chinese J. Catal.* 38 (2017) 389–395.
- [25] Y. Uragami, K. Otsuka, *J. Chem. Soc. Faraday Trans.* 88 (1992) 3605–3610.
- [26] X. Tu, M. Niwa, A. Arano, Y. Kimata, E. Okazaki, S. Nomura, *Appl. Catal. A Gen.* 549 (2018) 152–160.
- [27] M.O. Guerrero-Pérez, M.A. Peña, J.L.G. Fierro, M.A. Bañares, *Ind. Eng. Chem. Res.* 45 (2006) 4537–4543.
- [28] Hinago et al., United States Patent, (2000) 6063728.
- [29] L. Shi, D. Wang, W. Song, D. Shao, W.P. Zhang, A.H. Lu, *ChemCatChem* 9 (2017) 1788–1793.
- [30] A.A. Ayandiran, I.A. Bakare, H. Binous, S. Al-Ghamdi, S.A. Razzak, M.M. Hossain, *Catal. Sci. Technol.* 6 (2016) 5154–5167.
- [31] Colman et al., United States Patent, (2000) 6057475.
- [32] R. Cited, U.S.P. Documents, (1979).
- [33] S. Crone, F. Borgmeier, M. Duda, 2 (2012).
- [34] S. Paul, V. Le Courtois, D. Vanhove, *Ind. Eng. Chem. Res.* 36 (1997) 3391–3399.

- [35] Y. Liu, C. Xia, Q. Wang, L. Zhang, A. Huang, M. Ke, Z. Song, *Catal. Sci. Technol.* 8 (2018) 4916–4924.
- [36] S. Sakaguchi, S. Kato, T. Iwahama, Y. Ishii, *Bull. Chem. Soc. Jpn.* 71 (1998) 1237–1240.
- [37] M.J. Darabi Mahboub, J.L. Dubois, F. Cavani, M. Rostamizadeh, G.S. Patience, *Chem. Soc. Rev.* 47 (2018) 7703–7738.
- [38] A.W. Smith, I.T. Jackson, J. Yousefi, *Eur. J. Plast. Surg.* 22 (1999) 17–21.
- [39] K. Nagai, *Appl. Catal. A Gen.* 221 (2001) 367–377.
- [40] V.F. Coindre, S.M. Kinney, M. V. Sefton, *Biomaterials* 259 (2020) 120324.
- [41] K. Avasthi, A. Bohre, M. Grilc, B. Likozar, B. Saha, *Catal. Sci. Technol.* 10 (2020) 5411–5437.
- [42] F. Cavani, *Catal. Today* 157 (2010) 8–15.
- [43] N. Ballarini, F. Cavani, H. Degrand, E. Etienne, A. Pigamo, F. Trifirò, J.L. Dubois, *Methods Reagents Green Chem. An Introd.* (2007) 265–279.
- [44] Q. Deng, S. Jiang, T. Cai, Z. Peng, Z. Fang, *J. Mol. Catal. A Chem.* 229 (2005) 165–170.
- [45] S. Liu, L. Chen, G. Wang, J. Liu, Y. Gao, C. Li, H. Shan, *J. Energy Chem.* 25 (2016) 85–92.
- [46] M.R. Gogate, J.J. Spivey, J.R. Zoeller, *Catal. Today* 36 (1997) 243–254.
- [47] M. V. Kirillova, J.A.L. Da Silva, J.J.R.F. Da Silva, A.F. Palavra, A.J.L. Pombeiro, *Adv. Synth. Catal.* 349 (2007) 1765–1774.
- [48] J.M.M. Millet, J.C. Védrine, *Top. Catal.* 15 (2001) 139–144.
- [49] P.E.L. Shippen, (1988).
- [50] W. Bauer, *Ullmann's Encycl. Ind. Chem.* 16 (2011).
- [51] F. Jing, B. Katryniok, F. Dumeignil, E. Bordes-Richard, S. Paul, *J. Catal.* 309 (2014) 121–135.
- [52] Y. Liu, J. He, W. Chu, W. Yang, *Catal. Sci. Technol.* 8 (2018) 5774–5781.
- [53] S. Kendel, T. Brown, *Catal. Letters* 141 (2011) 1767–1785.
- [54] M. Sultan, S. Paul, M. Fournier, D. Vanhove, *Appl. Catal. A Gen.* 259 (2004) 141–152.
- [55] F. Cavani, R. Mezzogori, A. Pigamo, F. Trifirò, E. Etienne, *Catal. Today* 71 (2001) 97–

- 110.
- [56] J.C. Védrine, I. Fechete, *Comptes Rendus Chim.* 19 (2016) 1203–1225.
- [57] H. Krieger, L.S. Kirch, United States Patent, (1981) 4260822.
- [58] F. Cavani, R. Mezzogori, A. Pigamo, F. Trifirò, *Top. Catal.* 23 (2003) 119–124.
- [59] G. Centi, F. Cavani, F. Trifirò, *FUNDAMENTAL AND APPLIED CATALYSIS*, (2001) ISBN 978-1-4613-6872-4.
- [60] G. Busca, F. Cavani, E. Etienne, E. Finocchio, A. Galli, G. Sella, F. Trifirò, *J. Mol. Catal. A Chem.* 114 (1996) 343–359.
- [61] M. Misono, *Chem. Commun.* 1 (2001) 1141–1153.
- [62] N. Mizuno, M. Misono, *Chem. Rev.* 98 (1998) 199–217.
- [63] E. Bordes-Richard, *Catal. Today* (2019) 1–12.
- [64] D. Vanhove, *Appl. Catal. A Gen.* 138 (1996) 215–234.
- [65] H.L. Kee, H. Tang, *Angew. Chemie - Int. Ed.* 30 (2013) 1–59.
- [66] I. V. Kozhevnikov, *Chem. Rev.* 98 (1998) 171–198.
- [67] J. F. Keggin, *Proc. R. Soc. London Ser. A* 144 (1934) 75–100.
- [68] Y. Izumi, *Catal. Today* 33 (1997) 371–409.
- [69] J.B. Moffat, *J. Mol. Catal.* 26 (1984) 385–396.
- [70] B. Katryniok, *UCCS* (2010) 1–9.
- [71] S. Ganapathy, M. Fournier, J.F. Paul, L. Delevoye, M. Guelton, J.P. Amoureux, *J. Am. Chem. Soc.* 124 (2002) 7821–7828.
- [72] L. Barcza, M.T. Pope, *J. Phys. Chem.* 79 (1975) 92–93.
- [73] T. Okuhara, N. Mizuno, M. Misono, *Adv. Catal.* 41 (1996) 113–252.
- [74] M. Misono, *Heterogeneous Catalysis by Heteropoly Compounds of Molybdenum and Tungsten*, 1987.
- [75] C. Marchal-Roch, N. Laronze, R. Villanneau, N. Guillou, A. Tézé, G. Hervé, *J. Catal.* 190 (2000) 173–181.
- [76] F. Jing, B. Katryniok, F. Dumeignil, E. Bordes-Richard, S. Paul, *Catal. Sci. Technol.* 4 (2014) 2938–2945.

- [77] G.P. Schindler, C. Knapp, T. Ui, K. Nagai, *Top. Catal.* 22 (2003) 117–121.
- [78] J. Guan, Z. Wang, C. Xu, Y. Yang, B. Liu, X. Yu, Q. Kan, *Catal. Letters* 128 (2009) 356–362.
- [79] J. Guan, S. Jing, S. Wu, H. Xu, Z. Wang, Q. Kan, *React. Kinet. Catal. Lett.* 90 (2007) 27–33.
- [80] J. Guan, H. Xu, K. Song, B. Liu, F. Shang, X. Yu, Q. Kan, *Catal. Letters* 126 (2008) 293–300.
- [81] M. Langpape, J.M.M. Millet, *Appl. Catal. A Gen.* 200 (2000) 89–101.
- [82] N. Mizuno, H. Yahiro, *J. Phys. Chem. B* 102 (1998) 437–443.
- [83] N. Mizuno, M. Tateishi, M. Iwamoto, *J. Catal.* 163 (1996) 87–94.
- [84] L. Jalowiecki-Duhamel, A. Monnier, Y. Barbaux, G. Hecquet, *Catal. Today* 32 (1996) 237–241.
- [85] F. Liu-Cai, *React. Kinet. Catal. Lett.* 75 (2002) 305–314.
- [86] F. Jing, B. Katryniok, E. Bordes-richard, S. Paul, (n.d.).
- [87] F.J. Méndez, A. Llanos, M. Echeverría, R. Jáuregui, Y. Villasana, Y. Díaz, G. Liendo-Polanco, M.A. Ramos-García, T. Zoltan, J.L. Brito, *Fuel* 110 (2013) 249–258.
- [88] G. Karthikeyan, A. Pandurangan, *J. Mol. Catal. A Chem.* 311 (2009) 36–45.
- [89] N. Ballarini, F. Candiracci, F. Cavani, H. Degrand, J.L. Dubois, G. Lucarelli, M. Margotti, A. Patinet, A. Pigamo, F. Trifirò, *Appl. Catal. A Gen.* 325 (2007) 263–269.
- [90] W. Kuang, A. Rives, M. Fournier, R. Hubaut, *Appl. Catal. A Gen.* 250 (2003) 221–229.
- [91] S. Gao, J.B. Moffat, *Catal. Letters* 42 (1996) 105–111.
- [92] N. Legagneux, J.M. Basset, A. Thomas, F. Lefebvre, A. Goguet, J. Sá, C. Hardacre, *J. Chem. Soc. Dalt. Trans.* (2009) 2235–2240.
- [93] H. Jaramillo, L.A. Palacio, L. Sierra, *Stud. Surf. Sci. Catal.* 142 B (2002) 1291–1298.
- [94] K. Narasimharao, B.H. Babu, N. Lingaiah, P.S.S. Prasad, S.A. Al-Thabaiti, *J. Chem. Sci.* 126 (2014) 487–498.
- [95] L.R. Pizzio, P.G. Vázquez, C. V. Cáceres, M.N. Blanco, *Appl. Catal. A Gen.* 256 (2003) 125–139.

- [96] A. Lapkin, B. Bozkaya, T. Mays, L. Borello, K. Edler, B. Crittenden, *Catal. Today* 81 (2003) 611–621.
- [97] S.R. Mukai, T. Masuda, I. Ogino, K. Hashimoto, *Appl. Catal. A Gen.* 165 (1997) 219–226.
- [98] S. Damyanova, J.L.G. Fierro, *Appl. Catal. A Gen.* 144 (1996) 59–77.
- [99] M.L. Cubeiro, J.L.G. Fierro, *Catal. Letters* 49 (1997) 223–227.
- [100] L. Pizzio, P. Vázquez, C. Cáceres, M. Blanco, *Catal. Letters* 77 (2001) 233–239.
- [101] K.N. Rao, K.M. Reddy, N. Lingaiah, I. Suryanarayana, P.S.S. Prasad, *Appl. Catal. A Gen.* 300 (2006) 139–146.
- [102] H. Kim, J.C. Jung, D.R. Park, S.H. Baeck, I.K. Song, *Appl. Catal. A Gen.* 320 (2007) 159–165.
- [103] H. Kim, J.C. Jung, P. Kim, S.H. Yeom, K.Y. Lee, I.K. Song, *J. Mol. Catal. A Chem.* 259 (2006) 150–155.
- [104] M. Kanno, Y.K. Miura, T. Yasukawa, T. Hasegawa, W. Ninomiya, K. Ooyachi, H. Imai, T. Tatsumi, Y. Kamiya, *Catal. Commun.* 13 (2011) 59–62.
- [105] X. Cai, Y. Ma, Q. Zhou, Z. Zhang, W. Chu, W. Yang, *React. Kinet. Mech. Catal.* (2021).
- [106] S. Paul, W. Chu, M. Sultan, E. Bordes-Richard, *Sci. China Chem.* 53 (2010) 2039–2046.
- [107] J. Guan, K. Song, H. Xu, Z. Wang, Y. Ma, F. Shang, Q. Kan, *Catal. Commun.* 10 (2009) 528–532.
- [108] J. Guan, M. Jia, S. Jing, Z. Wang, L. Xing, H. Xu, Q. Kan, *Catal. Letters* 108 (2006) 125–129.
- [109] J. Guan, S. Wu, H. Wang, S. Jing, G. Wang, K. Zhen, Q. Kan, *J. Catal.* 251 (2007) 354–362.
- [110] J. Guan, S. Wu, M. Jia, J. Huang, S. Jing, H. Xu, Z. Wang, W. Zhu, H. Xing, H. Wang, Q. Kan, *Catal. Commun.* 8 (2007) 1219–1223.
- [111] P. Mars, D.W. van Krevelen, *Chem. Eng. Sci.* 3 (1954) 41–59.
- [112] G. Mazloom, S.M. Alavi, *React. Kinet. Mech. Catal.* 110 (2013) 387–403.
- [113] G. Mazloom, S.M. Alavi, *Part. Sci. Technol.* 36 (2018) 61–71.

- [114] S. Kwon, P. Deshlahra, E. Iglesia, *J. Catal.* 364 (2018) 228–247.
- [115] H.G. Lintz, A. Reitzmann, *Catal. Rev. - Sci. Eng.* 49 (2007) 1–32.
- [116] R. Zhao, J. Wang, Q. Dong, J. Liu, *J. Nat. Gas Chem.* 14 (2005) 88–94.
- [117] G. Mazloom, S.M. Alavi, *Part. Sci. Technol.* 33 (2015) 204–212.
- [118] B. Katryniok, R. Meléndez, V. Bellière-Baca, P. Rey, F. Dumeignil, N. Fatah, S. Paul, *Front. Chem.* 7 (2019).
- [119] J.L. Dubois, *Catal. Today* 99 (2005) 5–14.
- [120] R.M. Contractor, *Chem. Eng. Sci.* 54 (1999) 5627–5632.
- [121] S.D. Anuar Sharuddin, F. Abnisa, W.M.A. Wan Daud, M.K. Aroua, *Energy Convers. Manag.* 115 (2016) 308–326.
- [122] J. Worstell, *Adiabatic Fixed-Bed React.* (2014) 81–108.
- [123] V. Degirmenci, K. Eränen, V. Hessel, S.Y. Ivanov, T. Kilpiö, S.M. Mahajani, T. Noël, A.K. Ray, E. Rebrov, V. Russo, T. Salmi, E. Shahbazali, G. Vladisavljevic, Q. Wang, J. Wood, *Catal. React. III* (2015).
- [124] A. Chica, A. Corma, M.E. Dómine, *J. Catal.* 242 (2006) 299–308.
- [125] X. Wang, M. Economides, *Adv. Nat. Gas Eng.* (2009) 243–287.
- [126] *C. Int.* (2019).
- [127] W. Fang, Q.J. Ge, J.F. Yu, H.Y. Xu, *Ind. Eng. Chem. Res.* 50 (2011) 1962–1967.
- [128] A. Szöke, F. Solymosi, *Appl. Catal. A Gen.* 142 (1996) 361–374.
- [129] F. Cavani, J.H. Teles, *ChemSusChem* 2 (2009) 508–534.
- [130] T. Kane, Thesis, Université de Lille (2018).
- [131] S.T. Sie, *Appl. Catal. A Gen.* 212 (2001) 129–151.
- [132] J. B. GALESKI, *Canadian Journal of Chemical Engineering*, 48 (1970) 151–157.
- [133] N. Song, C. Rhodes, J.K. Bartley, S.H. Taylor, D. Chadwick, G.J. Hutchings, *J. Catal.* 236 (2005) 282–291.
- [134] G. Emig, K. Uihlein, C.J. Häcker, *Stud. Surf. Sci. Catal.* 82 (1994) 243–251.
- [135] X.P. Dai, R.J. Li, C.C. Yu, Z.P. Hao, *J. Phys. Chem. B* 110 (2006) 22525–22531.
- [136] R.M. Contractor, H.S. Horowitz, G.M. Sisler, E. Bordes, *Catal. Today* 37 (1997) 51–57.

- [137] J. Herguido, M. Menéndez, J. Santamaría, *Catal. Today* 100 (2005) 181–189.
- [138] C. TeHllez, M. Menéndez, J. Santamaría, *Chem. Eng. Sci.* 54 (1999) 2917–2925.
- [139] J. Soler, J.M. López Nieto, J. Herguido, M. Menéndez, J. Santamaría, *Catal. Letters* 50 (1998) 25–30.
- [140] X. Ye, Z. Wu, W. Li, H. Liu, Q. Li, B. Qing, M. Guo, F. Ge, *Colloids Surfaces A Physicochem. Eng. Asp.* 342 (2009) 76–83.
- [141] N. Essayem, Y. Ben Taârit, P.Y. Gayraud, G. Sapaly, C. Naccache, *J. Catal.* 204 (2001) 157–162.
- [142] M. Kanno, T. Yasukawa, W. Ninomiya, K. Ooyachi, Y. Kamiya, *J. Catal.* 273 (2010) 1–8.
- [143] R. Al-Faze, A. Finch, E.F. Kozhevnikova, I. V. Kozhevnikov, *Appl. Catal. A Gen.* 597 (2020) 117549.
- [144] P. Vazquez, L. Pizzio, C. Caceres, M. Blanco, H. Thomas, E. Alesso, L. Finkielsztein, B. Lantano, G. Moltrasio, J. Aguirre, *Journal of Molecular Catalysis A: Chemical* 161 (2000) 223–232.

# **Chapter 2**

## **Experimental**

## **Chapter 2 Experimental**

### **2.1 Characterization techniques**

Catalysts have been characterized by using different techniques such as microscopy, Thermogravimetric Analyzer (TGA), X-Ray Diffraction (XRD), IR-Raman spectroscopies, N<sub>2</sub> physisorption (BET), Temperature programmed reduction (TPR), Temperature-programmed desorption of ammonia (NH<sub>3</sub>-TPD) and X-ray photoelectron spectroscopy (XPS). Detailed information on the used characterization techniques is given below.

#### **2.1.1 Optical microscope**

Optical images were obtained using a ZEISS Axio Lab microscope. This microscope is available with differential interference contrasts (C-DIC) and equipped with a quintuple revolving nosepiece (ZEISS EC EPIPLAN), which keeps all relevant objectives ready for use [1]. In this work 5x objective and 10x eyepieces were used. The microscope camera AxioCam ERc 5s is equipped with a 5MP CMOS Sensor giving a resolution of 2560 (H) × 1920 (V).

#### **2.1.2 Thermogravimetric analysis**

The Thermogravimetric Analyzer (TGA) is an essential laboratory tool used for material characterization. It is a technique in which the mass of a substance is monitored as a function of temperature or time as the sample specimen is subjected to a controlled temperature program under a controlled atmosphere. A TGA consists of a sample pan that is supported by a precision balance. That pan resides in a furnace and is heated or cooled during the experiment. The mass of the sample is monitored during the experiment. A purge gas controls the sample environment. This gas may be inert or a reactive gas that flows over the sample and exits through an exhaust. In this work, the TGA was performed using a SETARAM instruments to study the thermal decomposition behavior of the catalysts. The catalysts were heated from 20 °C to 700 °C at a rate of 3 °C/min under air flow. A TGA thermal curve indicates a weight change occurred. The abscissa (X-axis) can be displayed as time or temperature and the ordinate (Y-axis) can be displayed as weight (mg) or percent of weight variation (%).

### 2.1.3 X-ray Diffraction

X-ray powder diffraction (XRD) is an analytical technique used in phase identification for a crystalline material. A crystal with planes oriented at an angle  $\theta$  to an incident X-ray beam of wavelength  $\lambda$  will diffract X-rays according to the Bragg's law:

$$2d.\sin\theta = n\lambda$$

Where,  $n$  is an integer,  $\lambda$  is the wavelength of the X-rays,  $\theta$  is the angle between the incident rays and the surface of the crystal, and  $d$  is the spacing between diffracting planes. The measurement of the different values of  $d$  allows identifying the phase. These particular directions appear as dots of light in a diffraction pattern, which are known as "*reflections*". Thus, an X-ray diffraction pattern is produced by an electromagnetic wave impinging on a regular array of scatterers [2].

In this work, X-ray diffraction patterns were recorded in ambient conditions using the Cu  $K\alpha$  radiation ( $\lambda = 1.5418 \text{ \AA}$ ; 40 kV, 30 mA) on a Siemens D5000 diffractometer, with a  $0.02^\circ$  scan step and 1 s time step in the  $10\text{-}80^\circ$  range. The interpretation of the diffractograms was performed using the Diffrac Eva software and by comparison by JCPDS reference files.

### 2.1.4 IR Raman spectroscopy

The Raman scattering of light by molecules was predicted by Smekal using classical quantum theory in 1923 and observed by Raman and Krishnan in 1928 [3]. Raman is a light-scattering technique in which molecules scatter incident light from a high-intensity laser source. Most of the scattered light has the same wavelength or color as the laser source, which is called Rayleigh scattering, and does not provide useful information. However, small amounts of light are scattered at different wavelengths or colors, depending on the chemical structure of the analyte, which is called Raman scattering. Raman spectra have many peaks, showing the intensity and wavelength position of Raman scattered light. Each peak corresponds to a specific molecular bond vibration, including individual bond (e.g., CC, C = C, NO, CH, etc.) and groups of bonds (e.g., polymer chain vibrations) [4].

In this work, IR-Raman spectra were collected on a Horiba Xplora using a laser beam of 532 nm wavelength for excitation in confocal mode. A 50x long working distance objective

(Olympus) was used for both focusing the excitation beam on the sample and collecting the scattered light. The latter was dispersed using an 1800 grooves spectrometer grating after having passed through a confocal hole of 300  $\mu\text{m}$ . A Peltier-cooled CCD detector was used for recording the Raman spectra.

### **2.1.5 Nitrogen adsorption/desorption**

The Brunauer-Emmett-Teller (BET) model serves as the basis for the measurement of the specific surface area of materials. Its theoretical basis was built in 1938 when Brunauer, Emmett and Teller [5] proposed a theory of nitrogen physisorption at  $-196\text{ }^\circ\text{C}$ . In this work,  $\text{N}_2$  physisorption isotherms at liquid nitrogen temperature were obtained on a TriStar II Plus gas adsorption analyzer (Micromeritics) after outgassing at  $130\text{ }^\circ\text{C}$  in vacuum overnight. Specific surface areas were evaluated with the BET model over the following range:  $P/P_0 = 0.05\text{-}0.30$ . The total pore volume was measured from the volume of  $\text{N}_2$  adsorbed at  $P/P_0 = 0.95$ .

### **2.1.6 Temperature-Programmed Reduction**

Temperature-Programmed Reduction (TPR) is an important technique for the characterization of oxidized materials. For TPR measurements, the reducing gas usually consists of a mixture of either hydrogen and nitrogen or hydrogen and argon. The reported hydrogen concentrations range from 3 to 15 %; the flow rates from 10 to 60 mL/min STP, and the sample volumes from 10 to 500  $\mu\text{mol}$  [6]. TPR allows estimating the nature of reducible species present in the catalyst, the amount of  $\text{H}_2$  required to reduce the material, and reveals the temperature at which the reduction of each species occurs in given conditions of catalyst mass, temperature ramp and flow rate [7].

In this work, TPR analyses were performed on an automated AutoChem II 2920 Chemisorption Analyzer from Micromeritics. 100 mg of catalyst were inserted into a glass reactor. The sample was flushed with a gas mixture comprising 5 vol.%  $\text{H}_2$  in Ar at room temperature with a flow rate of 50 mL/min STP. The temperature of the sample was increased linearly at a ramp rate of  $5\text{ }^\circ\text{C}/\text{min}$  up to  $1000\text{ }^\circ\text{C}$ . The consumption of hydrogen was monitored *via* a TCD signal converted by use of a calibration factor, to get quantitative information on the species present in the catalyst.

### 2.1.7 Temperature-Programmed Desorption of ammonia

Temperature-Programmed Desorption (TPD) of ammonia is a widely used and flexible techniques to determine the number of acid sites as well as their strength [8]. In this work, ammonia temperature-programmed desorption (NH<sub>3</sub>-TPD) combined with mass spectrometry (MS) was performed to quantify the amount and strength of the acid sites of the catalysts. A typical test was as follows: 50 mg of catalyst were pre-treated in a He flow (30 mL/min STP) at 130 °C for 2 h in order to notably remove physisorbed water. Then, NH<sub>3</sub> was absorbed on the surface by pulsed injections at 130 °C until saturation was stated from the MS signal. Then, the TPD profiles were monitored by MS and thermal conductivity detector and recorded from 130 to 650 °C at a heating rate of 10 °C/min.

As the desorption curve can involve several overlapping peaks, a deconvolution treatment was done by using a Gaussian shaped function to obtain separated peaks. The quantitative calculation was done as follows [9]:

- 1) Peaks identification and areas calculation by a Gaussian shaped function;
- 2) Calculation of the amount of NH<sub>3</sub> uptake according to the NH<sub>3</sub> calibration;
- 3) Calculation of the density of surface acidic sites using the following formula:

$$D_{\text{acidity}}, \mu\text{mol}/\text{m}^2 = \frac{\text{Acidity}, \text{mmol}/\text{g}_{\text{cat.}}}{S_{\text{BET}}, \text{m}^2/\text{g}_{\text{cat.}}}$$

Where  $D$ ,  $Acidity$ , and  $S_{\text{BET}}$  are the surface acidic sites density, the amount of NH<sub>3</sub> consumed and the specific surface area of samples, respectively.

### 2.1.8 X-ray Photoelectron Spectroscopy

Surface analyses by X-ray Photoelectron Spectroscopy (XPS) is a quantitative spectroscopic technique that can be used for the chemical analysis of the surface layers of a material [10]. XPS spectra are obtained by irradiating a material with a beam of X-rays (commonly Al K $\alpha$  or Mg K $\alpha$  radiations) in an ultra-high vacuum environment. Each element produces a characteristic set of XPS peaks at characteristic binding energies. The energy and intensity of the emitted photoelectrons allow identifying the elements and determining their surface concentration. In this work, XPS spectra were collected on an Axis Ultra DLD “2009” Kratos spectrometer using the monochromatic Al K $\alpha$  radiation ( $h\nu = 1486.6$  eV) as the

excitation source. The calibration of the XPS spectra was made using the carbon C 1s reference peak at 284.8 eV. Simulation of the experimental photopeaks was carried out using Casa XPS software.

## 2.2 Catalysts syntheses

### 2.2.1 Vanadium-substituted phosphomolybdic acids precursors

The formation of  $\text{H}_4\text{PMo}_{11}\text{VO}_{40}$  and  $\text{H}_5\text{PMo}_{10}\text{V}_2\text{O}_{40}$  starts from stoichiometric mixtures of phosphate, molybdate and vanadate as follows [11]:



The amounts of each reactant were stoichiometrically chosen for this preparation. The details are listed in Table 2.1 and Table 2.2:

**Table 2.1** Amounts of reactants used for  $\text{H}_4\text{PMo}_{11}\text{VO}_{40} \cdot x\text{H}_2\text{O}$  preparation.

Reactant	Molar ratio	Mole, mol	Mass, g
$\text{Na}_2\text{HPO}_4$	1.0	0.01	1.42
$\text{Na}_2\text{MoO}_4 \cdot 2\text{H}_2\text{O}$	11.0	0.11	26.6
$\text{NaVO}_3$	1.0	0.01	1.22

**Table 2.2** Amounts of reactants used for  $\text{H}_5\text{PMo}_{10}\text{V}_2\text{O}_{40} \cdot x\text{H}_2\text{O}$  preparation.

Reactant	Molar ratio	Mole, mol	Mass, g
$\text{Na}_2\text{HPO}_4$	1.0	0.01	1.42
$\text{Na}_2\text{MoO}_4 \cdot 2\text{H}_2\text{O}$	10.0	0.10	24.2
$\text{NaVO}_3$	2.0	0.02	2.44

For example, for the preparation of  $\text{H}_4\text{PMo}_{11}\text{VO}_{40}$ , 1.42 g of  $\text{Na}_2\text{HPO}_4$  (Sigma-Aldrich) were dissolved in a solution of 1.22 g of  $\text{NaVO}_3$  (Fluka) in 50 mL of boiling water under stirring. Then, after cooling to room temperature, 1 mL HCl (34-37 %) was added and the color turned to reddish brown. Following the addition of an aqueous solution of 26.6 g  $\text{Na}_2\text{MoO}_4 \cdot 2\text{H}_2\text{O}$  (Alfa Aesar) in 50 mL of water under stirring, the mixture was acidified with 40 mL HCl (34-37 %) and the color further changed to orange-red. The acidified mixture was kept at room temperature for 5 h and poured into a dividing funnel and then extracted with 70 mL of diethyl

ether. The extraction was accomplished by repeated shaking, after which the layers separated. The HPA etherate in the lowest layer was isolated, 7 mL of water was added and kept for crystallization at room temperature. The yield was 20.0 g (theoretical yield:  $\text{H}_4\text{PMo}_{11}\text{VO}_{40}$  without crystal water is 20.5 g), calculated for  $\text{H}_4\text{PMo}_{11}\text{VO}_{40}\cdot 30.5\text{H}_2\text{O}$ . Figure 2.1 shows schematically the different steps of the preparation of HPA.

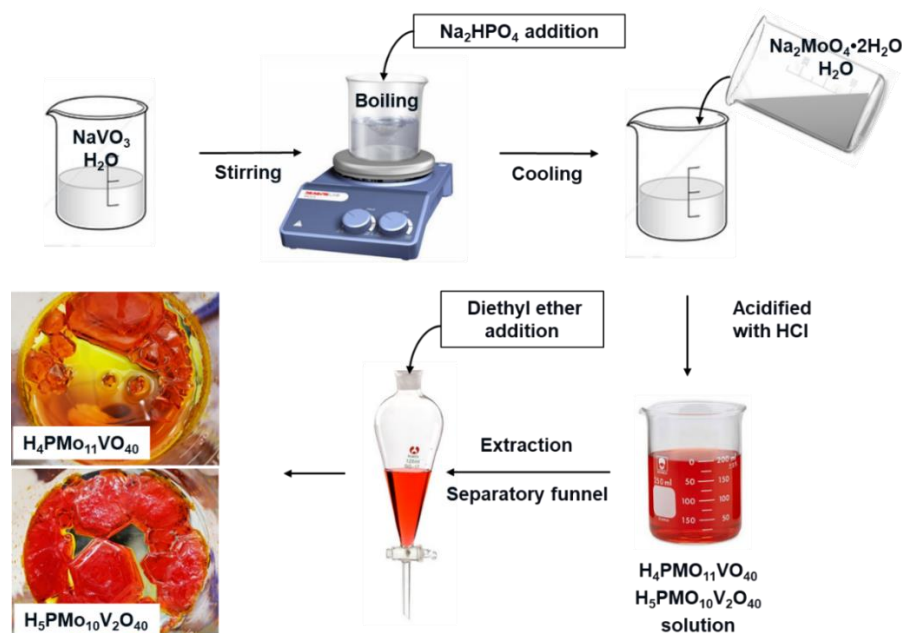
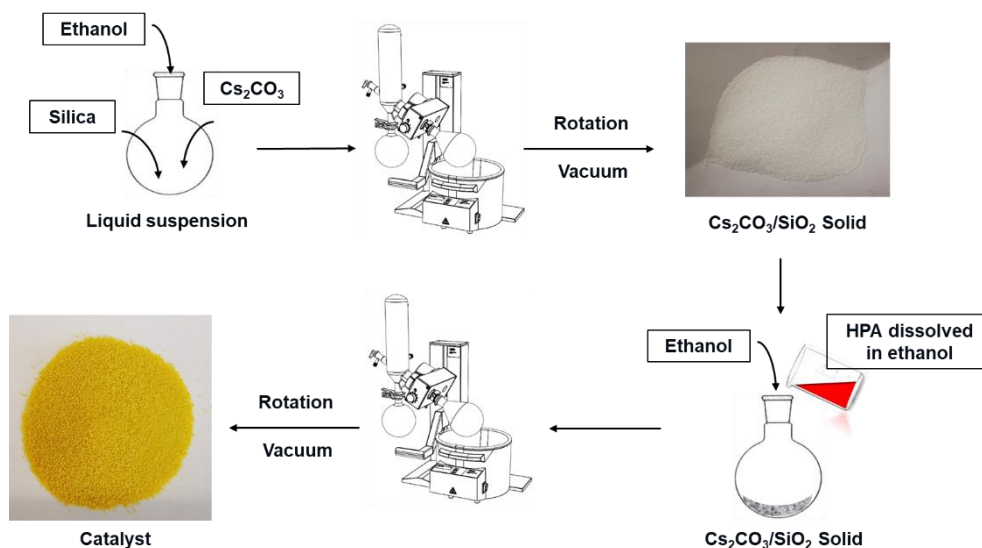


Figure 2.1 HPA synthesis.

### 2.2.2 Preparation of the supported catalysts

The CARiACT<sup>®</sup>  $\text{SiO}_2$ , commercially available from Fuji Silysia Chemical Company, was used as a support. The  $\text{SiO}_2$  with a specific surface area of  $264 \text{ m}^2/\text{g}$ , total pore volume of  $1.12 \text{ cm}^3/\text{g}$ , pore size of  $170 \text{ \AA}$ , average particle diameter of  $200 \mu\text{m}$ . The preparations of 10-50 wt.%  $\text{Cs}_2\text{H}_2\text{PMo}_{11}\text{VO}_{40}$ ,  $\text{Rb}_2\text{H}_2\text{PMo}_{11}\text{VO}_{40}$ ,  $\text{Cs}_{2.5}\text{H}_{2.5}\text{PMo}_{10}\text{V}_2\text{O}_{40}$  and  $\text{Rb}_{2.5}\text{H}_{2.5}\text{PMo}_{10}\text{V}_2\text{O}_{40}$  supported on  $\text{SiO}_2$  were carried out in two steps [12]: 1)  $\text{SiO}_2$  was impregnated with  $\text{Cs}_2\text{CO}_3$  (Fluka) or  $\text{Rb}_2\text{CO}_3$  (Aldrich). The support and 30 mL of 100 % ethanol were stirred at  $60 \text{ }^\circ\text{C}$ . Then, the desired amount of  $\text{Cs}_2\text{CO}_3$  or  $\text{Rb}_2\text{CO}_3$  was added as solids. After 30 min, the solvent was evaporated under vacuum at  $60 \text{ }^\circ\text{C}$  for 1.5 h. 2) The as-prepared support was then impregnated with HPA. The prepared  $\text{Cs}_2\text{CO}_3/\text{SiO}_2$  (or  $\text{Rb}_2\text{CO}_3/\text{SiO}_2$ ) was suspended in 30 mL of 100 % ethanol, and subsequently the required amount of HPA ( $\text{H}_4\text{PMo}_{11}\text{VO}_{40}$  or

H<sub>5</sub>PMo<sub>10</sub>V<sub>2</sub>O<sub>40</sub>) dissolved in a minimum quantity of ethanol was added. After 30 min, the solvent was evaporated under vacuum at 60 °C until the obtained solid was dry. Figure 2.2 shows schematically the impregnation of the silica carrier with cesium carbonate and subsequently with HPA acid.



**Figure 2.2** Catalyst preparation by impregnation.

In order to make comparisons easier between the different catalysts, the formulation of the series of catalysts Cs<sub>2</sub>H<sub>2</sub>PMo<sub>11</sub>VO<sub>40</sub>/SiO<sub>2</sub>, Cs<sub>2.5</sub>H<sub>2.5</sub>PMo<sub>10</sub>V<sub>2</sub>O<sub>40</sub>/SiO<sub>2</sub> and Rb<sub>2.5</sub>H<sub>2.5</sub>PMo<sub>10</sub>V<sub>2</sub>O<sub>40</sub>/SiO<sub>2</sub> are labelled in the followings as CsV<sub>1</sub>/SiO<sub>2</sub>, CsV<sub>2</sub>/SiO<sub>2</sub> and RbV<sub>2</sub>/SiO<sub>2</sub>, respectively. Catalysts with different loadings of active phase on the SiO<sub>2</sub> support  $x$  wt.% Cs<sub>2</sub>H<sub>2</sub>PMo<sub>11</sub>VO<sub>40</sub>/SiO<sub>2</sub>,  $x$  wt.% Cs<sub>2.5</sub>H<sub>2.5</sub>PMo<sub>10</sub>V<sub>2</sub>O<sub>40</sub>/SiO<sub>2</sub> and  $x$  wt.% Rb<sub>2.5</sub>H<sub>2.5</sub>PMo<sub>10</sub>V<sub>2</sub>O<sub>40</sub>/SiO<sub>2</sub> are labelled in the following as  $x$ CsV<sub>1</sub>,  $x$ CsV<sub>2</sub> and  $x$ RbV<sub>2</sub>, respectively, where  $x$  ranges from 10 to 50.

## 2.3 Experimental set-ups and catalytic performance evaluation

### 2.3.1 Fixed-bed reactor

#### 2.3.1.1 Description of the experimental set-up and operation conditions

The catalytic reactions for the selective oxidation of *isobutane* to methacrolein and methacrylic acid were first performed in a downflow fixed-bed reactor under atmospheric

pressure as depicted in Figure 2.3. As shown in the figure, the overall catalytic set-up is composed of three parts: the feeding zone, the reaction zone and the analysis zone, respectively.

For the feeding zone, *isobutane* and O<sub>2</sub> are necessary as reactants, and inert helium gas was introduced as the diluent and carrier gas. The flow-rates of each gas are regulated by mass flow controllers (MFC - BROOKS). Water was introduced *via* a saturation system keeping 10 % partial pressure of water in the gas stream. Regulated temperature of the saturation system was calculated according to the following Antoine equation (2.1):

$$T = \frac{1435.26}{4.65 - \log_{10}\left(\frac{P}{P_0}\right)} + 64.85 \quad (2.1)$$

Where the units of pressure ( $P$ ) and temperature ( $T$ ) are Pa and K, respectively. The catalytic reaction was carried out under 1 atmosphere (101325 Pa). The reactants mixture was fed at a constant total flow-rate of 10 mL/min STP (molar ratio 28 % IBAN; 12 % O<sub>2</sub>; 10 % H<sub>2</sub>O; 50 % He), corresponding to a WHSV (weight hourly space velocity) of 0.75 L·g<sup>-1</sup>·h<sup>-1</sup>.

When the gas leaves the feeding zone and enters the reaction zone, a four-way valve directs the feed stream through the reactor or to the by-pass line. The reactor is made of a stainless-steel tube, with an inner diameter of 10 mm and a length of 240 mm. The details of the reactor with the loaded catalyst are depicted on Figure 2.3. The reactor was loaded with 0.8 g of catalyst sandwiched by carborundum (SiC, 0.21 mm diameter) to keep the catalytic bed in the isothermal zone of the reactor. The reactor was heated to reaction temperature at a 5 °C/min heating rate under atmospheric pressure. The reactant gas will enter the reactor from the top, after flowing through the catalyst, the product gas will leave the reactor from the bottom. Downstream to the reactor, the effluent fills a 1 mL loop of the six-way valve, which is connected to the analysis zone. The reaction conditions were always kept the same as above unless otherwise stated.

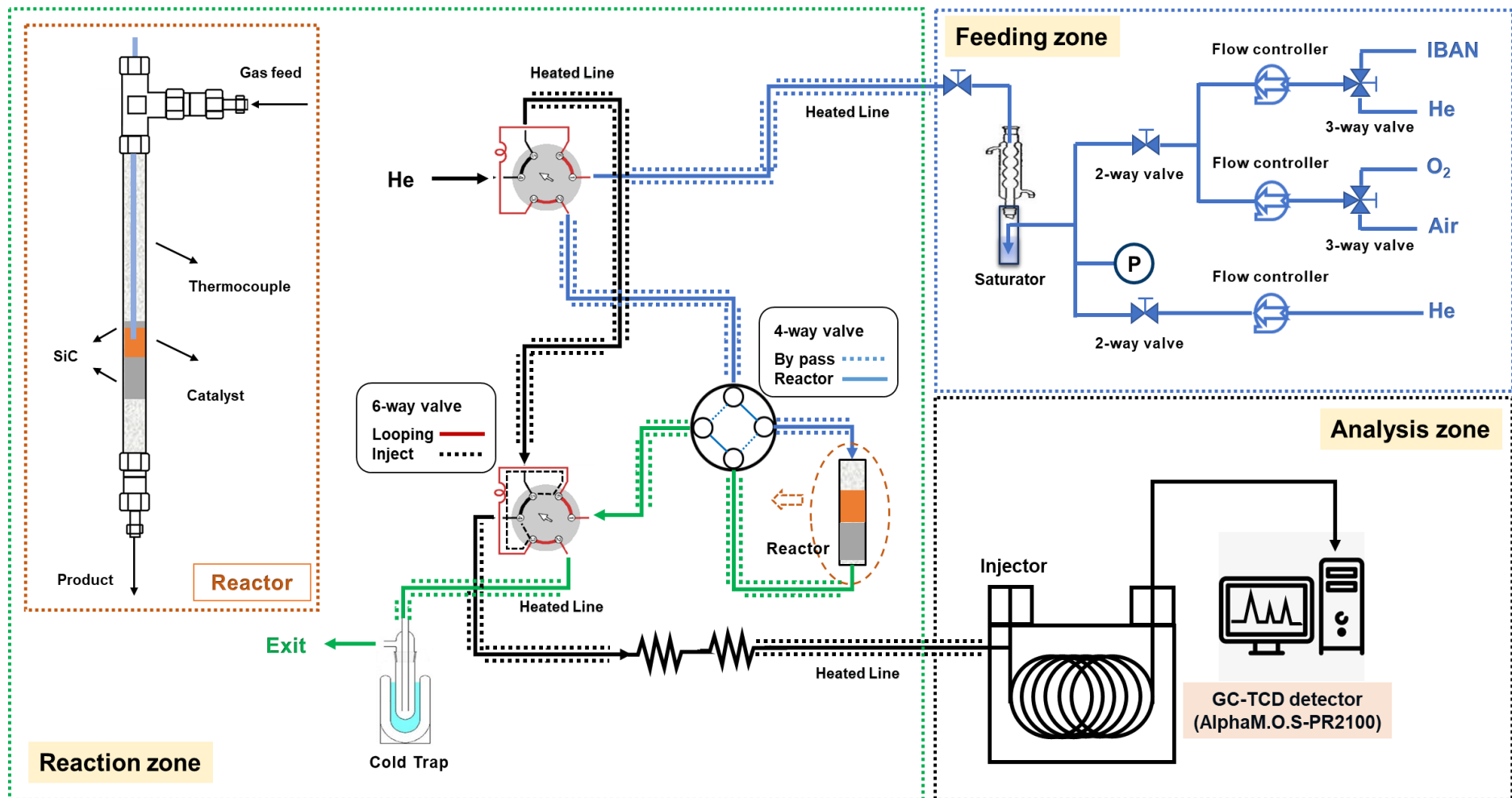


Figure 2.3 Fixed bed reactor system used for the selective oxidation of isobutane to MAC and MAA.

Coming to the analysis zone, all products were analyzed on-line by gas chromatography (GC). The reaction data were obtained under stream at steady state conditions.

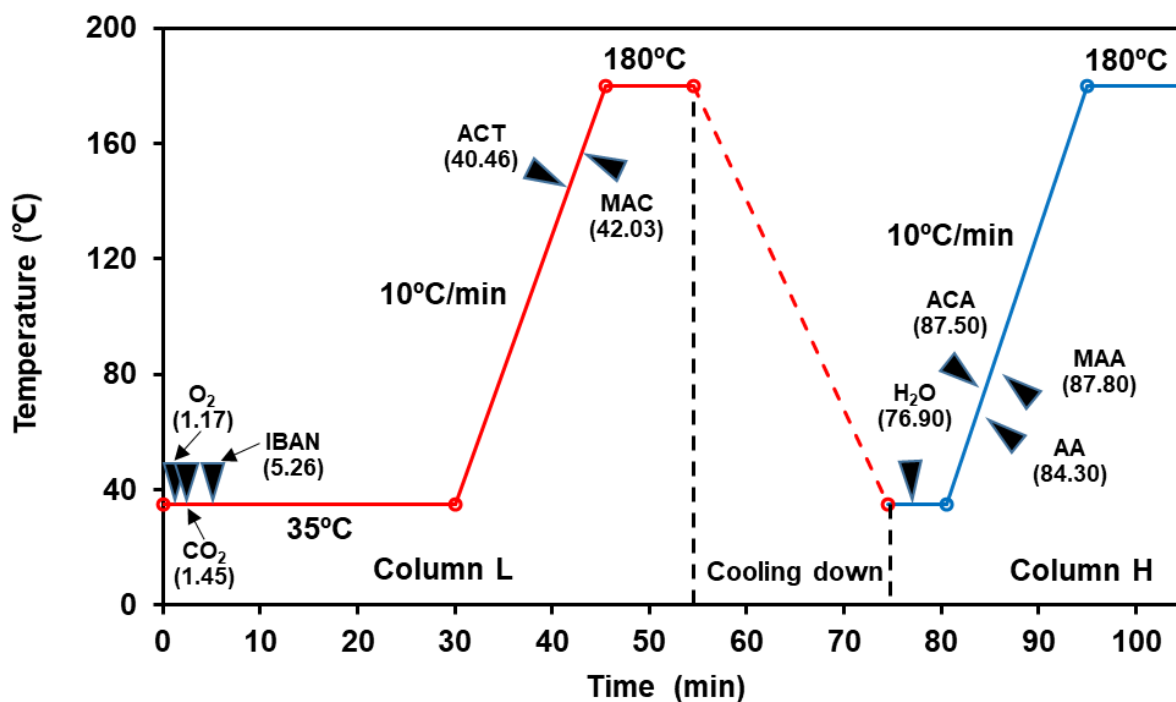


Figure 2.4 Detailed conditions of the analytical method (GC)

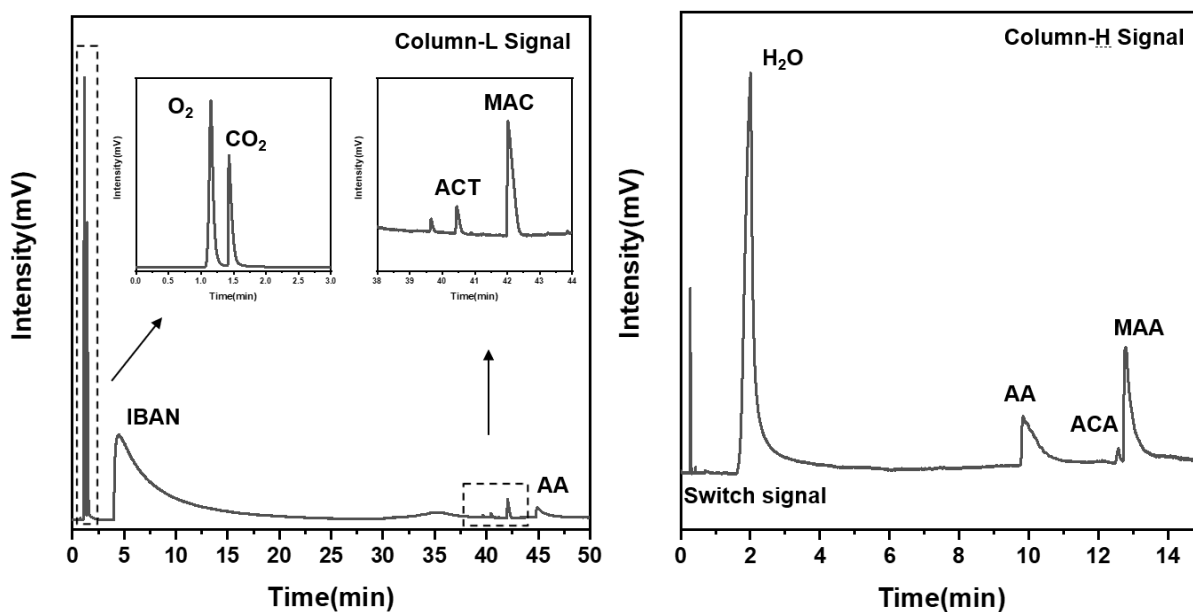


Figure 2.5 A typical analysis result over a Keggin-type heteropolycompounds catalyst using 2 combined Columns (A: Column L, Rt-U-BOND Column, B: Column H, OV-351 Column).

For online analysis of the products, alternated injections were performed on two chromatographic columns L and H by switching a specific valve in the Gas Chromatograph (AlphaM.O.S-PR2100). The light products such as CO<sub>2</sub>, O<sub>2</sub>, *isobutane*, acetone (ACT) and methacrolein (MAC) were analyzed by a GC-TCD detector on Column-L (Rt-U-BOND Column, 30 m × 0.53 mm × 20 μm). After that, H<sub>2</sub>O and the heavy products like methacrylic acid (MAA), acetic acid (AA) and acrylic acid (ACA) were analyzed on a Column-H (OV-351 Column, 30 m × 0.53 mm × 1 μm). The detailed conditions of the method are shown in Figure 2.4 and a typical analysis using the two columns is shown in Figure 2.5.

### 2.3.1.2 Catalytic performances measurements

All the reactants and the different products were used for GC calibration, and all the calibration curves have a linear correlation > 99.9 %. The conversion of IBAN and O<sub>2</sub>, the selectivity and the yield in all products were determined using equations (2.2), (2.3), (2.4) and (2.5) listed below, respectively. The carbon balance was also determined using equation (2.6). Calculation of the conversions of the reactants:

$$IBAN \text{ conversion } (\%) = \frac{n_{IBAN,in} - n_{IBAN,out}}{n_{IBAN,in}} \times 100\% \quad (2.2)$$

$$O_2 \text{ conversion } (\%) = \frac{n_{O_2,in} - n_{O_2,out}}{n_{O_2,in}} \times 100\% \quad (2.3)$$

Determination of the selectivity to each product:

$$Selectivity (\%) = \frac{\gamma_i}{\gamma_{IBAN}} \times \frac{n_i}{n_{IBAN,in} - n_{IBAN,out}} \times 100\% \quad (2.4)$$

Determination of the yield to each product:

$$Yield (\%) = \frac{n_i}{n_{IBAN,in}} \times 100\% \quad (2.5)$$

Calculation of the carbon balance:

$$Carbon \text{ balance} = \frac{4n_{IBAN,out} + n_{CO_2} + 4n_{MAC} + 3n_{ACT} + 2n_{AA} + 3n_{ACA} + 4n_{MAA}}{4n_{IBAN,in}} \times 100\% \quad (2.6)$$

Where  $\gamma_i$  is carbon numbers of the product,  $n_i$  corresponds to the molar amount of each product detected: CO<sub>2</sub>, methacrolein (MAC), acetone (ACT), acrylic acid (ACA), acetic acid (AA) and methacrylic acid (MAA).

## 2.3.2 Periodic reactor

### 2.3.2.1 Description of the experimental set-up and operation conditions

Selective oxidation of *isobutane* to MAC and MAA was also carried out in semi-regenerative operation conditions. The idea is that the experiment can be done intermittently. The reaction can be stopped temporarily and the oxidized feed is then injected into the same reactor for a fixed period of time. In this case, catalytic reaction and catalyst regeneration are carried out in a fixed periodic cycle [13]. Schematic diagram of the system is given below. It consists on three main zones, as shown in Figure 2.6.

For the feeding zone, *isobutane* and O<sub>2</sub> are necessary as reactants, and inert helium gas (green lines) was introduced as the internal standard. The blue and red lines allow the preparation of the reductant (IBAN) and oxidant (O<sub>2</sub>) flows. The black lines allow the preparation of three Argon flows: (*i*) central Ar flow is fed continuously whereas (*ii*) two lateral Ar serve for replacing the reactant or oxidant gases. The flow-rates of each gas are regulated by mass flow controllers (MFC - BROOKS). Calibration of the gas flows can be performed before the experiment to tune precise flows, and these are done manually by using bubble flow meter. Water was introduced by central argon gas via a saturation system keeping 10 % partial pressure of water in the gas stream was calculated according to the Antoine equation (2.1), and was kept at a constant flow rate thank to the permutation of reactant gas or oxidant gas with equivalent Ar flows. In order to obtain 10 % water in the system, central argon-rich stream was required to introduce 31.2 mol.% of water, and the theoretical required temperature was 70 °C at 101325 Pa.

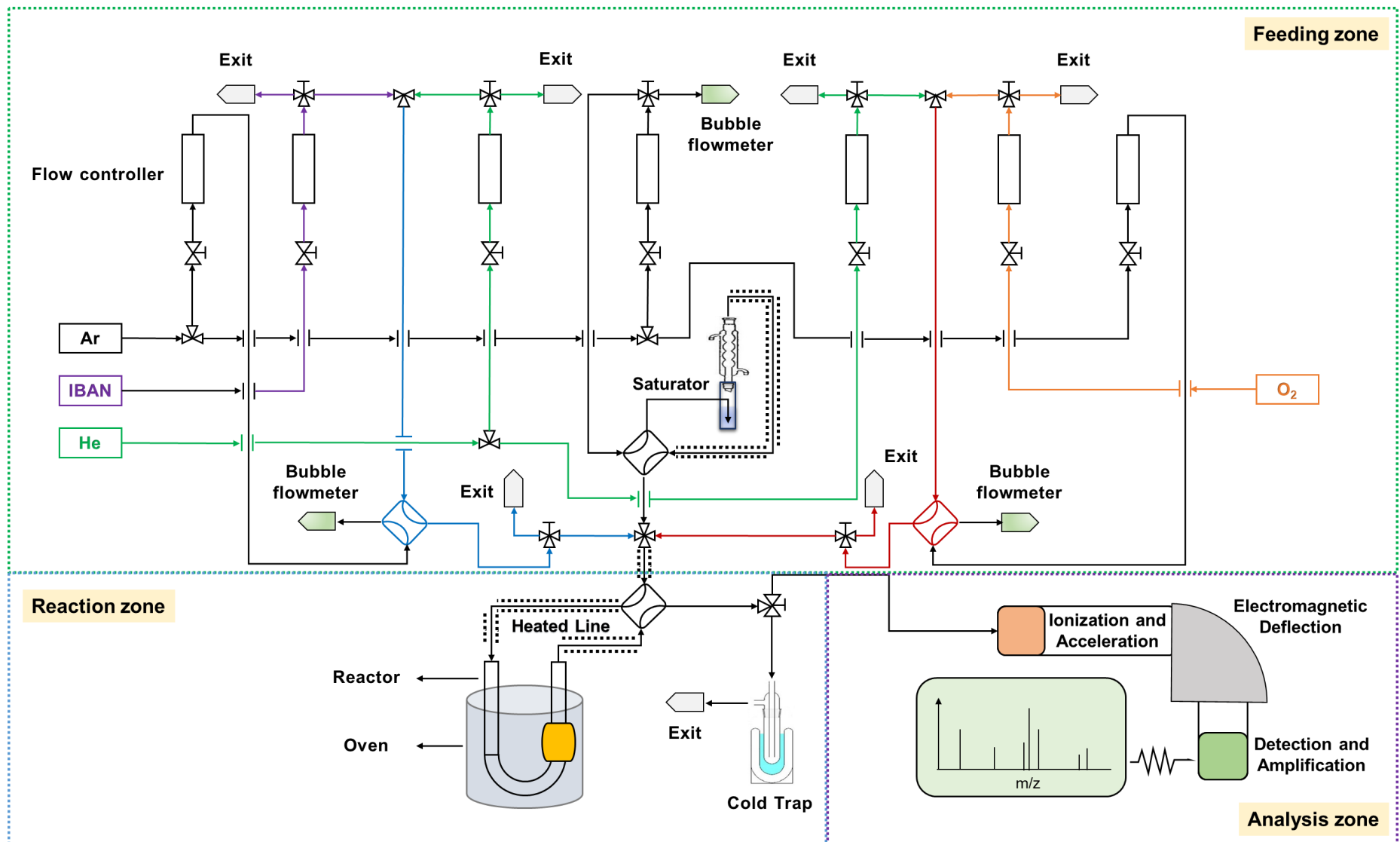


Figure 2.6 Schematic diagram for the lab scale periodic feed setup

The reaction zone consists of the reactor itself, oven and subsequent cold trap. The reactor is a “U”-shaped quartz tube connected to a 4 way-valve. The valve is operated with high-pressure air actuators and used to isolate (by-pass mode) or pass through (reaction mode) the reactor. Thus, the reactant flow is never interrupted except for the short time needed for valve rotation.

The principle of the alternating flows consists of having three gas flows: a central Ar flow continuous feeding of 10 mL/min and introducing 4.5 mL/min of water; two side flows, which contain He/IBAN (8 mL/min and 7 mL/min) or He/O<sub>2</sub> (5 mL/min and 10 mL/min). On each side, argon gas is present, which acts as a substitute for the corresponding reactant or oxidant, respectively. By this way, the mixture fed during periodic operation remains at a constant total flow-rate of 44.5 mL/min STP. The molar ratios were 56.2 % Ar, 10.1 % H<sub>2</sub>O, 15.7 % IBAN and 18.0 % He (or 22.5 % O<sub>2</sub> and 11.2 % He), corresponding to a contact time of 3 s (*approx.* WHSV is 1.8 L·g<sup>-1</sup>·h<sup>-1</sup>). During a typical periodic feed cycle, the reductant gas (IBAN/He) passes through the reactor for 2 min. To remove this gas from the reactor, inert gas (Ar) passes through the system for 1 min. Next, oxidant gas (O<sub>2</sub>/He) flows through the system for 3 min to oxidize the solid. To remove unreacted or excess oxygen from the system, Ar gas flows through the reactor for another 1 min. The whole process takes 7 min, and is repeated sequentially as represented in Figure 2.7.



**Figure 2.7** Schematic diagram of alternating flow of reactant and oxidant in a periodic system.

The catalytic reaction being carried out under 1 atmosphere. The temperature range explored is between 320 and 360 °C. Typically 1.5 g of catalyst solid were employed. Reactant gas from one end into the U-shaped reactor, flow through the catalyst and leaves the reactor from the other end. The outlet is connected to the analysis zone with a T-joint allowing part of the product to enter into the mass spectrometer for analysis, and the rest of the gas flow through the cold trap, and then discharged. Reaction conditions are always the same as above unless otherwise stated.

## Experimental

**Table 2.3** Ion fraction distribution for main components.

m/z	Ar	He	H <sub>2</sub> O	O <sub>2</sub>	CO <sub>2</sub>	CO	IBAN	MAC	MAA	ATH	ACT	AA	ACA
4		100											
12					9.5	5							
15							12.0			37.7	12.5	17.7	
16				22.4	10.5					6.3			
17			21.1										
18			100										
20	14.6												
26										6.3	5.2		29.3
27							48.9	10.1			7.3		55.6
28					10.5	100	4.5						8.7
29							10.4	14.1		100		10.4	5
32				100									
37								8.3	8.9				
38								14.1	15.8				
39							17.7	67.7	79.1				
40	100							13.1	23.7				
41							45.4	100	100	5.2			
42							37.4	16.2	9.9	12.8	10.4	13.5	
43							100		8.9	48.2	100	100	8
44					100					82.8			19.2
45									18.8			90.6	38.4
55													87.9
58									8.9		25		
60												75	
68									10.9				
69								8	17.8				
70								82.8					
71													6
72													100
86									90.9				

IBAN = *isobutane*, MAA = *methacrylic acid*, MAC = *methacrolein*, AA = *acetic acid*, ACT = *acetone*, ATH = *acetaldehyde* and ACA = *acrylic acid*.

For the analysis zone, all the products were analyzed by online mass spectrometer (Balzers, TSH052). The mass spectrometer (MS) continuously samples approximately 15 mL/min of the flow from the outlet of the reactor. The most significant  $m/z$  ratio is used for each component but interference between different gases have also to be taken into account as shown in Table 2.3. At the beginning and end of each test, the Ar, He, IBAN and O<sub>2</sub> sensitivities were calculated using a by-pass periodic feed sequence. The calculation for the product relies on the methodology of catalytic testing, which calibrated the detection sensitivity of each product on this MS based on the results of the test co-feed conditions. The mass spectrometer background signals were also determined during this sequence.

### 2.3.2.2 Catalytic performances measurements

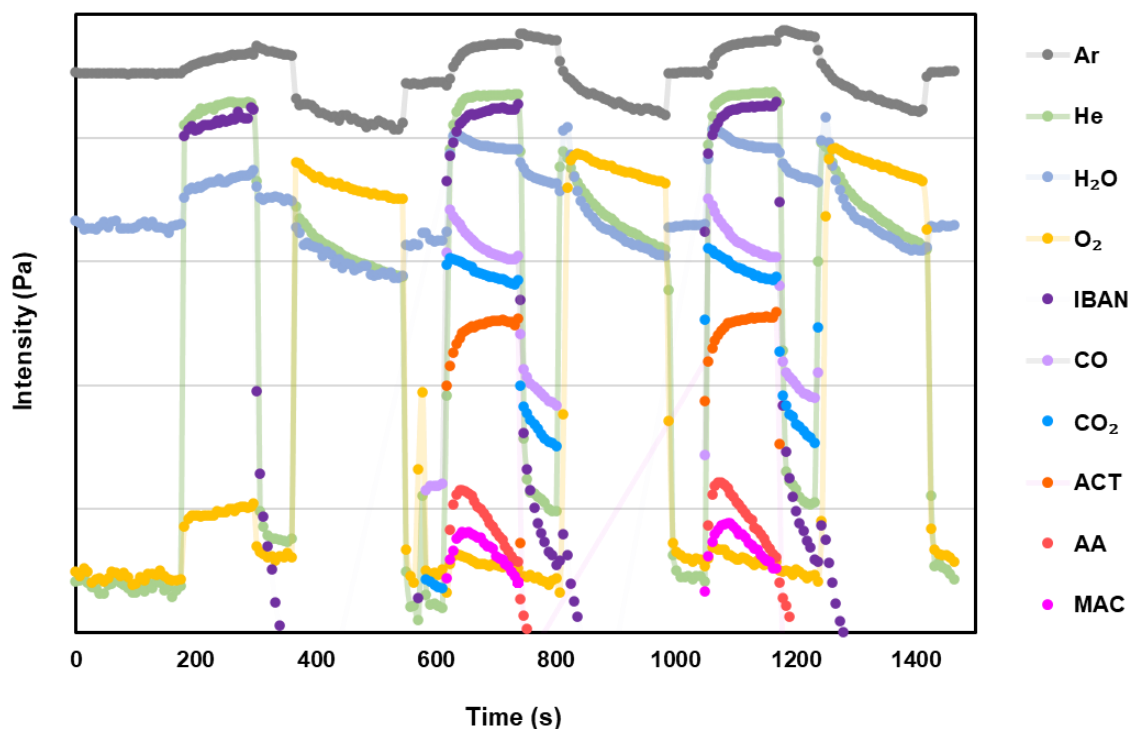


**Figure 2.8** Typical MS curves obtained during the experiments.

After the gas passes through the catalyst, different MS signals are obtained. Figure 2.8 illustrates the partial pressures evolution on a typical experiment during the cycles. The first cycle is through the by-pass, and the last two cycles are through the reactor. The “*Reaction step*” corresponds to IBAN (purple) diluted with Helium (green) passing through the catalyst, and the “*Oxidant step*” is carried out with oxygen (yellow) diluted with helium.

As for the calculation, during the first two and last two cycles of the reaction, the reactor was closed to obtain a reference by-pass value for analyzer calibration. Such cycles allow background definition, and remove the background baseline. As shown in Figure 2.9 and

Equation (2.7) below. The dotted line position in the figure is the data position after subtracting the background.

$$I_{baseline} = (I_{AVERAGE (before)} + I_{AVERAGE (after)})/2 \quad (2.7)$$

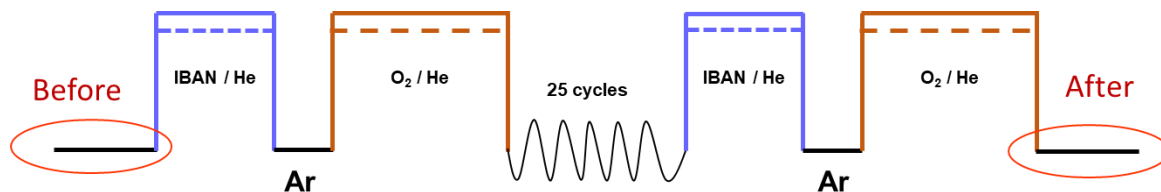


**Figure 2.9** Subtraction of the background baseline from the experimental results

In the following, the interference is removed according to ion fraction distribution. In the mass analyzer, the gas is ionized through electron bombardment, then, the ions are separated by the  $m/z$  ratio. For each component the most significant  $m/z$  is used, but interferences between different gases must also be considered, shown in Table 2.3. Here, the calculation of *isobutane* is illustrated, as shown in the following formula (2.8):

$$I_{IBAN} = I_{43} - \left(\frac{100}{25}\right) \times I_{58 (ACT)} - \left(\frac{100}{75}\right) \times I_{60 (AA)} - \left(\frac{8.9}{90.9}\right) \times I_{86 (MAA)} \quad (2.8)$$

The sensitivity of the online mass spectrometer is determined relatively to Ar. The sensitivity of the mass spectrometer to each component is different, He, IBAN and O<sub>2</sub> sensitivity are calculated during each experiment using the by-pass periodic feed sequence at the beginning and end of each test, and the calculation of the products relies on the methodology of catalytic testing, which calibrates the relative sensitivity of the products according to the results of the test co-feed conditions. According to the relative sensitivity of each component to Ar, the partial pressure of each component can be calculated by the Equation (2.9),

$$P_i = \frac{I_i \times f_i}{\sum(I_i \times f_i)} \times 101325 \text{ (Pa)} \quad (2.9)$$

Where  $I_i$  is the intensity of each component,  $f_i$  corresponds to the relative sensitivity factor of each component. Where  $f_{Ar} = 1.00$ , calculated as  $f_{He} = 1.00$ ,  $f_{IBAN} = 1.00$ , and  $f_{O_2} = 0.60$  based on by-pass during the test. The products calibrated based on the results of the co-feed conditions were  $f_{CO} = 1.50$ ,  $f_{CO_2} = 1.60$ ,  $f_{ACT} = 1.1$ ,  $f_{AA} = 0.02$ ,  $f_{MAC} = 0.03$ , and  $f_{MAA} = 0.01$ , respectively. At this stage of the study, quantitative information is obtained by integrating the reactant or product during a full cycle. Thus, the following quantitative results represent an average on a full cycle. The main quantitative data that are retrieved are the following:

IBAN conversion (%) is obtained by integrating the outlet flow and comparing this to the theoretical inlet calculated from the He tracer.

$$IBAN \text{ conversion } (\%) = \frac{n_{IBAN,in} - n_{IBAN,out}}{n_{IBAN,in}} \times 100\% \quad (2.10)$$

The O<sub>2</sub> conversion (%) is obtained from the theoretical oxygen consumption and is calculated by calculating the oxygen content in the products formed after the reaction.

$$O_2 \text{ conversion } (\%) = \frac{n_{O_2,consumption}}{n_{O_2,in}} \times 100\% \quad (2.11)$$

The selectivity (%) to each product in reductant phase is calculated by integrating the outlet flow:

$$Selectivity (\%) = \frac{\gamma_i}{\gamma_{IBAN}} \times \frac{n_i}{n_{IBAN,in} - n_{IBAN,out}} \times 100\% \quad (2.12)$$

Calculation of the carbon balance:

$$Carbon \text{ balance } (\%) = \frac{\sum \gamma_i^{IBAN} \times n_i}{4 n_{IBAN,in}} \times 100\% \quad (2.13)$$

Where  $\gamma_i$  is carbon numbers of product,  $n_i$  corresponds to the molar amount of each product detected: CO, CO<sub>2</sub>, acetaldehyde (ATH), acetone (ACT), acetic acid (AA) methacrolein (MAC) and methacrylic acid (MAA).

### 2.3.3 Two zones fluidized-bed reactor

#### 2.3.3.1 Description of the experimental set-up and operation conditions

A two zones fluidized bed reactor (TZFBR) was also employed for the selective oxidation of *isobutane*. As discussed in Chapter 1, the TZFBR configuration is used in this work to achieve the continuous catalyst reoxidation without contacting oxygen and hydrocarbon. Tests were performed with the following approach: 1) the hydrodynamic behavior was studied, 2) the feasibility of the concept of selective oxidation of *isobutane* in TZFBR was verified, and 3) the effect of operating conditions on the reaction was investigated. The complete experimental setup is schematically displayed in Figure 2.10, and in the following are described the main components of the experimental setup as well as their functions.

As shown in Figure 2.10, the overall catalytic set-up is composed of three parts: the feeding zone, the reaction zone and the analysis zone, respectively. The feeding zone is mainly divided into two parts: oxidizing gas (air) along with fluidized gas (nitrogen) from the bottom of the reactor into the system; the reaction gas (*isobutane*) and carrier gas (helium) entrainment water vapor into the system through the nozzle in the center of the reactor. Nitrogen was used as fluidization gas, regulated by a rotameter, model Q-Flow by Vögtlin with a measuring range from 21 to 227 L/h STP. The air stream for the regeneration of the catalyst was controlled by a mass flow meter (MFC-Brooks) with measuring range is from 0 to 360 mL/min STP. Water was introduced *via* saturation in the gas stream – like for the fixed bed reactor.

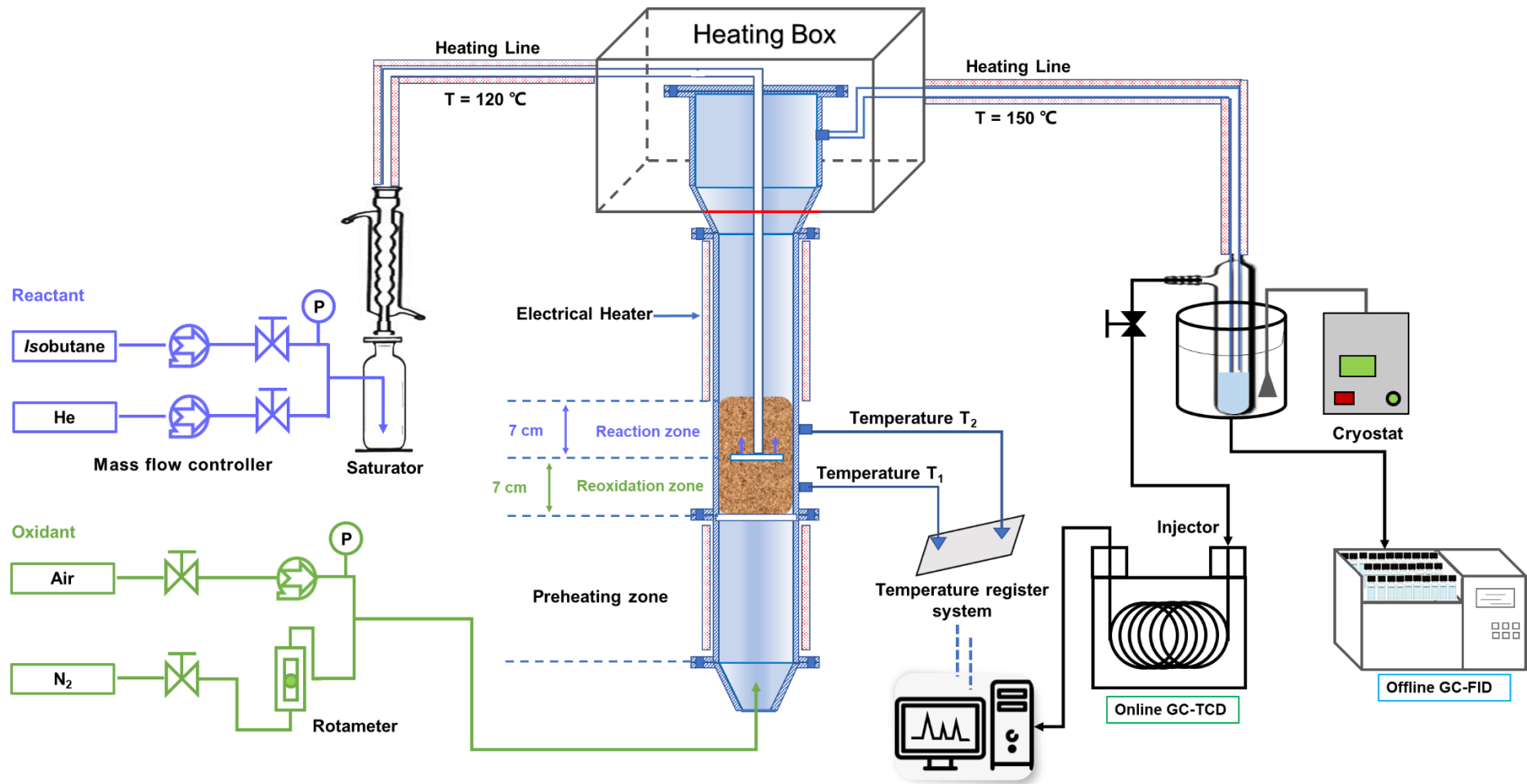


Figure 2.10 Schematics of the TZFBR set-up.

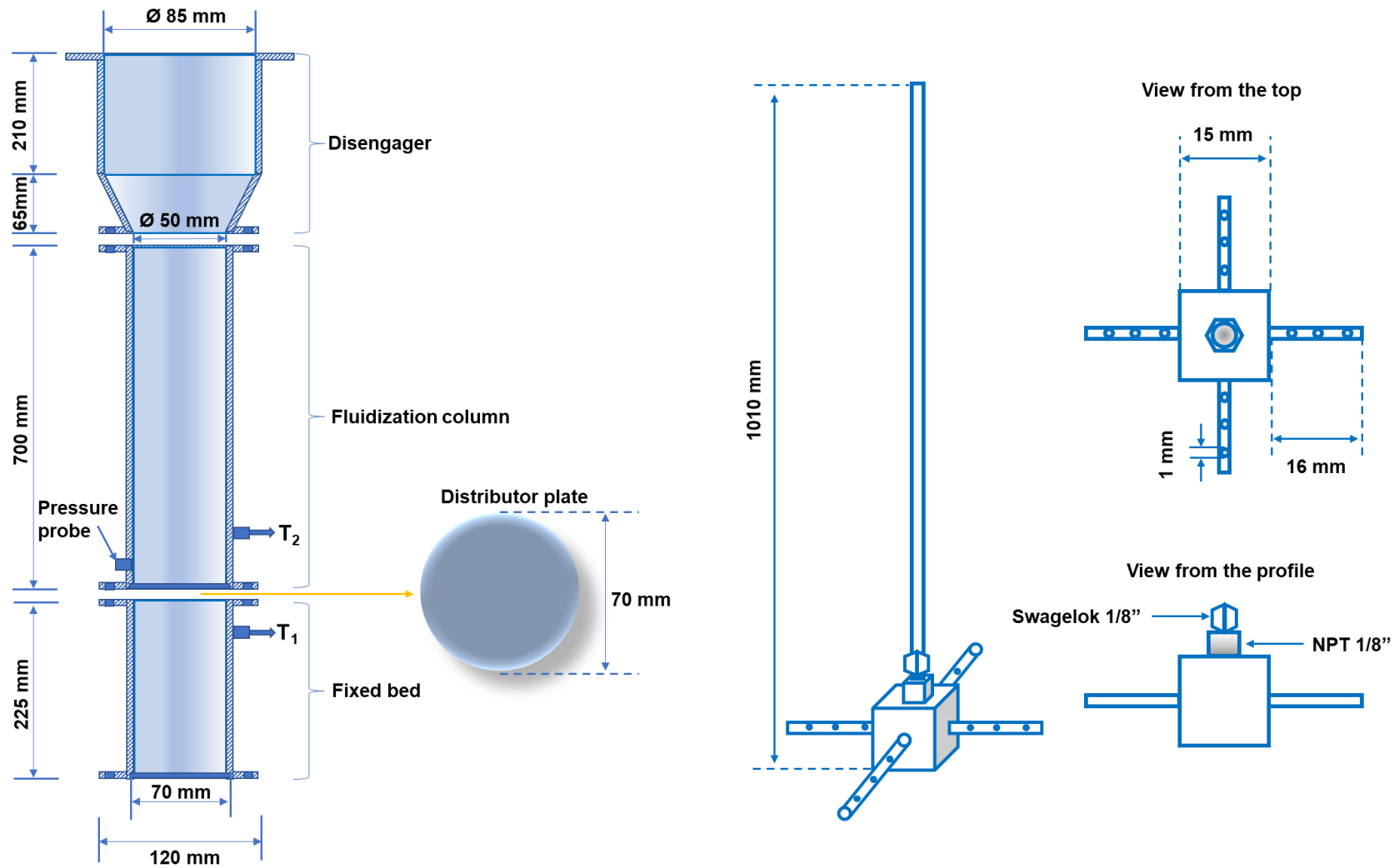


Figure 2.11 Schematics of different TZFBR components

The reaction zone is a fluidized bed reactor made of stainless steel, shown in Figure 2.11, which comprises the following elements:

1) The pre-heating system is a fixed bed that heats the fluidized gas before they enter the fluidizing column. It is made of stainless steel with an inner diameter of 50 mm and a height of 225 mm. To improve the heat transfer inside the bed, SiC beads are filled inside. The heat is provided by an electric heater installed outside the bed and the temperature is regulated by means of a thermocouple in the upper zone of the bed.

2) A distribution plate is located at the bottom of the fluidization column and is made of Inconel with a diameter of 70 mm and a thickness of 2 mm to ensure the uniform distribution of gas entering the reactor.

3) The fluidized column has an inner diameter of 50 mm and a height of 700 mm, and is equipped with a thermocouple to measure the temperature. A pressure probe is connected to the U-tube manometer system to measure the pressure drop across the catalytic bed.

4) The disengager has an inner diameter of 85 mm and 50 mm respectively at the top and bottom sections, and a height of 275 mm. It is used to reduce the velocity of the gas and prevent the catalyst particles entrainment by the gas.

5) A feed tube equipped with a nozzle for the injection of reactant gas is installed in the fluidized column. The material is stainless steel, the height and the diameter are 1010 mm and 3 mm, respectively. As shown in Figure 2.11, the reactant gas is dispersed in the catalytic bed through a cross-shaped porous nozzle, which are 16 mm long tubes with the holes of 1 mm diameter. It is located within the catalyst bed, 70 mm from the distribution plate.

The reaction conditions used were as follows: The reactants mixture was fed at a constant total flow-rate of 20 mL/min STP (molar ratio 35 % IBAN; 10 % H<sub>2</sub>O; 55 % He). The fluidized gas is controlled by the rotameter (Q-Flow-Vögtlin) and the flow rate of 70 L/h STP (the gas velocity of 2 times the minimum experimental fluidization velocity). The oxidants gas was fed at the flow rate with molar ratio O<sub>2</sub> to IBAN of 0.6, 2, 3, and 6 depending on the catalytic test. The catalytic experiments were performed using 20 g of catalyst (40 wt.% of Cs<sub>2</sub>H<sub>2</sub>PMo<sub>11</sub>O<sub>40</sub> on SiO<sub>2</sub>) diluted in 80 g of SiO<sub>2</sub>, the total is 100 g. Afterwards, the column was heated up to reaction temperature (either 325 or 340 °C), and the reactant gas was injected *via* the inlet tube when the temperature was reached. The products and non-reacted IBAN were analyzed by gas-chromatography and cold traps, respectively, as detailed in the following. The operating parameters are summarized in Table 2.4.

**Table 2.4** Operating parameters for catalytic tests in the TZFBR.

Reactor	
Temperature of pre-heating	320 °C
Temperature of bed catalytic	325 or 340 °C
Input streams	
Nature of fluidization gas	N <sub>2</sub> mixed with air
Fluidization gas	70 L/h - STP
Air for regeneration	1.3, 4.0, 6.0 or 12.0 L/h - STP
Molar ratio of oxygen / IBAN	0.6, 2, 3 or 6
IBAN flow rate	7 mL/min
Sampling	
Cooling temperature	0 °C
Catalyst	
Catalyst mass (40 wt.% Cs <sub>2</sub> H <sub>2</sub> PMO <sub>11</sub> VO <sub>40</sub> / SiO <sub>2</sub> )	20 g
CARiACT <sup>®</sup> SiO <sub>2</sub> mass	80 g

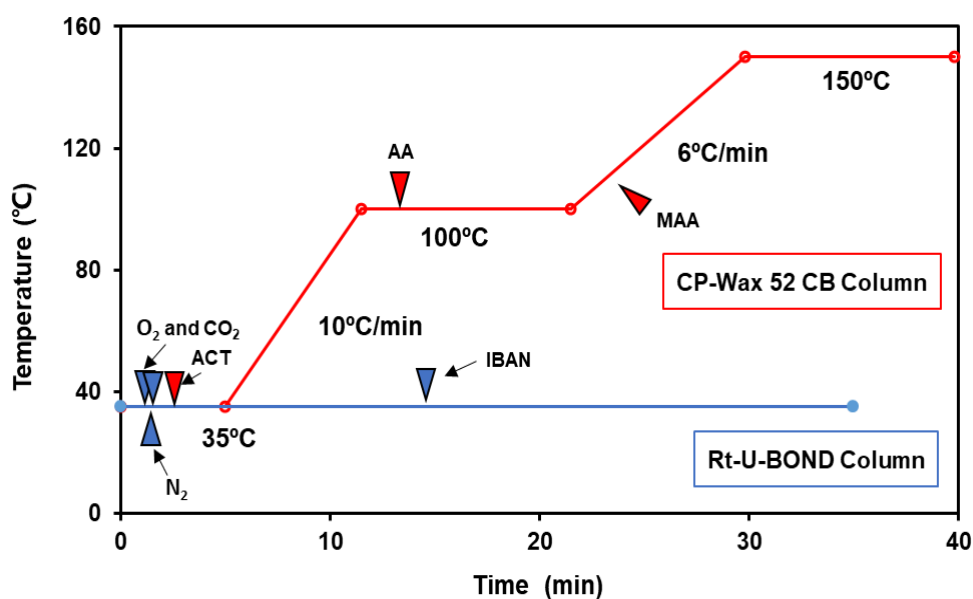


**Figure 2.12** Detailed conditions of the analytical method (red: GC-FID, blue: GC-TCD).

At the outlet of the fluidization column, the effluent stream was heated to avoid condensation of products inside the tubing. The gas was then fed to a cold trap to condensate the reaction products. The trap was cooled by a refrigerant at a temperature of 0 °C controlled by a cooler, and then quantitatively analyzed by an offline gas chromatograph (Agilent-7890B, GC-FID, CP-Wax 52 CB columns, 30m × 250µm × 0.25µm). For the output streams, a needle valve was used to control the flow rate before entering the online GC. The online analysis of the IBAN, injected by switching a six-way valve, was performed on a GC-TCD detector on a

Rt-U-BOND column (30 m × 0.53 mm × 20 μm). The detailed conditions of the method are shown in Figure 2.12.

### 2.3.2.2 Catalytic performances measurements

The reactant IBAN was used for online GC calibration, and the different products were used for offline GC calibration, and all the calibration curves have a linear correlation > 99.9 %. The conversion of IBAN, the selectivity and the yield in all products were determined by equations (2.6), (2.7), and (2.8) listed below, respectively.

Calculation of the conversions of the reactants:

$$IBAN \text{ conversion } (\%) = \frac{n_{IBAN,in} - n_{IBAN,out}}{n_{IBAN,in}} \times 100\% \quad (2.14)$$

Determination of the selectivity to each product:

$$Selectivity (\%) = \frac{\gamma_i}{\gamma_{IBAN}} \times \frac{n_i}{n_{IBAN,in} - n_{IBAN,out}} \times 100\% \quad (2.15)$$

Where  $\gamma_i$  is carbon numbers of product,  $n_i$  corresponds to the molar amount of each product detected.

## References

- [1] <https://www.zeiss.com/microscopy>. Apr. 14, 2021.
- [2] D. Shi, Thesis, Centrale Lille, (2019).
- [3] R.R. Jones, D.C. Hooper, L. Zhang, D. Wolverson, V.K. Valev, *Nanoscale Res. Lett.* 14 (2019).
- [4] [https://www.horiba.com/en\\_en/](https://www.horiba.com/en_en/). Apr. 14, 2021.
- [5] S. Brunauer, P. H. Emmett, E. Teller, Adsorption of gases in multimolecular layers, 60 (1938) 309–319.
- [6] D.A.M. Monti, A. Baiker, *J. Catal.* 83 (1983) 323–335.
- [7] J. Zhu, H. Li, L. Zhong, P. Xiao, X. Xu, X. Yang, Z. Zhao, J. Li, *ACS Catal.* 4 (2014) 2917–2940.
- [8] M. Niwa, N. Katada, M. Sawa, Y. Murakami, *J. Phys. Chem.* 99 (1995) 8812–8816.
- [9] F. Jing, Thesis, Université de Lille 1 (2012).
- [10] T. Yamashita, P. Hayes, *Appl. Surf. Sci.* 254 (2008) 2441–2449.
- [11] G.A. Tsigdinos, C.J. Hallada, *Inorg. Chem.* 7 (1968) 437–441.
- [12] E. Tsukuda, S. Sato, R. Takahashi, T. Sodesawa, *Catal. Commun.* 8 (2007) 1349–1353.
- [13] T. Kane, Thesis, Université de Lille (2018).

**Chapter 3**  
**Catalytic selective oxidation of IBAN to MAA**  
**and MAC in a fixed-bed reactor**

## Chapter 3 Catalytic selective oxidation of IBAN to MAA and MAC in a fixed-bed reactor

### 3.1 Introduction

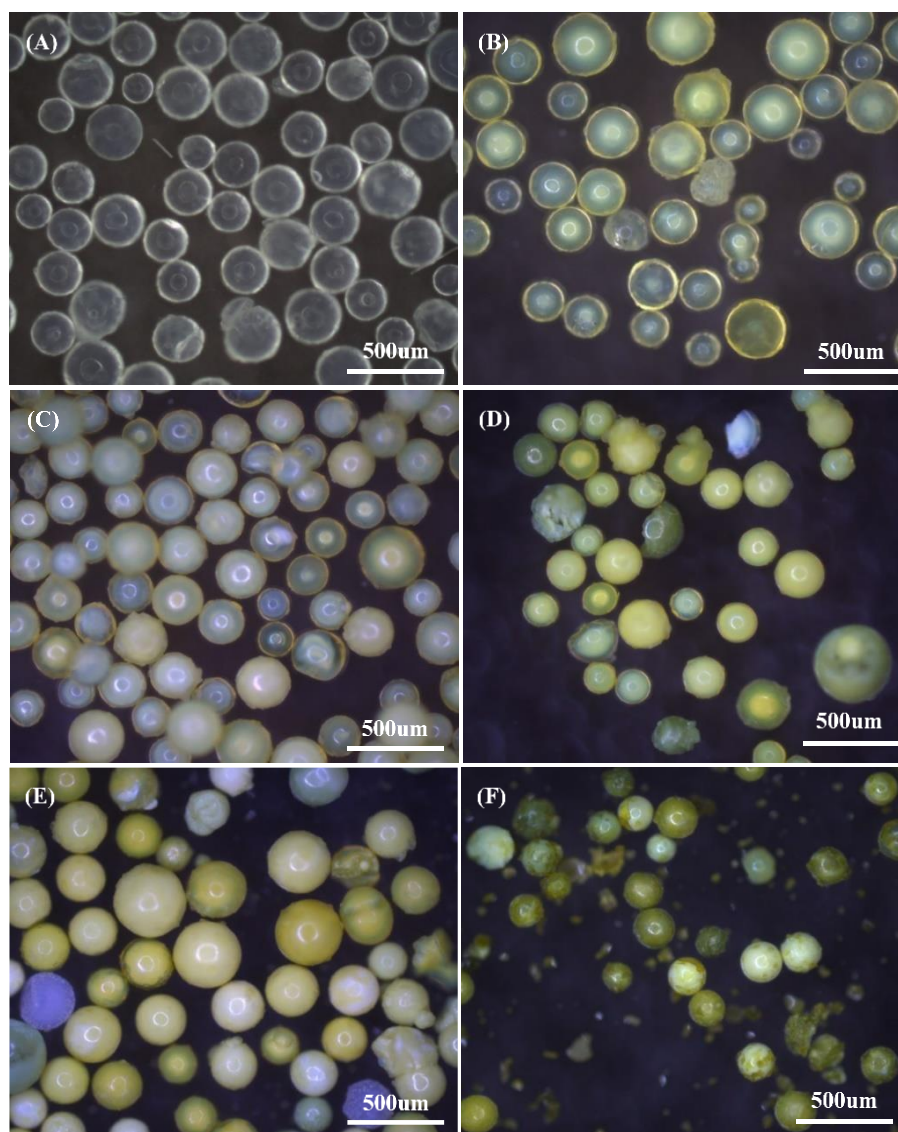
Silica-supported catalysts based on Keggin-type HPAs containing rubidium or cesium as counter cations have been prepared by the impregnation method described in Chapter 2 and evaluated in the selective oxidation of *isobutane* to methacrolein and methacrylic acid. Keggin-type heteropolycompounds are particularly interesting for catalytic selective oxidation reactions because of their strong and tunable acidity and redox properties [1]. However, Keggin-type polyoxometalates as catalyst are suffering from low specific surface area, which may become an obvious drawback for their application [2]. In order to increase the available surface area, the active phases  $\text{Cs}_2\text{H}_2\text{PMo}_{11}\text{VO}_{40}$ ,  $\text{Cs}_{2.5}\text{H}_{2.5}\text{PMo}_{10}\text{V}_2\text{O}_{40}$ ,  $\text{Rb}_2\text{H}_2\text{PMo}_{11}\text{VO}_{40}$  and  $\text{Rb}_{2.5}\text{H}_{2.5}\text{PMo}_{10}\text{V}_2\text{O}_{40}$  were supported on commercial CARiACT  $\text{SiO}_2$  carriers, with loadings of 10-50 wt.%. The catalysts were characterized by various techniques such as XRD,  $\text{N}_2$  physisorption, TGA, Raman spectroscopy,  $\text{H}_2$ -TPR, and  $\text{NH}_3$ -TPD in order to study their thermal stability, structural, and textural properties, acidity and reducibility. In this chapter, we will focus on the influence of the different loadings and on the influence of the different counter cations, and textural properties of the catalysts on their structure and performance. The selective oxidation of IBAN to MAC and MAA was performed under co-feed conditions. In order to determine the best catalysts and optimize their performance, catalysts with different active phases and different loadings were studied at various reaction temperatures under atmospheric pressure, in order to establish the relationship between catalyst properties and catalytic performance.

### 3.2 Physicochemical properties of the catalysts

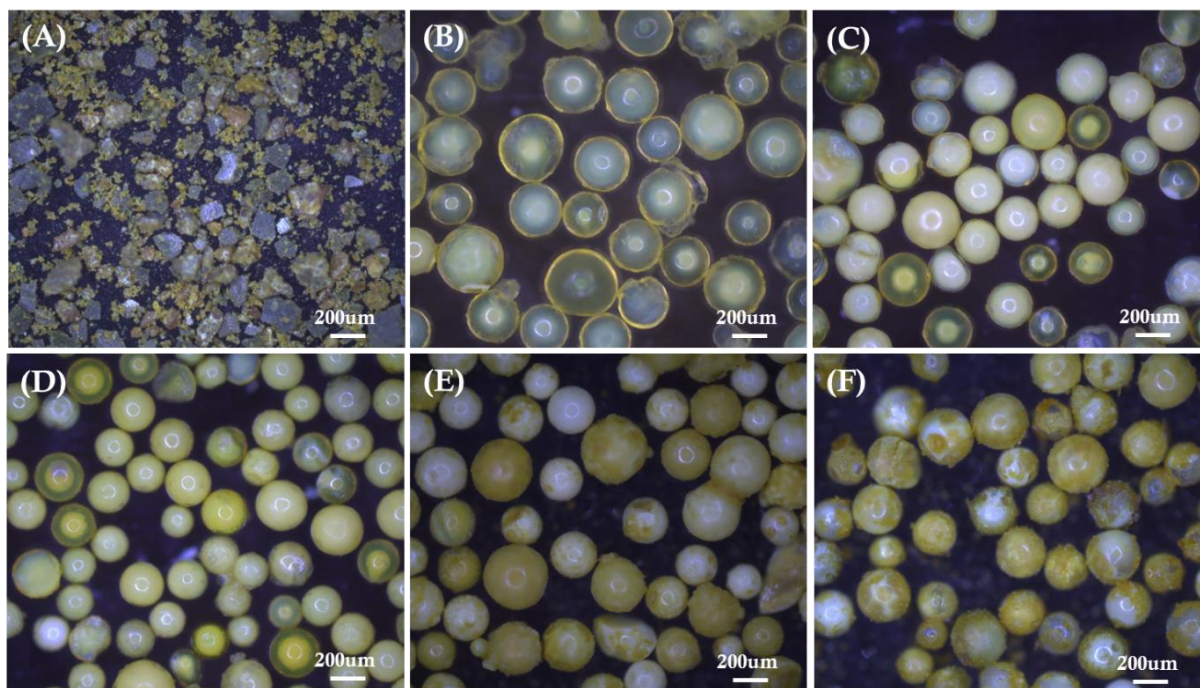
#### 3.2.1 Macrostructure of the catalysts

Figure 3.1 shows typical optical microscope images of  $\text{SiO}_2$  and  $x\text{CsV}_1/\text{SiO}_2$  spheres with  $x = 10$  to 50 wt.%. CARiACT  $\text{SiO}_2$  spheres possess good uniformity with an average diameter of  $\sim 200 \mu\text{m}$ , as expected (Figure 3.1A). After coating of the  $\text{CsV}_1$  active phase, core-shell

CsV<sub>1</sub>/SiO<sub>2</sub> spheres were formed, which maintain similar uniformity in shape. Upon increasing the amount of active phase, the colors of the surfaces of the CsV<sub>1</sub>/SiO<sub>2</sub> spheres change progressively from white to yellow. Actually, as the loading increased, the color changed from light to dark. For the 10 wt.%-20 wt.% loadings (Figure 3.1B and C), a bright yellow shell was observed, while for the 30 wt.% - 40 wt.% loadings (Figure 3.1D and E) the yellow color was more homogeneous. For the 50 wt.% loading (Figure 3.1F), the shell was too thick and partly detached from the silica surface whereby small pieces of debris (CsV<sub>1</sub>) were clearly visible on the image. Similar results, were obtained for CsV<sub>2</sub>/SiO<sub>2</sub> and RbV<sub>2</sub>/SiO<sub>2</sub> catalysts (Figure 3.2 and Figure 3.3).



**Figure 3.1** Typical optical microscope images of SiO<sub>2</sub> and xCsV<sub>1</sub> spheres with  $x = 10$  to 50. (A) SiO<sub>2</sub>, (B) 10CsV<sub>1</sub>, (C) 20CsV<sub>1</sub>, (D) 30CsV<sub>1</sub>, (E) 40CsV<sub>1</sub>, (F) 50CsV<sub>1</sub>.



**Figure 3.2** Typical optical microscope images of: (A) pure  $\text{CsV}_2$ , (B)  $10\text{CsV}_2$ , (C)  $20\text{CsV}_2$ , (D)  $30\text{CsV}_2$ , (E)  $40\text{CsV}_2$ , (F)  $50\text{CsV}_2$ .

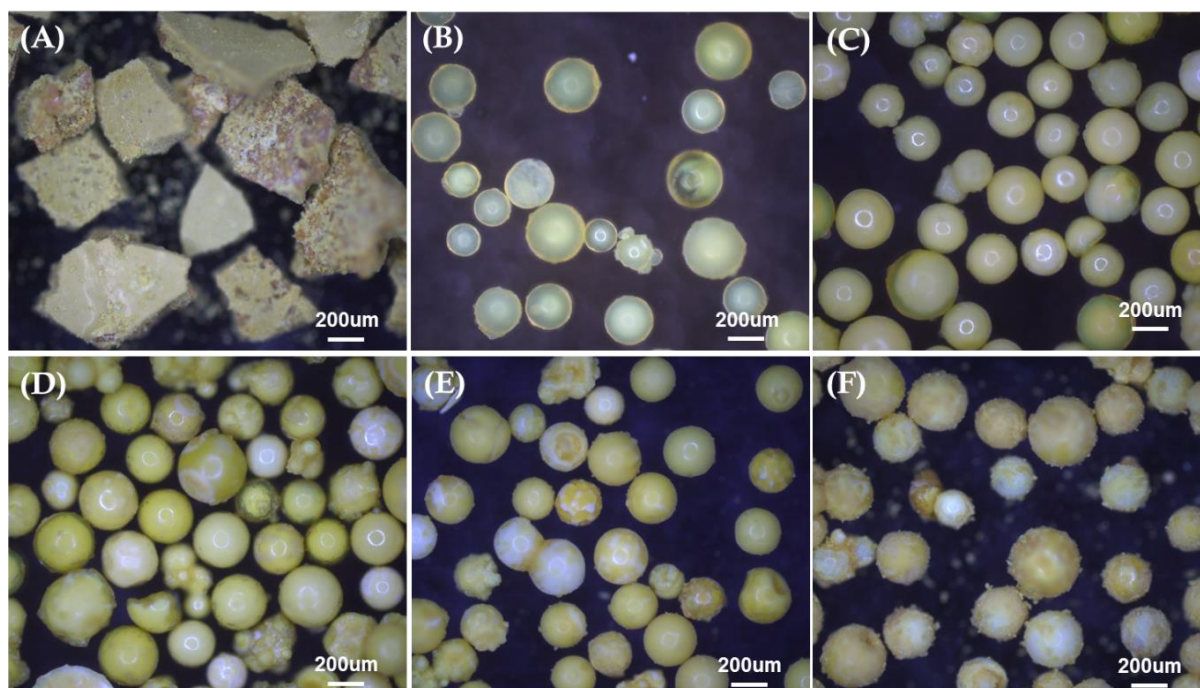


**Figure 3.3** Typical optical microscope images of: (A) pure  $\text{RbV}_2$ , (B)  $10\text{RbV}_2$ , (C)  $20\text{RbV}_2$ , (D)  $30\text{RbV}_2$ , (E)  $40\text{RbV}_2$ , (F)  $50\text{RbV}_2$ .

Figure 3.4 shows the  $30\text{CsV}_1$  catalyst before and after reaction. Some parts of the catalyst after the reaction turned green, some turned blue, corresponding to the aforementioned "heteropoly blue" species caused by the reduction of the initial catalyst.

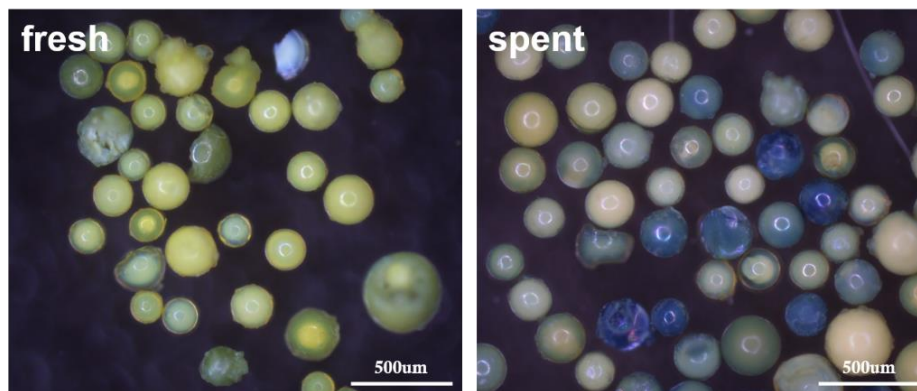


Figure 3.4 Optical microscope images of 30CsV<sub>1</sub> before and after the reaction.

### 3.2.2 Thermal decomposition of the fresh catalysts – TGA

According to the thermogravimetric curves presented in Figure 3.5, the weight loss of the catalysts can be divided into two stages. The first stage is at a temperature below 100 °C. Here, this weight loss is obviously caused by the desorption of physisorbed water. The second weight loss - observed in the 150 °C to 340 °C range, and is caused by the loss of crystal water. According to the literature [3], phosphomolybdic acid loses its constitution water at 375 °C and as the catalysts used here are based on alkaline heteropoly salt, one can see that the thermal stability is improved compared to the literature. As a matter of fact, below 400 °C, the catalysts only lose crystal water, but no constitution water, whereby the acidic protons are retained, which is important with respect to the chosen reaction temperature (< 400 °C).

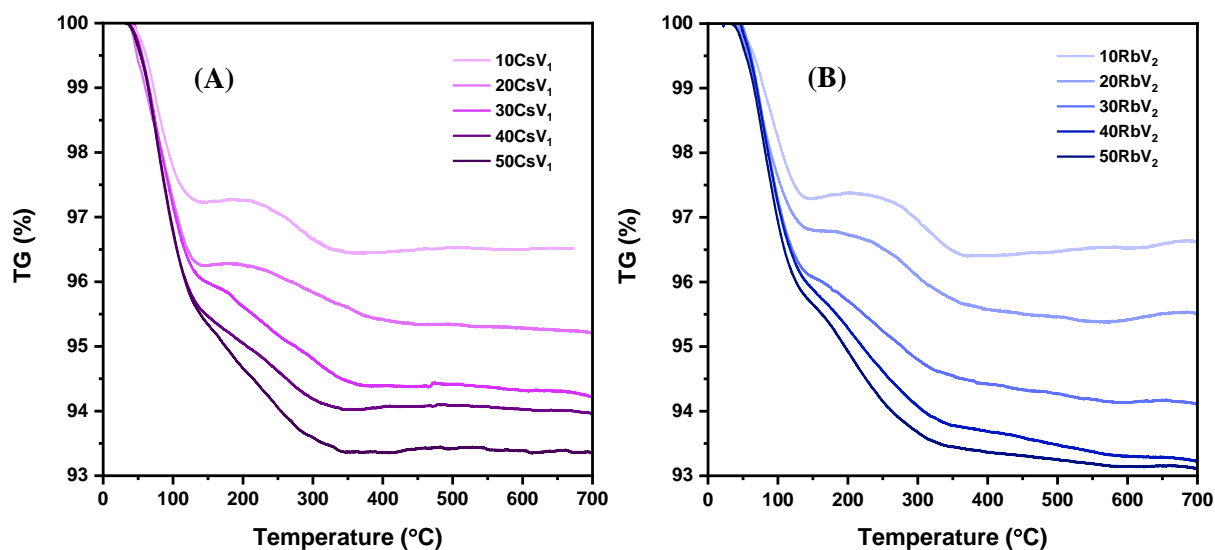
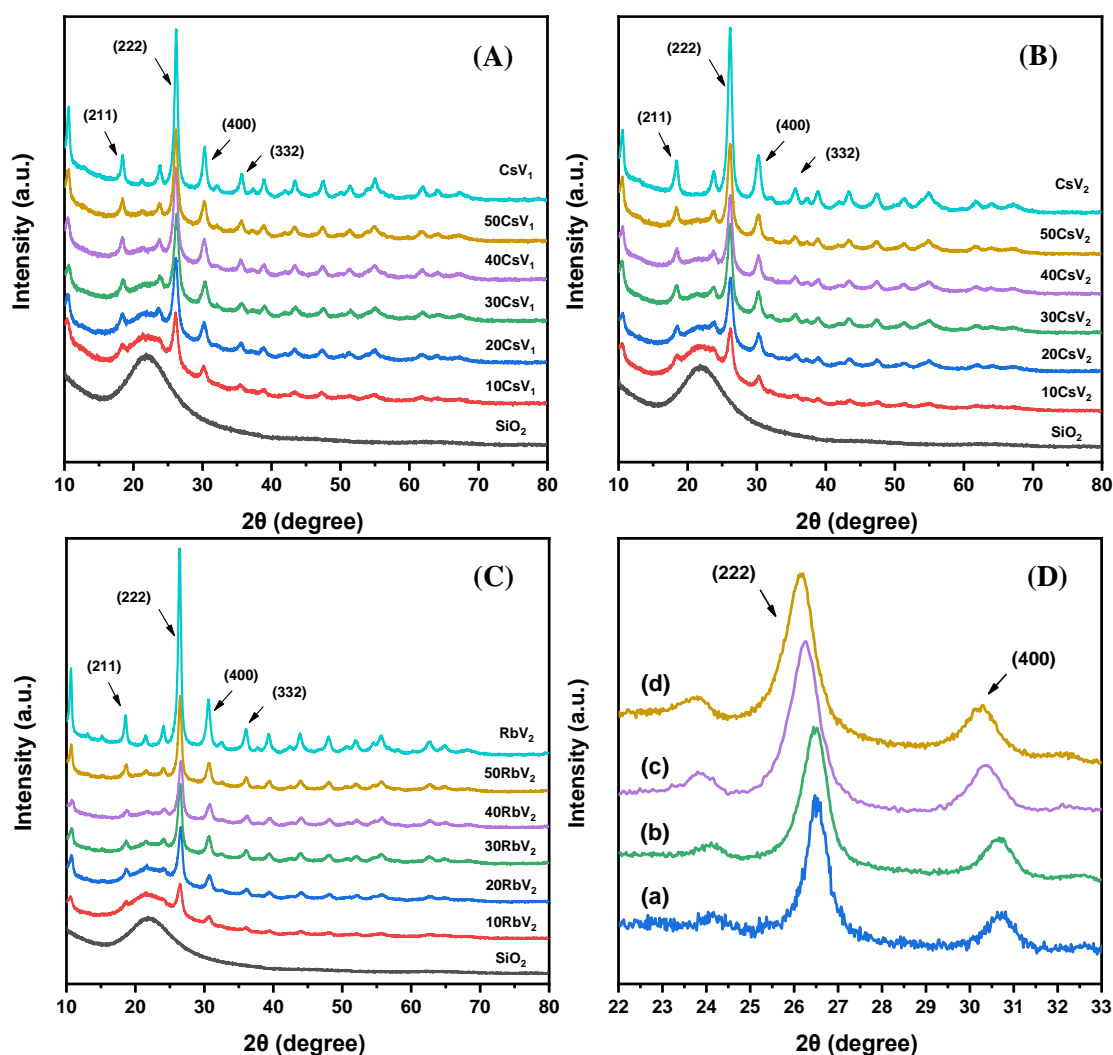


Figure 3.5 TGA curves of the catalysts (A) CsV<sub>1</sub>/SiO<sub>2</sub> catalysts, (B) RbV<sub>2</sub>/SiO<sub>2</sub> catalysts.

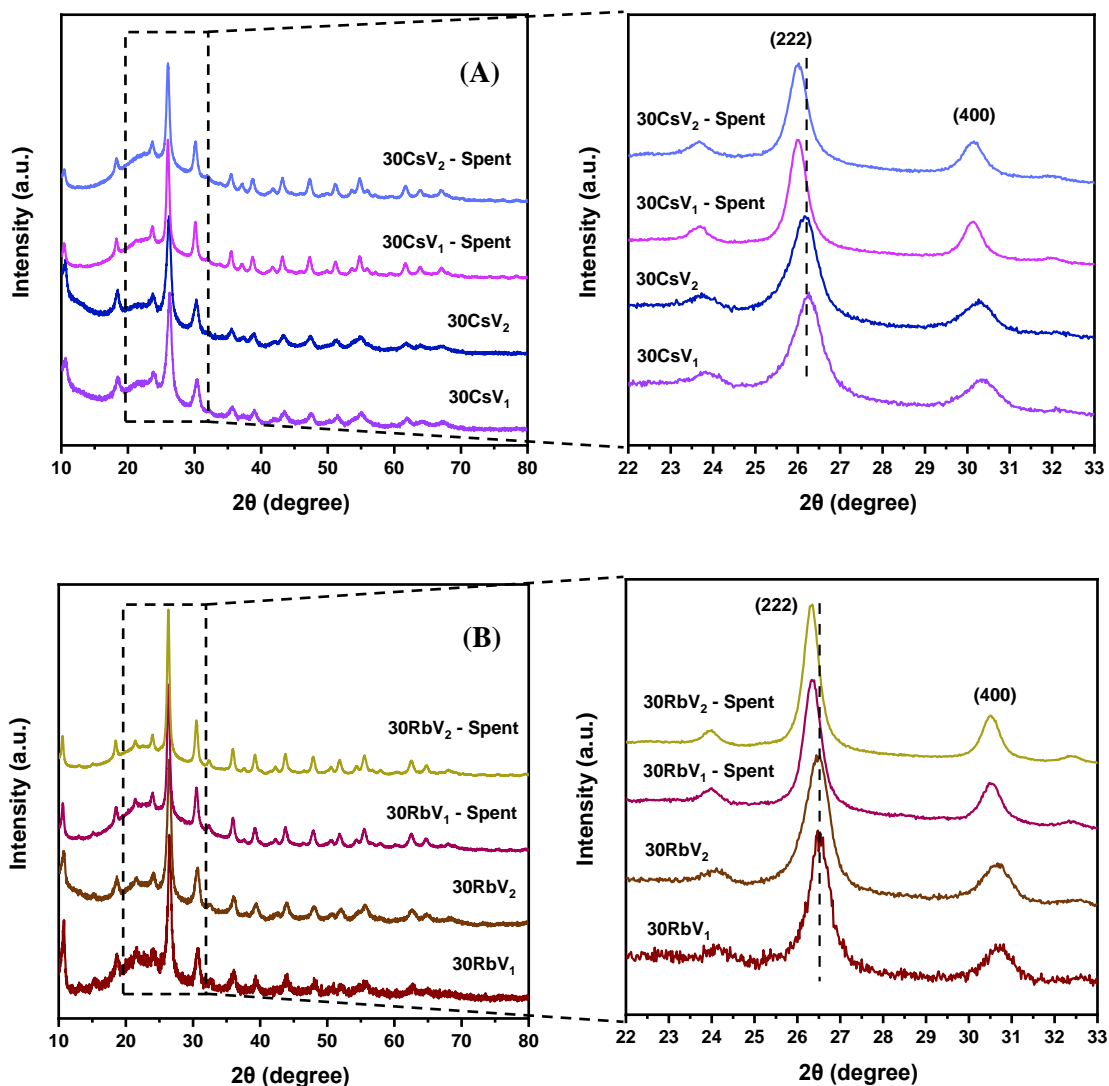
### 3.2.3 Crystal phases analysis of the samples - XRD

Figure 3.6 shows the typical XRD patterns of  $\text{SiO}_2$ ,  $\text{CsV}_1/\text{SiO}_2$  catalysts (Figure 3.6A),  $\text{CsV}_2/\text{SiO}_2$  catalysts (Figure 3.6B) and  $\text{RbV}_2/\text{SiO}_2$  catalysts (Figure 3.6C). The patterns exhibit diffraction peaks at  $2\theta = 18.5^\circ$ ,  $23.9^\circ$ ,  $26.2^\circ$ ,  $30.4^\circ$  and  $35.8^\circ$  assigned to the (211), (310), (222), (400), and (332) lattice planes of both cubic  $\text{CsV}_1/\text{SiO}_2$  and  $\text{CsV}_2/\text{SiO}_2$  catalysts, respectively, which are characteristic for Keggin-type compounds. For  $\text{RbV}_2/\text{SiO}_2$  catalysts, the observed diffraction peaks at  $2\theta = 18.6^\circ$ ,  $24.1^\circ$ ,  $26.5^\circ$ ,  $30.7^\circ$  and  $36.2^\circ$  can be assigned to the (211), (310), (222), (400), and (332) lattice planes, respectively. With the increase in active phase amounts, the intensities of the diffraction peaks corresponding to the (211), (310), (222), (400), and (332) lattice planes belonging to the Keggin-type compounds were largely increased, suggesting a higher degree of crystallization of the active phase. As a matter of fact, the interplanar spacing was expanded as  $\text{Cs}^+$  has a larger ionic radius than  $\text{Rb}^+$ , ascribed to  $d$ -spacing decrease when the protons were substituted by Rb cations in comparison with by Cs cations. The  $d$ -spacing of the (222) plane increased from 0.3362 nm for  $\text{Rb}_2\text{H}_2\text{PVMo}_{11}\text{O}_{40}$  to 0.3393 nm for  $\text{Cs}_2\text{H}_2\text{PMo}_{11}\text{VO}_{40}$ . Therefore, the diffraction peaks of Rb-containing catalysts were slightly shifted to higher angles in comparison with the diffraction peaks of Cs-containing catalysts, as can be clearly observed in Figure 3.6D.



**Figure 3.6** XRD patterns of (A)  $\text{SiO}_2$  and  $\text{CsV}_1/\text{SiO}_2$  catalysts, (B)  $\text{SiO}_2$  and  $\text{CsV}_2/\text{SiO}_2$  catalysts, (C)  $\text{SiO}_2$  and  $\text{RbV}_2/\text{SiO}_2$  catalysts with various loadings: 10–50 wt.%, (D) Catalysts with loading 30 wt.%: (a)  $30\text{RbV}_1$ , (b)  $30\text{RbV}_2$ , (c)  $30\text{CsV}_1$ , (d)  $30\text{CsV}_2$ .

Figure 3.7 shows the XRD patterns of the catalysts with 30 wt.% before and after reaction. It is worth mentioning that no new diffraction peak was found for the spent catalysts, which indicated that the catalysts did not significantly decompose into metal oxides during the reaction process, meaning that the catalysts were quite stable under the reaction conditions. However, the spent catalysts exhibit a slight shift of the diffraction peak, compared to the fresh catalysts. This was ascribed to the loss of crystal water causing a modification of the lattice parameter, which is consistent with the results of TG analysis. It should also be noted that the diffraction peaks of the spent catalyst become narrower compared to those of the fresh one, implying an increase in crystallinity of the catalyst after reaction, probably due to sintering.



**Figure 3.7** XRD patterns of fresh and spent catalysts: (A) 30CsV<sub>1</sub> and 30CsV<sub>2</sub> catalysts, (B) 30RbV<sub>1</sub> and 30RbV<sub>2</sub> catalysts.

### 3.2.4 BET specific surface area and pore volume of the catalysts

The specific surface areas of the SiO<sub>2</sub> (CARiACT) support and of the catalysts are gathered in Table 3.1. The specific surface area of the catalysts decreased with increasing the amount of active phase, from 264.2 m<sup>2</sup>/g (SiO<sub>2</sub> support) to 150.9 m<sup>2</sup>/g (50CsV<sub>1</sub>), 197.8 m<sup>2</sup>/g (50CsV<sub>2</sub>) and 194.2 m<sup>2</sup>/g (50RbV<sub>2</sub>), respectively. Theoretical values obtained from the calculation (assuming that the active phase was well and homogeneously dispersed as referred to [4]) are also given in brackets in Table 3.1. When comparing the experimental and theoretical BET values, it can be seen that all the catalysts display a higher specific surface area than the calculated theoretical one (Figure 3.8). This indicates that the active phase (CsV<sub>1</sub>, CsV<sub>2</sub>, RbV<sub>2</sub>) partially contributes

to the specific surface area, meaning that new surface is created due to the porous structure of the active phase. The mean value of the coverage of active phase on the support for the different loadings was calculated based on a Keggin unit occupancy of  $1.44 \text{ nm}^2$  [5,6]. The coverage of the support is expressed as the number of active phase layers stacked on the surface.

**Table 3.1** Textural properties of the supported catalysts and coverage of active phase.

Catalysts	SiO <sub>2</sub> (CARIACT)	10CsV <sub>1</sub>	20CsV <sub>1</sub>	30CsV <sub>1</sub>	40CsV <sub>1</sub>	50CsV <sub>1</sub>	CsV <sub>1</sub>
$S_{BET}$ , m <sup>2</sup> /g	264.2	233.0 (237.8) <sup>a</sup>	226.0 (211.4) <sup>a</sup>	219.8 (184.9) <sup>a</sup>	179.4 (158.5) <sup>a</sup>	150.9 (132.1) <sup>a</sup>	70.4
$V_{pore}$ , cm <sup>3</sup> /g	1.12	0.94	0.81	0.69	0.49	0.4	0.05
Catalysts		10CsV <sub>2</sub>	20CsV <sub>2</sub>	30CsV <sub>2</sub>	40CsV <sub>2</sub>	50CsV <sub>2</sub>	CsV <sub>2</sub>
$S_{BET}$ , m <sup>2</sup> /g	-	242.3 (237.8) <sup>a</sup>	234.9 (211.4) <sup>a</sup>	217.5 (184.9) <sup>a</sup>	215.0 (158.5) <sup>a</sup>	197.8 (132.1) <sup>a</sup>	122.3
$V_{pore}$ , cm <sup>3</sup> /g	-	0.96	0.81	0.66	0.6	0.46	0.09
Catalysts		10RbV <sub>2</sub>	20RbV <sub>2</sub>	30RbV <sub>2</sub>	40RbV <sub>2</sub>	50RbV <sub>2</sub>	RbV <sub>2</sub>
$S_{BET}$ , m <sup>2</sup> /g	-	236.1 (237.8) <sup>a</sup>	232.3 (211.4) <sup>a</sup>	215.2 (184.9) <sup>a</sup>	206.3 (158.5) <sup>a</sup>	194.2 (132.1) <sup>a</sup>	120.1
$V_{pore}$ , cm <sup>3</sup> /g	-	0.94	0.82	0.68	0.65	0.48	0.08
Coverage, layer	-	0.2	0.46	0.79	1.33	1.84	

<sup>a</sup> theoretical values were calculated according to the specific surface area of SiO<sub>2</sub> measured in the same conditions.

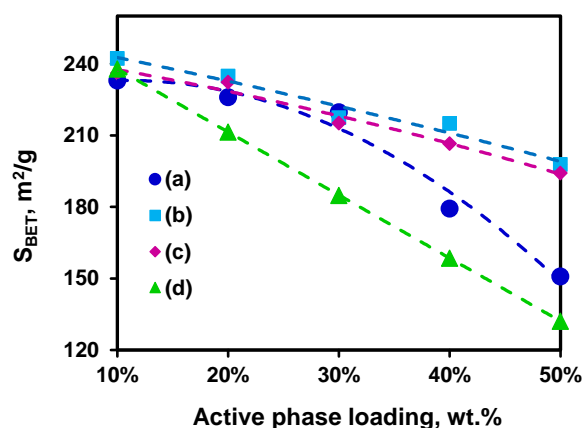


**Figure 3.8** Relationship between the active phase loadings and the specific surface area: (a) 10-50 wt.% CsV<sub>1</sub>/SiO<sub>2</sub>, (b) 10-50 wt.% CsV<sub>2</sub>/SiO<sub>2</sub>, (c) 10-50 wt.% RbV<sub>2</sub>/SiO<sub>2</sub> catalysts, (d) theoretical values for the various catalysts' loadings.

### 3.2.5 Structural features of the catalysts - Raman spectroscopy

The catalysts were also studied using Raman spectroscopy (Figure 3.9) to further confirm the integrity of the Keggin structure in the salt of the HPA samples. The observed bands corresponded to the characteristic Keggin vibrations [4,7]: *vs* Mo=O<sub>d</sub> at  $983 \text{ cm}^{-1}$ , *vas* Mo-O<sub>b</sub>-Mo at  $871 \text{ cm}^{-1}$ , *vas* Mo-O<sub>c</sub>-Mo at  $600 \text{ cm}^{-1}$  and  $\delta(\text{Mo-O-Mo})$  255 and  $235 \text{ cm}^{-1}$ , respectively.

The P-O vibration in Keggin units is Raman-inactive [8]. These results also indicate that the Keggin structure of the catalyst has been effectively formed, confirming the XRD results.

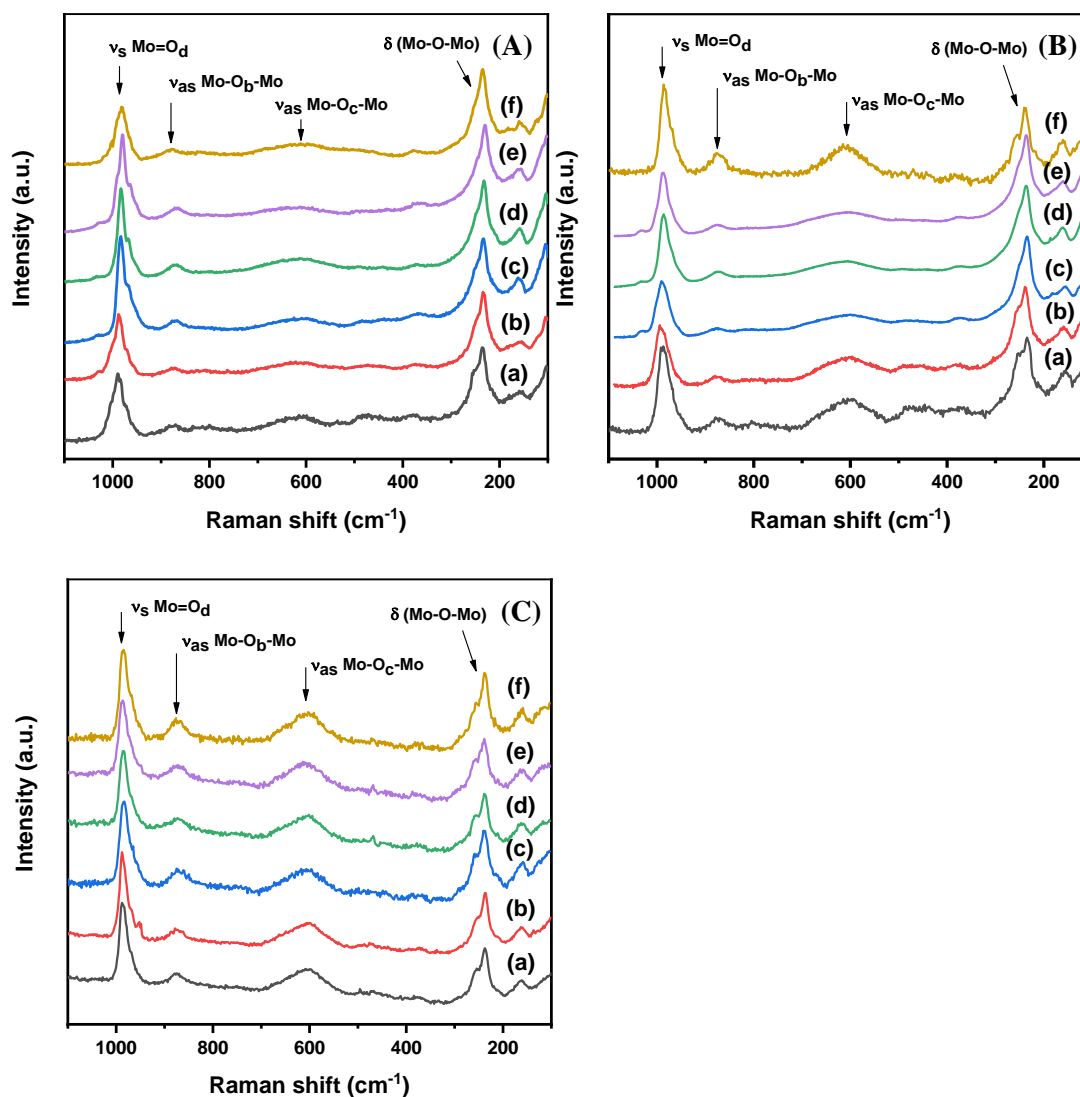


**Figure 3.9** Raman spectra for the catalysts: (A) the series of  $\text{Cs}_2\text{H}_2\text{PMo}_{11}\text{VO}_{40}/\text{SiO}_2$  catalysts, (B) the series of  $\text{Cs}_{2.5}\text{H}_{2.5}\text{PMo}_{10}\text{VO}_{40}/\text{SiO}_2$  catalysts, (C) the series of  $\text{Rb}_{2.5}\text{H}_{2.5}\text{PMo}_{10}\text{VO}_{40}/\text{SiO}_2$  catalysts with (a) 10 wt.%, (b) 20 wt.%, (c) 30 wt.%, (d) 40 wt.%, (e) 50 wt.%, (f) bulk active phase.

### 3.2.6 Reducibility measurements - TPR

Figure 3.10 shows the reducibility of the three series of catalysts, which were examined by  $\text{H}_2$ -TPR measurements. All samples exhibited significant  $\text{H}_2$  consumption. The reduction at lower temperatures starting from 550 °C is ascribed to the first step of the reduction of the  $\text{Mo}^{6+}$  species (from  $\text{Mo}^{6+}$  to  $\text{Mo}^{4+}$ ). The reduction peak at the higher temperature of approximately from 800 °C was attributed to the reduction of  $\text{Mo}^{4+}$  species to  $\text{Mo}^0$  [9]. The broad peaks observed hereby indicated a rather complex reduction process composed of one or more

transition states [4]. Concerning vanadium, its content was too low to observe its reduction, which should occur at a lower temperature. Since the  $H_2$  consumption increased linearly with the loading, one can clearly state that the reduced species originated from the active phase and not from the  $SiO_2$  support (Figure 3.10D) and further that the active phase was well dispersed allowing the access of  $H_2$  to all Mo atoms. In addition, with the increase in the loading, the reduction peak shifted to lower temperature, before shifting back when the loading reached 50 wt.%. This maximum indicates that the catalyst with 40 wt.% exhibited the highest reducibility. This can be explained by the fact that the active phase stacking results in less accessible sites when the loading is higher than 40 wt.%.

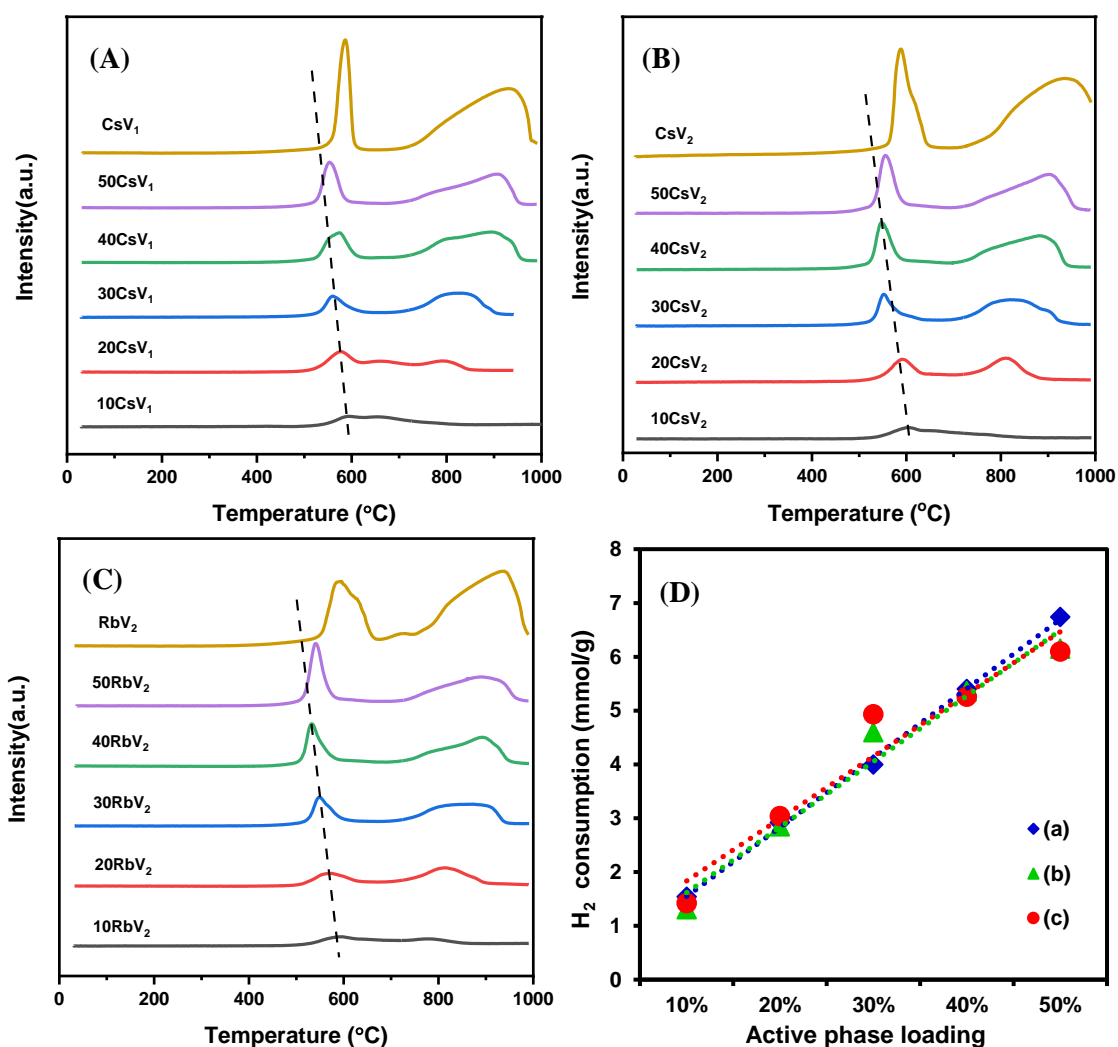


**Figure 3.10** TPR profiles of the catalysts: (A)  $CsV_1$  and  $CsV_1/SiO_2$  catalysts, (B)  $CsV_2$  and  $CsV_2/SiO_2$  catalysts, (C)  $RbV_2$  and  $RbV_2/SiO_2$  catalysts with various loadings: 10-50 wt.%, (D)  $H_2$  consumption as a function of active phase loading for the three series of catalysts (a)  $CsV_1/SiO_2$  catalysts, (b)  $CsV_2/SiO_2$  catalysts, (c)  $RbV_2/SiO_2$  catalysts.

### 3.2.7 Quantification and strength of the acid sites - NH<sub>3</sub>-TPD

The amount and strength of acid sites of the three series of catalysts ( $x\text{CsV}_1/\text{SiO}_2$ ,  $x\text{CsV}_2/\text{SiO}_2$  and  $x\text{RbV}_2/\text{SiO}_2$  catalysts) were determined by ammonia temperature-programmed desorption (NH<sub>3</sub>-TPD). The desorption temperature profiles are plotted in Figure 3.11 and the quantitative calculation for the NH<sub>3</sub> uptakes are listed in Table 3.2, Table 3.3 and Table 3.4.

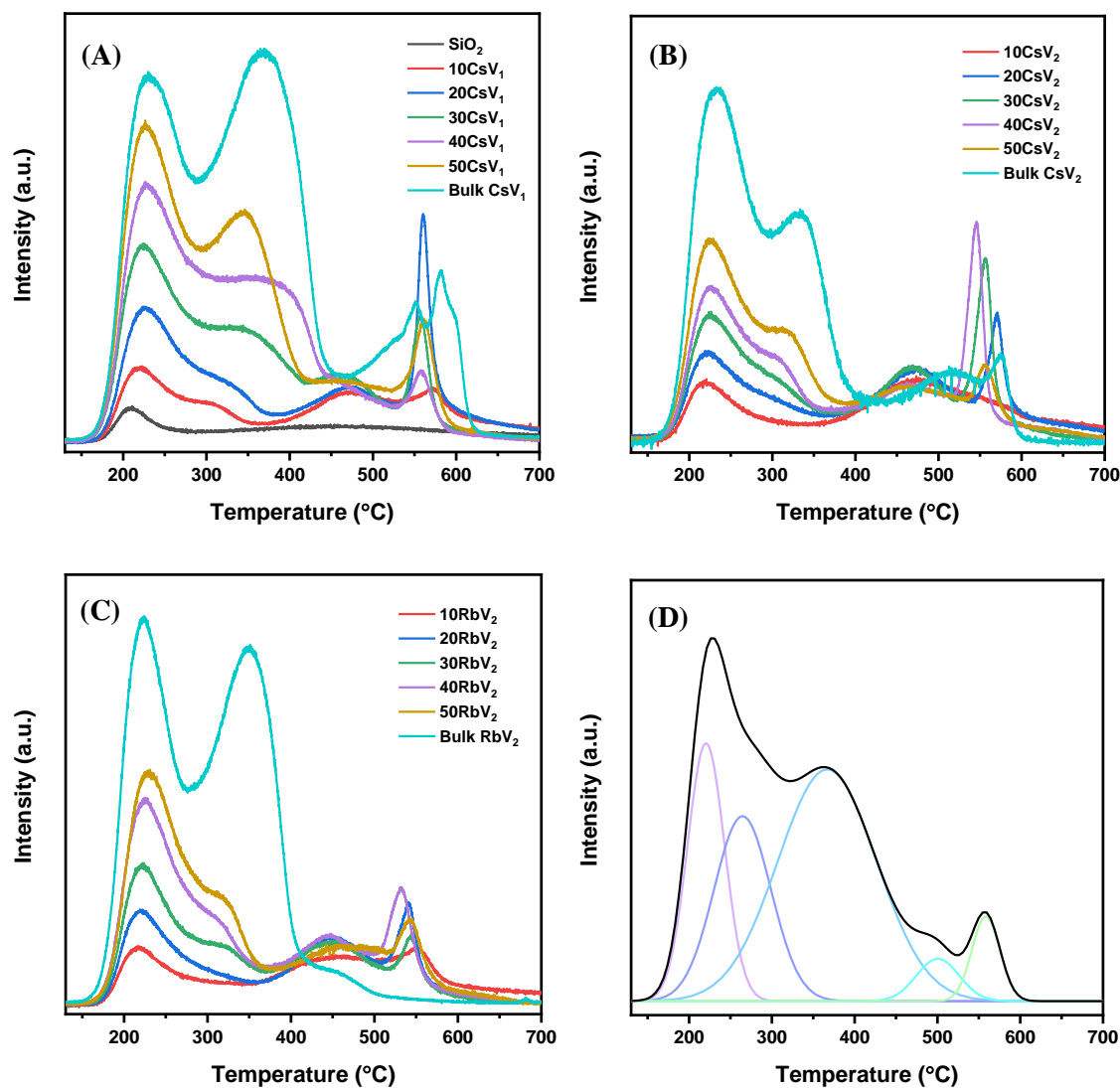


**Figure 3.11** NH<sub>3</sub>-TPD profiles for: (A) CsV<sub>1</sub> and CsV<sub>1</sub>/SiO<sub>2</sub> catalysts, (B) CsV<sub>2</sub> and CsV<sub>2</sub>/SiO<sub>2</sub> catalysts, (C) RbV<sub>2</sub> and RbV<sub>2</sub>/SiO<sub>2</sub> catalysts with various loadings: 10-50 wt.%, (D) NH<sub>3</sub>-TPD deconvolution curve of 40CsV<sub>1</sub> sample shown as an example.

**Table 3.2** Distribution of acid sites and acid strengths over CsV<sub>1</sub>/SiO<sub>2</sub> catalysts.

Catalyst	Acidity, NH <sub>3</sub> uptake, $\mu\text{mol}/\text{m}^2$ cat (mmol/g)				Total acidity
	130-300 °C weak	300-450 °C medium	450-560 °C strong	560-700 °C very strong	
SiO <sub>2</sub> (CARIACT)	0.10 (0.03)	-	0.09 (0.02)	-	0.19 (0.05)
10CsV <sub>1</sub>	0.35 (0.08)	-	0.22 (0.05)	0.11 (0.03)	0.68 (0.16)
20CsV <sub>1</sub>	0.68 (0.15)	0.12 (0.03)	0.30 (0.07)	0.14 (0.03)	1.24 (0.28)
30CsV <sub>1</sub>	0.50 (0.11)	0.68 (0.15)	0.35 (0.08)	-	1.53 (0.34)
40CsV <sub>1</sub>	1.08 (0.20)	1.24 (0.22)	0.23 (0.04)	-	2.55 (0.46)
50CsV <sub>1</sub>	1.40 (0.21)	1.33 (0.20)	0.48 (0.07)	0.12 (0.02)	3.33 (0.50)
CsV <sub>1</sub>	4.86 (0.35)	4.27 (0.30)	1.17 (0.08)	0.58 (0.04)	10.88 (0.77)

**Table 3.3** Distribution of acid sites and acid strengths over CsV<sub>2</sub>/SiO<sub>2</sub> catalysts.

Catalyst	Acidity, NH <sub>3</sub> uptake, $\mu\text{mol}/\text{m}^2$ cat (mmol/g)				Total acidity
	130-300 °C weak	300-450 °C medium	450-560 °C strong	560-700 °C very strong	
10CsV <sub>2</sub>	0.23 (0.06)	-	0.45 (0.10)	-	0.68 (0.16)
20CsV <sub>2</sub>	0.36 (0.09)	-	0.44 (0.10)	0.09 (0.02)	0.89 (0.21)
30CsV <sub>2</sub>	0.59 (0.13)	-	0.60 (0.13)	-	1.19 (0.26)
40CsV <sub>2</sub>	0.74 (0.16)	-	0.64 (0.14)	-	1.38 (0.30)
50CsV <sub>2</sub>	1.16 (0.23)	-	0.56 (0.11)	-	1.72 (0.34)
CsV <sub>2</sub>	2.26 (0.27)	2.37 (0.29)	0.71 (0.09)	0.14 (0.02)	5.48 (0.67)

**Table 3.4** Distribution of acid sites and acid strengths over RbV<sub>2</sub>/SiO<sub>2</sub> catalysts.

Catalyst	Acidity, NH <sub>3</sub> uptake, $\mu\text{mol}/\text{m}^2$ cat (mmol/g)				Total acidity
	130-300 °C weak	300-450 °C medium	450-560 °C strong	560-700 °C very strong	
10RbV <sub>2</sub>	0.22 (0.05)	-	0.45 (0.11)	-	0.67 (0.16)
20RbV <sub>2</sub>	0.35 (0.08)	0.32 (0.07)	0.08 (0.02)	0.08 (0.02)	0.83 (0.19)
30RbV <sub>2</sub>	0.56 (0.12)	0.30 (0.07)	0.10 (0.02)	-	0.96 (0.21)
40RbV <sub>2</sub>	0.81 (0.17)	0.04 (0.01)	0.52 (0.10)	-	1.37 (0.28)
50RbV <sub>2</sub>	1.04 (0.20)	0.02 (0.01)	0.48 (0.09)	-	1.54 (0.30)
RbV <sub>2</sub>	3.03 (0.37)	1.20 (0.14)	0.16 (0.02)	-	4.39 (0.53)

For the silica support, a weak desorption peak was observed, which indicates that the carrier has a weak acidity. For the other three series of silica-supported catalysts, four NH<sub>3</sub> desorption peaks could be distinguished: weak acid sites (100-300°C), medium acid sites (300-450°C), strong acid sites (450-560°C) and very strong acid sites (560-700°C) [6]. There is no clear tendency regarding the distribution of acid strength and therefore there is not a clear clue regarding the distribution of catalytic activity with acid strength. However, the number of acid sites has an effect on the catalytic activity (*cf. section 3.3.3*). All the series of catalysts followed

the same trend. The total amount of acid sites increased with the amount of active phase, as expected. For  $\text{Cs}_2\text{H}_2\text{PMo}_{11}\text{VO}_4/\text{SiO}_2$  catalysts, for example, from 10 wt.% to 50 wt.%, the ammonia uptakes were 0.16, 0.28, 0.34, 0.46 and 0.50 mmol/g, respectively. However, for lower loadings, the number of acid sites of the catalysts increased significantly, but only moderately for higher loadings from 40 to 50 wt.% (Figure 3.12A). This was ascribed to overloading with active phase leading to non-accessible sites and the formation of isolated detached bulk  $\text{CsV}_1$ , as evidenced in the microscope images. In addition, by comparing the three series of catalysts, we found that the  $\text{CsV}_1/\text{SiO}_2$  series catalysts has the highest number of acid sites, followed by the  $\text{CsV}_2/\text{SiO}_2$  series catalysts, and the  $\text{RbV}_2/\text{SiO}_2$  series (Figure 3.12).

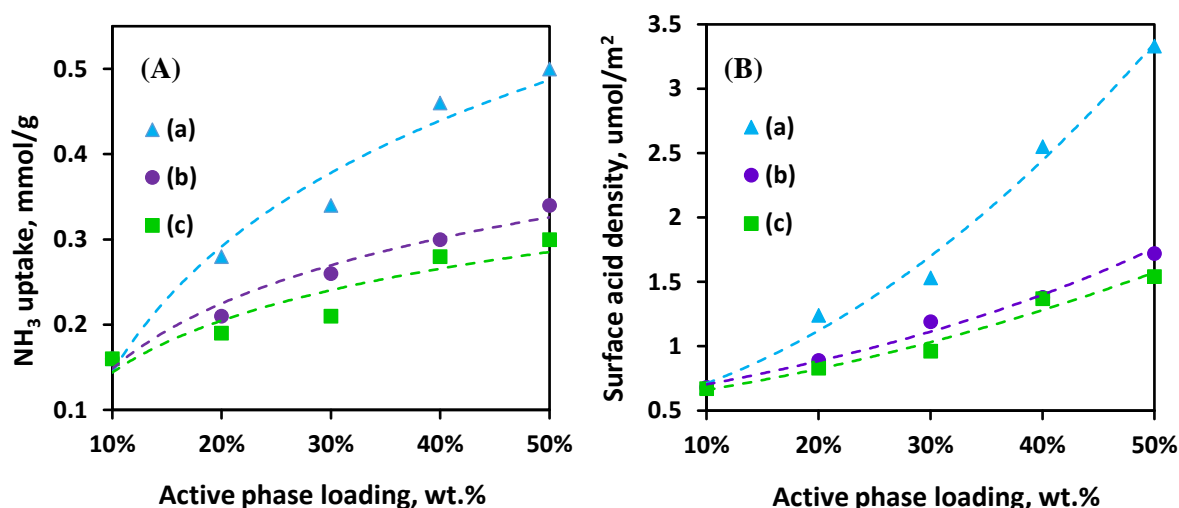


**Figure 3.12** (A) Amount of acid sites as a function of the active phase loading. (B) Relationship between the active phase loading and the surface acid density: (a)  $\text{CsV}_1/\text{SiO}_2$  catalysts, (b)  $\text{CsV}_2/\text{SiO}_2$  catalysts, (c)  $\text{RbV}_2/\text{SiO}_2$  catalysts.

### 3.3 Catalytic evaluation in selective oxidation of isobutane in a fixed-bed reactor

#### 3.3.1 Effect of the support

First, the catalytic performances of the bulk and the supported catalyst were evaluated in the selective oxidation of *isobutane* to MAC and MAA in the same operating conditions (Figure 3.13). In order to take into account the presence of silica, the bulk catalyst was employed as a mechanical mixture of 0.24 g of bulk  $\text{CsV}_1$  with 0.56 g CARIAC (Hereinafter referred to as M-30 $\text{CsV}_1$ ). Significant lower IBAN conversion ( $X_{\text{IBAN}} = 3.7\%$ ) was found for bulk  $\text{CsV}_1$  compared to the supported 30 $\text{CsV}_1$  catalyst (6.0%, Table 3.5). This low conversion was related

to the rather low specific surface area ( $70.4 \text{ m}^2/\text{g}$ ) of bulk  $\text{CsV}_1$  (cf. Table 3.1). With respect to the promising results obtained for the supported catalyst, the silica was chosen as support for the following studies.

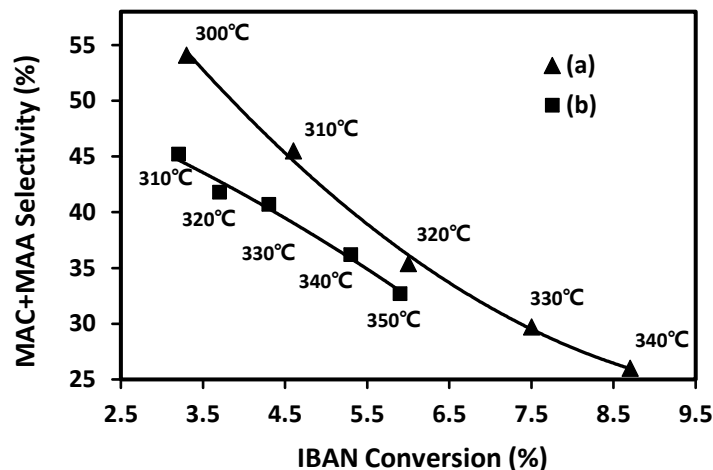


**Figure 3.13** Relationship between IBAN conversion and selectivity to (MAC+MAA) obtained at different temperatures for (a)  $30\text{CsV}_1$  and (b) 30 wt.% pure  $\text{CsV}_1$  mechanically mixed with 70 wt.%  $\text{SiO}_2$ .

**Table 3.5** Catalytic performance in IBAN oxidation of M- $30\text{CsV}_1$ ,  $30\text{CsV}_1$  catalyst and  $\text{SiO}_2$  support.

Catalysts	Conversion <sup>a</sup> , %		Selectivity, %						$Y_{(\text{MAC+MAA})}$ , %	Carbon balance, %
	$\text{O}_2$	IBAN	MAA	MAC	$\text{CO}_2$	AA	ACT	ACA		
M- $30\text{CsV}_1$	19.6	3.7	27.5	14.3	23.0	19.9	9.9	3.0	1.54	99.9
$30\text{CsV}_1$	43.0	6.0	23.5	11.9	27.6	26.0	7.3	2.3	2.12	99.9
$\text{SiO}_2$	0	0	-	-	-	-	-	-	-	-

<sup>a</sup> Reaction conditions: Temperature  $320 \text{ }^\circ\text{C}$ , atmospheric pressure, WHSV:  $0.75 \text{ L}\cdot\text{g}^{-1}\cdot\text{h}^{-1}$

IBAN = *isobutane*, MAA = methacrylic acid, MAC = methacrolein, AA = acetic acid, ACT = acetone and ACA = acrylic acid.

### 3.3.2 Effect of the active phase

The catalytic performances of the catalysts with a constant amount of 30 wt.% of active phase on the  $\text{SiO}_2$  support, namely  $30\text{CsV}_1$ ,  $30\text{CsV}_2$ ,  $30\text{RbV}_1$  and  $30\text{RbV}_2$  were studied. The catalytic performances in terms of *isobutane* conversion, and  $\text{CO}_2$ , MAC, MAA selectivity are shown in Table 3.6 to Table 3.9.

**Table 3.6** Catalytic performance in IBAN oxidation of 30CsV<sub>1</sub> at various temperatures.

Temperature, °C	Conversion <sup>a</sup> , %				Selectivity, %				$Y_{(MAC+MAA)}$ , %	Carbon balance, %
	O <sub>2</sub>	IBAN	MAA	MAC	CO <sub>2</sub>	AA	ACT	ACA		
340	61.2	8.7	17.2	8.8	30.0	31.5	6.3	2.3	2.25	99.6
330	56.4	7.5	19.8	9.9	28.4	29.9	6.1	2.3	2.23	99.7
320	43.0	6.0	23.5	11.9	27.6	26.0	7.3	2.3	2.12	99.9
310	35.3	4.6	31.1	14.4	17.6	24.5	8.9	2.5	2.09	99.9
300	24.2	3.3	36.8	17.3	13.8	20.3	11.1	-	1.77	99.9

<sup>a</sup> Reaction conditions: Temperature 300-340 °C, atmospheric pressure, WHSV: 0.75 L•g<sup>-1</sup>•h<sup>-1</sup>

Molar ratio: 28 % IBAN, 12 % O<sub>2</sub>, 10 % steam, 50 % He

IBAN = *isobutane*, MAA = *methacrylic acid*, MAC = *methacrolein*, AA = *acetic acid*, ACT = *acetone* and ACA = *acrylic acid*.

**Table 3.7** Catalytic performance for IBAN oxidation of 30CsV<sub>2</sub> catalyst at various temperatures.

Temperature, °C	Conversion, %				Selectivity, %				$Y_{(MAC+MAA)}$ , %	Carbon balance, %
	O <sub>2</sub>	IBAN	MAA	MAC	CO <sub>2</sub>	AA	ACT	ACA		
350	53.2	7.7	16.3	9.8	31.3	30.6	6.8	2.2	2.01	99.7
340	45.3	7.0	17.6	9.9	30.9	29.5	7.1	2.1	1.94	99.8
330	31.2	5.4	21.4	11.8	26.3	26.8	8.5	2.4	1.78	99.8
320	19.5	4.0	27.8	13.8	20.2	22.5	10.3	2.6	1.65	99.8
310	15.8	2.8	35.3	17.4	9.8	22.9	13.6	-	1.48	99.9

**Table 3.8** Catalytic performance in IBAN oxidation of 30RbV<sub>1</sub> at various temperatures.

Temperature, °C	Conversion, %				Selectivity, %				$Y_{(MAC+MAA)}$ , %	Carbon balance, %
	O <sub>2</sub>	IBAN	MAA	MAC	CO <sub>2</sub>	AA	ACT	ACA		
350	54.3	7.3	17.6	10.1	28.6	31.2	7.8	2.1	2.03	99.8
340	41.4	5.7	22.6	12.6	27.7	24.1	8.5	2.1	2.01	99.8
330	33.9	5.0	24.9	13.5	25.7	22.7	9.0	2.2	1.94	99.9
320	25.5	4.3	27.9	14.6	24.2	19.2	10.1	2.6	1.82	99.9
310	19.5	3.8	30.5	13.8	23.3	19.5	10.1	2.8	1.68	99.9

**Table 3.9** Catalytic performance in IBAN oxidation of 30RbV<sub>2</sub> at various temperatures.

Temperature, °C	Conversion, %				Selectivity, %				$Y_{(MAC+MAA)}$ , %	Carbon balance, %
	O <sub>2</sub>	IBAN	MAA	MAC	CO <sub>2</sub>	AA	ACT	ACA		
350	40.0	5.5	19.0	12.5	28.8	26.2	8.5	2.5	1.73	99.8
340	36.5	5.1	20.0	12.5	26.7	26.8	9.2	2.7	1.65	99.8
330	24.2	3.6	27.4	14.8	20.8	24.2	11.3	-	1.53	99.9
320	19.2	2.9	33.7	16.0	15.6	18.7	13.2	-	1.44	99.9

The *isobutane* conversion over the four kinds of catalysts increased with the reaction temperature, as expected. Maximum conversions of 8.7 % for the 30CsV<sub>1</sub> catalyst at 340 °C, 7.7 % for the 30CsV<sub>2</sub> catalyst, 7.3 % for the 30RbV<sub>1</sub> catalyst and 5.5 % for the 30RbV<sub>2</sub> catalyst at 350 °C were observed. It is worth noting that with the temperature increase, the increase in the IBAN conversion was accompanied with an over-stoichiometric increase in O<sub>2</sub> conversion leading to CO<sub>2</sub> formation and a decrease in the selectivity to the main products of interest, namely MAC and MAA (Figure 3.14). For the byproducts such as acetic acid and acetone, the selectivity showed an opposite trend with respect to temperature according to Table 3.6 to Table 3.9. Acetone also decomposes further with increasing temperature to form C<sub>2</sub> and C<sub>1</sub>. In addition, in all cases the carbon balance was >99.6 %, which means that at least 96 % of the products were detected even at the lower *isobutane* conversions.

These results are in good agreement with the reaction network proposed by Paul *et al.* [10,11]: MAC, MAA and degradation products could be formed through parallel reactions from *isobutane* directly. At a high reaction temperature, more over-oxidation products are produced, obviously resulting in the formation of less desired products. At the same time, the initially formed MAC is easier to transform to degradation products as the rate of degradation was found around 50 times higher than that of *isobutane* conversion. This reaction network was also proposed by Busca *et al.*[12]. Therefore, it can be assumed that the reaction network is composed of the conversion of *isobutane* to MAA, MAC and other by-products, and that the consecutive reactions for the oxidative degradation of MAA and MAC to AA and CO<sub>2</sub> are responsible for the decrease of desired products (*cf. section 1.1.2.2*). Liu *et al.* also reported [13], in the view of the whole reaction network, that MAC and MAA are both intermediates to complete oxidation products. At high *isobutane* conversion, the selectivity to MAC and MAA both decreased because of the complete oxidation. Therefore, maintaining the high selectivity of the desired product requires that the temperature of the oxidation operation should be moderate.

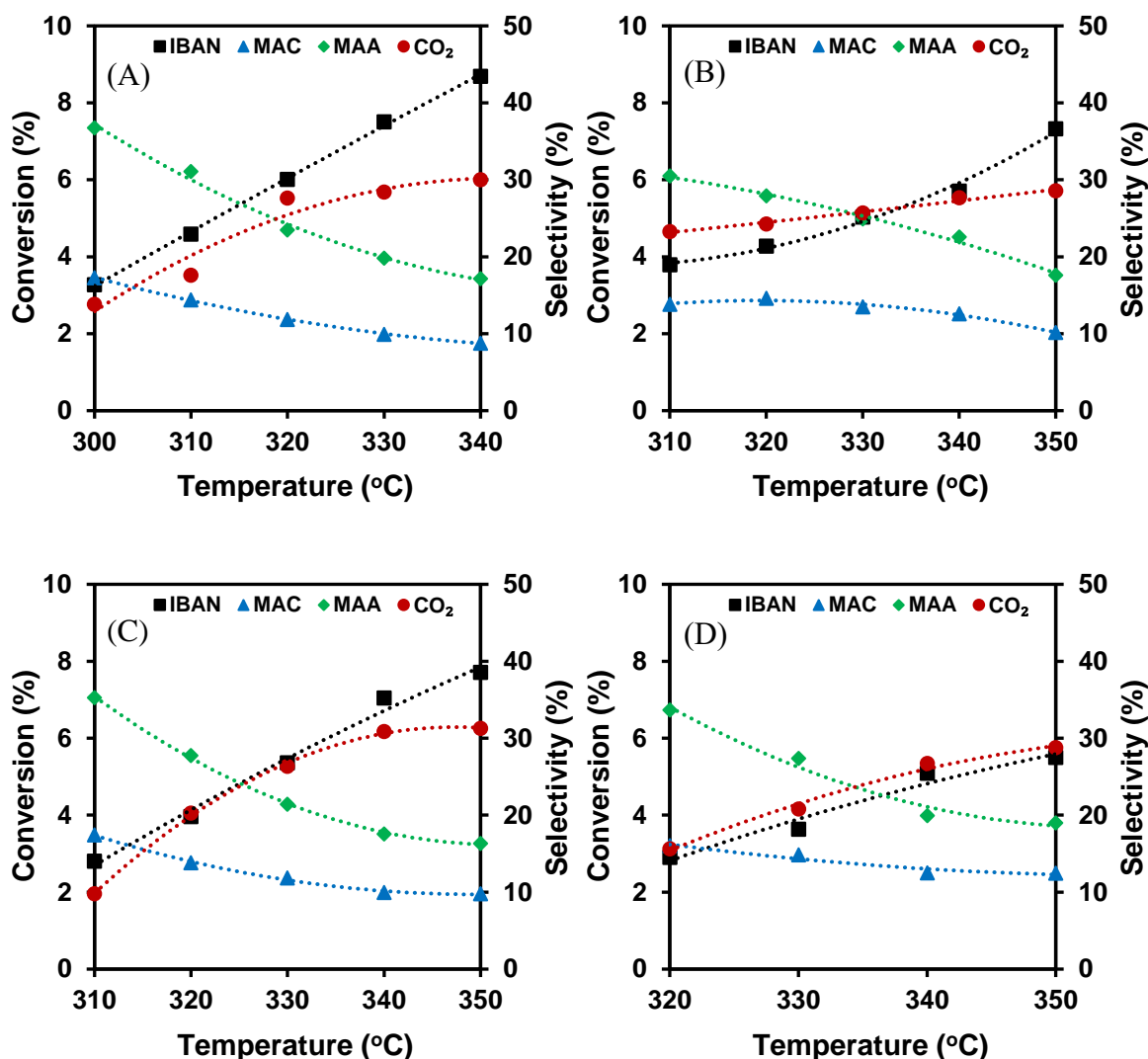


**Figure 3.14** Effect of the reaction temperature on the catalytic performance of (A) 30CsV<sub>1</sub>, (B) 30RbV<sub>1</sub>, (C) 30CsV<sub>2</sub>, and (D) 30RbV<sub>2</sub>. (IBAN = *isobutane*, MAC = methacrolein, MAA = methacrylic acid).

The conversions of *isobutane* over the Cs-based catalysts at different reaction temperatures were almost twice higher than those obtained over the rubidium-based catalyst. For example, at 320 °C, the conversion of *isobutane* was 6.0 % for 30CsV<sub>1</sub>, while for 30RbV<sub>2</sub>, it was 2.9 %. Hence, although there have been some reports about rubidium-doped catalysts in alcohol catalytic conversion [14,15], rubidium seems not to be the best choice for the catalytic oxidation of *isobutane*. Figure 3.15 shows the IBAN conversion as a function of the MAC+MAA selectivity for 30CsV<sub>1</sub>, 30CsV<sub>2</sub>, 30RbV<sub>1</sub> and 30RbV<sub>2</sub> catalysts. The 30CsV<sub>1</sub> catalyst exhibits the highest selectivity in the main products at a given conversion, meanwhile, it possesses the highest *isobutane* conversion at a given selectivity. The trend was observed for the performance

followed the order:  $30\text{CsV}_1 > 30\text{RbV}_1 > 30\text{CsV}_2 > 30\text{RbV}_2$ . This clearly evidenced that the use of cesium as counter cation is more favorable than rubidium and that replacing molybdenum by one vanadium is better than that by two vanadium. The lower performance over di-vanado substituted phosphomolybdic acid may be related to the absence of a stoichiometric phase. In fact, the compounds with vanadium stoichiometry  $> 1$  cannot be obtained in a pure state, but consist of a mixture of polyanions, which is disadvantageous for the catalytic activity [16–18]. Another postulate is that the decrease in activity of a catalyst at a stoichiometric vanadium content of 2 would be related to the formation of  $\text{VO}_2$  species, which does not contribute to the selectivity of the products [17,19,20].

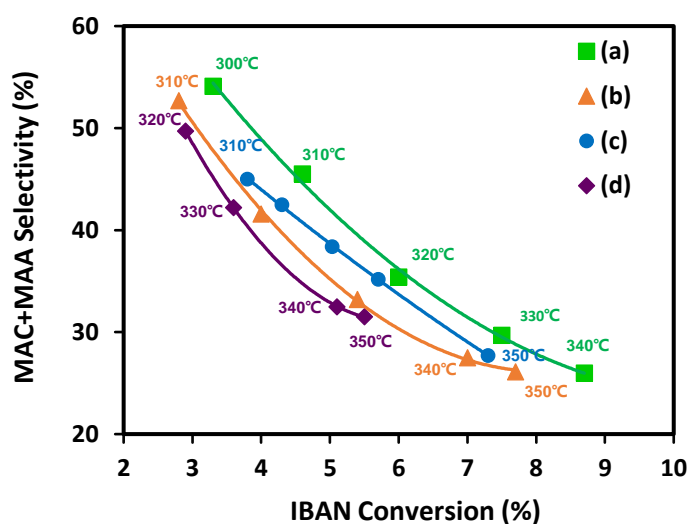


**Figure 3.15** Relationship between IBAN conversion and selectivity (MAC+MAA) of (a)  $30\text{CsV}_1$ , (b)  $30\text{CsV}_2$ , (c)  $30\text{RbV}_1$  and (d)  $30\text{RbV}_2$  catalysts at different temperatures.

The difference in the catalytic performance between CsV and RbV can be explained by taking a closer look to their respective acidities. In fact, according to the  $\text{NH}_3$ -TPD analysis, a correlation was attempted between acidity and catalytic activity, defined as follows [6]:

$$\text{Activity} = \frac{F_{\text{IBAN}} \times X_{\text{IBAN}}}{S_{\text{BET}} \times m_{\text{cat}}}$$

where  $F_{\text{IBAN}}$  is the molar flowrate of fed *isobutane*,  $X_{\text{IBAN}}$  the *isobutane* conversion (320 °C),  $S_{\text{BET}}$  the specific surface area and  $m_{\text{cat}}$  the mass of catalyst. By plotting activity vs. acidity, a linear relationship was obtained (Figure 3.16). Therefore, the number of acid sites in the  $30\text{CsV}_1$  catalyst is higher than that in the other three catalysts, confirming that the acidic sites are mainly

required for the C-H bond activation step [12].

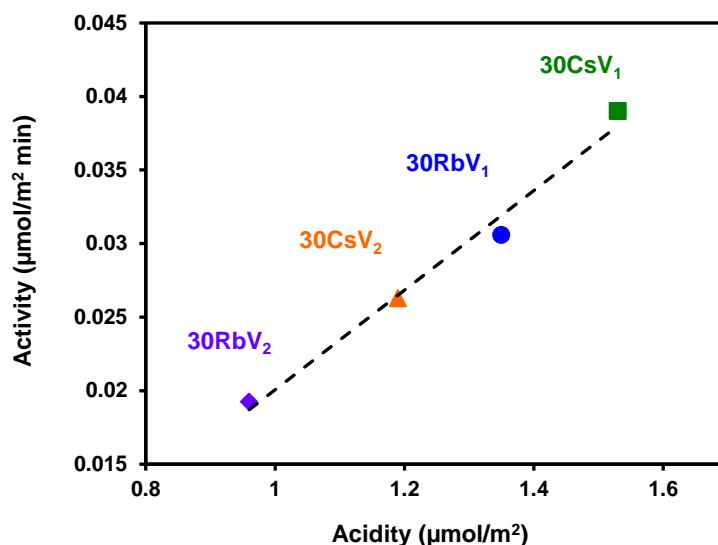


**Figure 3.16** Correlation between the activity in *isobutane* oxidation and the acidity of catalysts.

### 3.3.3 Effect of active phase amount

The catalytic performance of the three series of catalysts with different loadings are summarized in Table 3.10 to Table 3.12. For 10CsV<sub>1</sub>, the conversion of *isobutane* was quite low (0.4 %). The most plausible explanation is the low loading of active phase resulting in low amounts of active sites - in agreement with the low total acidity measured by ammonia TPD. For the other catalysts containing 20 wt.%-50 wt.% of CsV<sub>1</sub> on SiO<sub>2</sub>, the *isobutane* conversion increased (from 5.0 % for 20CsV<sub>1</sub> to 10.1 % for 50CsV<sub>1</sub>), obviously with the increase in loading of active phase, indicating that the conversion of *isobutane* is related to the amount of active phase and the quantity of acid sites – as observed before. The catalytic performances of the other two series of catalysts, CsV<sub>2</sub>/SiO<sub>2</sub> and RbV<sub>2</sub>/SiO<sub>2</sub>, showed a similar trend. The highest IBAN conversion was 8.9 % for 50CsV<sub>2</sub> and 7.7 % for 50RbV<sub>2</sub>. However, the selectivities to byproducts also increased with the increased amount of active phase, especially concerning the selectivity to CO<sub>2</sub> and acetic acid. Figure 3.17 shows the selectivity to the main products of interest (MAA+MAC) for the three series of catalysts as a function of *isobutane* conversion. It can be clearly seen that the catalytic performances of catalysts at a given selectivity or conversion follows the order CsV<sub>1</sub>/SiO<sub>2</sub> > CsV<sub>2</sub>/SiO<sub>2</sub> > RbV<sub>2</sub>/SiO<sub>2</sub>.

**Table 3.10** Catalytic performance in IBAN oxidation of CsV<sub>1</sub>/SiO<sub>2</sub> with different loadings.

Catalysts	Conversion <sup>a</sup> , %				Selectivity, %				Y <sub>(MAC+MAA)</sub> , %	Carbon balance, %
	O <sub>2</sub>	IBAN	MAA	MAC	CO <sub>2</sub>	AA	ACT	ACA		
50CsV <sub>1</sub>	82.1	10.1	17.5	5.0	36.4	29.1	6.4	2.0	2.3	99.6
40CsV <sub>1</sub>	53.4	7.3	24.1	10.0	27.2	27.0	7.1	2.1	2.4	99.8
30CsV <sub>1</sub>	43.0	6.0	23.5	11.9	27.6	26.0	7.3	2.3	2.1	99.9
20CsV <sub>1</sub>	31.5	5.0	24.4	13.3	24.9	23.1	8.6	2.2	1.9	99.8
10CsV <sub>1</sub>	8.2	0.4	-	-	-	-	-	-	-	-

<sup>a</sup> Reaction conditions: Temperature = 320 °C, atmospheric pressure, WHSV: 0.75 L•g<sup>-1</sup>•h<sup>-1</sup>.

Molar ratio: 28 % IBAN, 12 % O<sub>2</sub>, 10 % steam, 50 % He

IBAN = *isobutane*, MAA = *methacrylic acid*, MAC = *methacrolein*, AA = *acetic acid*, ACT = *acetone* and ACA = *acrylic acid*.

**Table 3.11** Catalytic performance in IBAN oxidation of CsV<sub>2</sub>/SiO<sub>2</sub> with different loadings.

Catalysts	Conversion <sup>a</sup> , %				Selectivity, %				Y <sub>(MAC+MAA)</sub> , %	Carbon balance, %
	O <sub>2</sub>	IBAN	MAA	MAC	CO <sub>2</sub>	AA	ACT	ACA		
50CsV <sub>2</sub>	72.9	8.9	15.5	5.7	35.7	33.7	5.3	1.9	1.88	99.8
40CsV <sub>2</sub>	59.0	7.2	17.8	7.5	34.0	29.7	6.5	2.1	1.81	99.8
30CsV <sub>2</sub>	31.2	5.4	21.4	11.8	26.3	26.8	8.5	2.4	1.78	99.8
20CsV <sub>2</sub>	22.8	3.5	26.6	15.2	22.5	18.5	11.3	2.9	1.48	99.8
10CsV <sub>2</sub>	12.7	0.7	-	-	-	-	-	-	-	-

<sup>a</sup> Reaction conditions: Temperature = 330 °C, atmospheric pressure, WHSV: 0.75 L•g<sup>-1</sup>•h<sup>-1</sup>.

**Table 3.12** Catalytic performance in IBAN oxidation of RbV<sub>2</sub>/SiO<sub>2</sub> with different loadings.

Catalysts	Conversion <sup>a</sup> , %				Selectivity, %				Y <sub>(MAC+MAA)</sub> , %	Carbon balance, %
	O <sub>2</sub>	IBAN	MAA	MAC	CO <sub>2</sub>	AA	ACT	ACA		
50RbV <sub>2</sub>	66.2	7.7	14.0	6.5	38.1	30.8	6.4	1.9	1.58	99.8
40RbV <sub>2</sub>	52.9	6.6	16.3	9.0	32.0	29.7	8.0	2.5	1.67	99.8
30RbV <sub>2</sub>	36.5	5.1	20.0	12.5	26.7	26.8	9.2	2.7	1.65	99.8
20RbV <sub>2</sub>	14.7	1.6	-	27.2	13.1	33.6	25.2	-	0.43	99.9
10RbV <sub>2</sub>	14.7	1.4	-	29.5	11.4	28.5	29.1	-	0.40	99.9

<sup>a</sup> Reaction conditions: Temperature = 340 °C, atmospheric pressure, WHSV: 0.75 L•g<sup>-1</sup>•h<sup>-1</sup>.

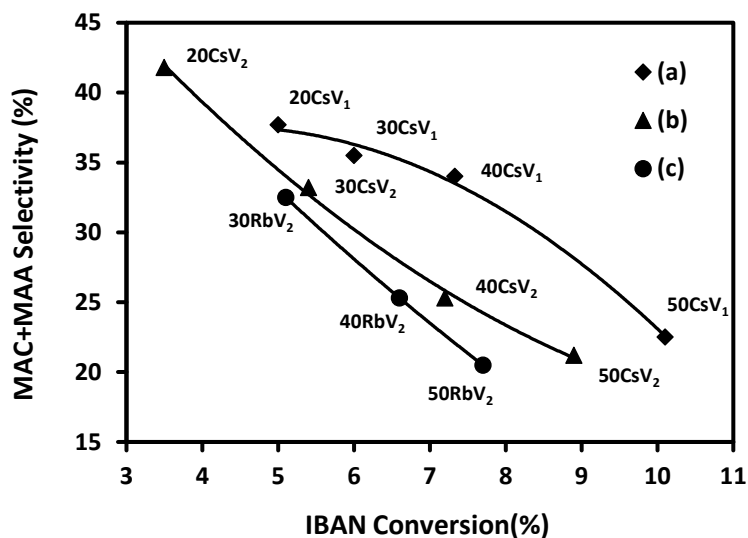


**Figure 3.17** Relationship between conversion and selectivity of (a) CsV<sub>1</sub>/SiO<sub>2</sub>, (b) CsV<sub>2</sub>/SiO<sub>2</sub>, (c) RbV<sub>2</sub>/SiO<sub>2</sub> catalysts with various loadings.

It is well known that the first step in the selective *isobutane* oxidation is the dehydrogenation of the tertiary carbon atoms, which is the rate determining step of the reaction [4]. The acidic sites on the surface effectively promote the hydrocarbon activation and lead to the C=C bond formation by oxidative dehydrogenation. Therefore, the density of acidic sites on the catalyst surface plays a key role in the activation of *isobutane*. Figure 3.18 actually shows the relationship between the IBAN conversion and the surface acid density of these three series catalysts (CsV<sub>1</sub>/SiO<sub>2</sub> catalysts, CsV<sub>2</sub>/SiO<sub>2</sub> catalysts, RbV<sub>2</sub>/SiO<sub>2</sub> catalysts). As shown in the illustration, the *isobutane* conversion increases when increasing the surface acidity, which is caused by increasing the active phase loading. Furthermore, for the lower loadings, the activity of the catalysts increased significantly with increased total acidity for cesium catalysts (10 wt.% to 20 wt.%) and rubidium catalysts (20 wt.% to 30 wt.%). For higher loadings, > 30 wt.%, the conversion of *isobutane* only moderately increased with increased acidity. This indicates that the effect of acidity on catalytic properties is not linear [4], and that the activity of the catalysts is controlled by the surface acid sites density.

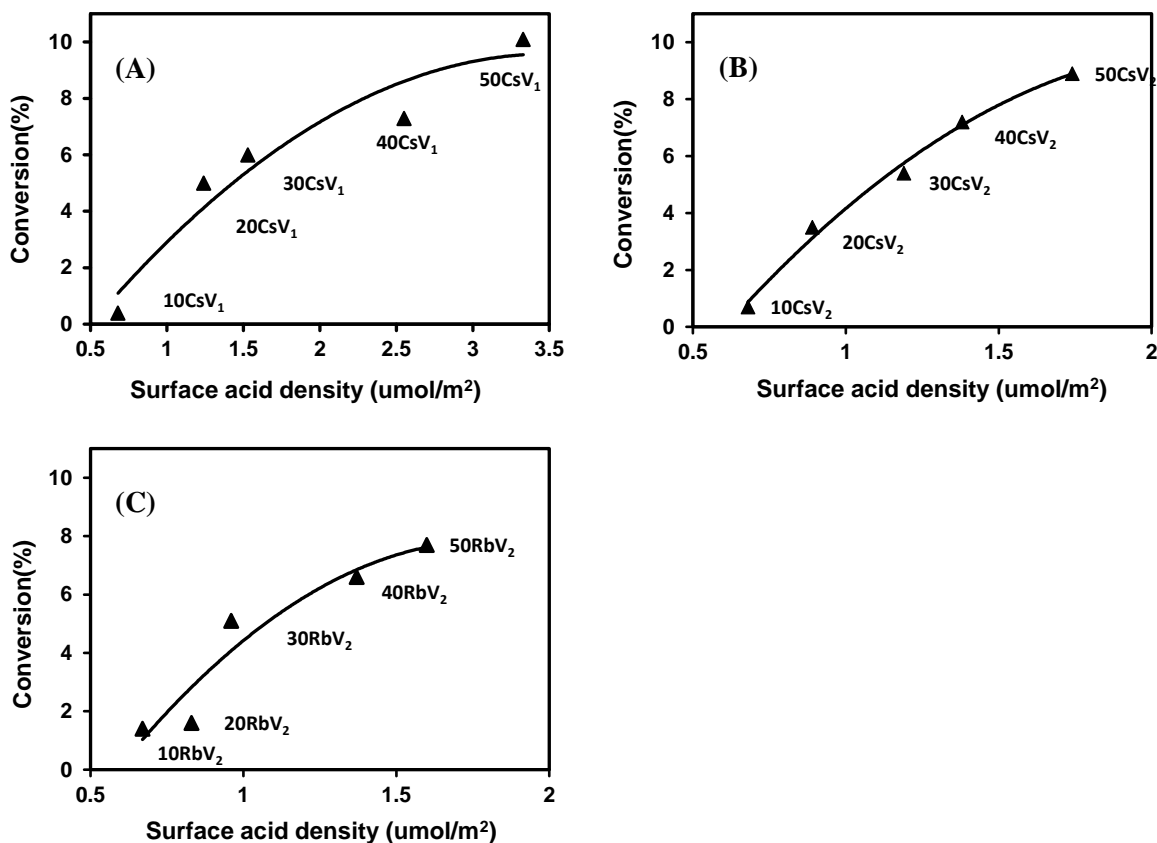


**Figure 3.18** Relationship between the IBAN conversion and the surface acid density over (A) CsV<sub>1</sub>/SiO<sub>2</sub> catalysts, (B) CsV<sub>2</sub>/SiO<sub>2</sub> catalysts, (C) RbV<sub>2</sub>/SiO<sub>2</sub> catalysts.

After that, in order to determine the optimal loading of active phase, the selectivity to the main products was studied at the same level of IBAN conversion, which is shown in Table 3.13 and Table 3.14. According to the discussion about the effect of reaction temperature and catalytic performances on the catalytic activity in the last section, the selectivity for these series of catalysts have been compared with catalysts loaded with 30 wt.% of active phase. At a first glance, one can see that, except for catalysts with 10-20 wt.% loading failing to achieve the desired IBAN conversion due to too low loading, the best selectivity to the desired products (MAC+MAA) was observed for CsV<sub>1</sub>/SiO<sub>2</sub> and RbV<sub>2</sub>/SiO<sub>2</sub> series with 39.1 % (IBAN conversion at 6.0 %) of 40CsV<sub>1</sub>, and 32.9 % (IBAN conversion at 5.0 %) of 40RbV<sub>2</sub>. Thus, the optimal loading is 40 wt.% (Figure 3.19). This conclusion is consistent with the characterization results showing that the 40 wt.% samples had high acidity, highest reducibility and a good dispersion on the surface of the silica support.

**Table 3.13** Selectivity of CsV<sub>1</sub>/ SiO<sub>2</sub> catalyst at the IBAN isoconversion.

Catalysts	Conversion <sup>a</sup> , %		Selectivity, %						Y <sub>(MAC+MAA)</sub> , %	Carbon balance, %
	O <sub>2</sub>	IBAN	MAA	MAC	CO <sub>2</sub>	AA	ACT	ACA		
50CsV <sub>1</sub>	49.0	6.2	25.3	9.0	27.8	27.1	2.2	7.4	2.14	99.9
40CsV <sub>1</sub>	40.5	6.0	27.9	11.2	25.7	23.9	2.2	7.5	2.34	99.9
30CsV <sub>1</sub>	42.0	6.0	23.5	11.9	27.6	25.6	2.3	7.3	2.12	99.9
20CsV <sub>1</sub>	33.5	5.2	23.3	13.2	24.4	24.4	2.3	8.4	1.9	99.8
10CsV <sub>1</sub>	7.9	0.5	-	-	-	-	-	-	-	100.0

<sup>a</sup> Reaction conditions: atmospheric pressure, WHSV: 0.75 L•g<sup>-1</sup>•h<sup>-1</sup>.

Molar ratio: 28 % IBAN, 12 % O<sub>2</sub>, 10 % steam, 50 % He

**Table 3.14** Selectivity of RbV<sub>2</sub>/ SiO<sub>2</sub> catalyst at the IBAN isoconversion.

Catalysts	Conversion <sup>a</sup> , %		Selectivity, %						Y <sub>(MAC+MAA)</sub> , %	Carbon balance, %
	O <sub>2</sub>	IBAN	MAA	MAC	CO <sub>2</sub>	AA	ACT	ACA		
50RbV <sub>2</sub>	41.5	5.3	20.1	8.7	30.4	29.9	2.2	8.2	1.53	99.9
40RbV <sub>2</sub>	38.2	5.0	21.4	11.5	27.2	27.0	2.4	9.0	1.65	99.9
30RbV <sub>2</sub>	36.5	5.1	20.0	12.4	26.7	26.8	2.7	9.2	1.64	99.8
20RbV <sub>2</sub>	15.7	1.5	-	27.8	16.5	25.7	-	27.7	0.41	99.9
10RbV <sub>2</sub>	15.7	1.5	-	29.5	16.2	26.0	-	27.8	0.44	99.9

<sup>a</sup> Reaction conditions: atmospheric pressure, WHSV: 0.75 L•g<sup>-1</sup>•h<sup>-1</sup>.

Molar ratio: 28 % IBAN, 12 % O<sub>2</sub>, 10 % steam, 50 % He

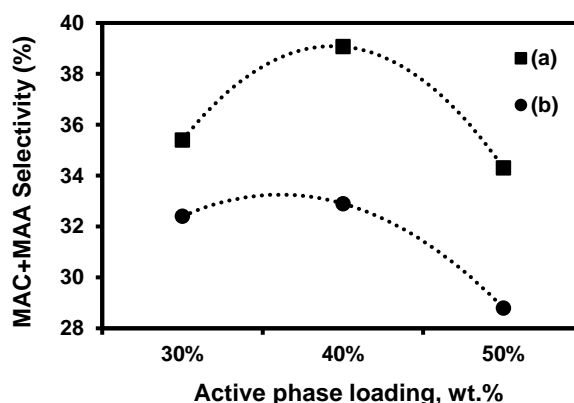


**Figure 3.19** Relationship between active phase loading and selectivity to MAC and MAA for: (a) CsV<sub>1</sub>/SiO<sub>2</sub>, (b) RbV<sub>2</sub>/SiO<sub>2</sub> at the same level of IBAN conversion (6 % for CsV<sub>1</sub>/SiO<sub>2</sub> and 5 % for RbV<sub>2</sub>/SiO<sub>2</sub>).

### 3.3.4 Effect of the weight hourly space velocity (WHSV)

In order to study the impact of the WHSV on the catalytic selective oxidation of isobutane at different reaction temperatures (310 - 340 °C), the former was increased from 0.75 to 1.5 L•g<sup>-1</sup>•h<sup>-1</sup>. The results are reported in Figure 3.20. As one can see, the IBAN conversion

decreased from 8.7, 7.5, 6.0, 4.6 % to 6.3, 5.0, 4.1, 3.7 % with WHSV of 0.75 and 1.5 L•g<sup>-1</sup>•h<sup>-1</sup>, respectively. However, with respect to the product distribution, no increase in MAC and MAA selectivity was observed for the same level of conversion as a result of increasing WHSV, meaning that longer contact time (WHSV of 0.75 L•g<sup>-1</sup>•h<sup>-1</sup>) is not automatically leading to over-oxidation to non-selective species.

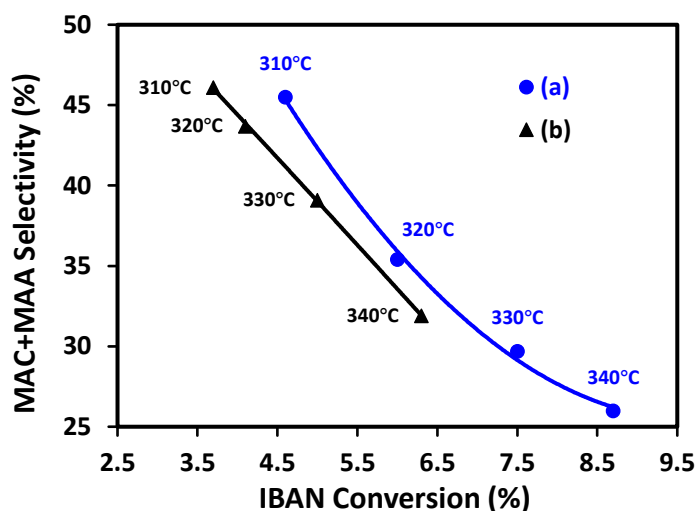


**Figure 3.20** Relationship between IBAN conversion and selectivity of 30CsV<sub>1</sub> catalysts at different reaction temperatures: (a) WHSV = 0.75 L•g<sup>-1</sup>•h<sup>-1</sup>, (b) 1.5 L•g<sup>-1</sup>•h<sup>-1</sup>.

### 3.4 Conclusions

As a conclusion, three series of catalysts with 10 to 50 wt.% loadings of Keggin-type catalysts ( $x\text{CsV}_1/\text{SiO}_2$ ,  $x\text{CsV}_2/\text{SiO}_2$  and  $x\text{RbV}_2/\text{SiO}_2$  catalysts) were prepared. The textural properties of the catalysts were evaluated showing that the theoretical specific surface area was larger than the actual ones, suggesting that the active phase itself is developing its own specific surface area. Catalysts containing different amounts of active phase differ in homogeneity, acidity, and reducibility:

- 1) At high loadings (50 wt.%), the active phase is detached from the support,
- 2) The catalyst with 40 wt.% loading of active phase exhibited optimal reducibility and the high amount of acid sites,
- 4) Monolayer coverage was obtained for 30-40 wt.% loading.

From the characterization study, it can be concluded that the optimum loading of catalyst is 30-40 wt.%. Subsequently, their catalytic performances for the selective oxidation of

*isobutane* to methacrylic acid and methacrolein were evaluated. First, catalysts loaded with 30 wt.% of heteropoly salt were selected to assess the effect of reaction temperature on the catalytic performances. We found that the counter cation and the degree of vanadium substitution had significant impact on the catalytic performance: Rubidium-containing catalysts require higher reaction temperatures to convert *isobutane*, which did not favor the selectivity to the desired product. Cs<sup>+</sup> as a counter-ion in the presence of one vanadium atom in the primary Keggin structure achieved the higher MAA and MAC selectivities at a given level of *isobutane* conversion. In the following, the performance of catalysts with active phase contents ranging from 10 to 50 wt.% were studied. The higher contents of active phase - up to a certain extent - led to an increase in conversion. This could be explained by the fact that acidity is the key to activate the C-H bond: with the increase in the active phase loading, the surface acid sites density increased, which led to an increase in catalytic activity. Hence, a loading of 40 wt.% on the CARiACT silica support used was found to be the optimum for the selective oxidation of *isobutane* (IBAN) to methacrylic acid (MAA), which not only enabled high acidity, but also a highly homogeneous dispersion of the active phase on the support. Within all the catalysts tested, through the above test comparison, 40CsV<sub>1</sub> has shown the best catalytic performance.

## References

- [1] I. V. Kozhevnikov, K.R. Kloetstra, A. Sinnema, H.W. Zandbergen, H. Van Bekkum, J. Mol. Catal. A Chem. 114 (1996) 287–298.
- [2] N. Mizuno, M. Tateishi, M. Iwamoto, J. Catal. 163 (1996) 87–94.
- [3] I. V. Kozhevnikov, J. Mol. Catal. A Chem. 305 (2009) 104–111.
- [4] F. Jing, B. Katryniok, F. Dumeignil, E. Bordes-Richard, S. Paul, J. Catal. 309 (2014) 121–135.
- [5] M. Kanno, T. Yasukawa, W. Ninomiya, K. Ooyachi, Y. Kamiya, J. Catal. 273 (2010) 1–8.
- [6] F. Jing, B. Katryniok, E. Bordes-Richard, S. Paul, Catal. Today 203 (2013) 32–39.
- [7] A. Brückner, G. Scholz, D. Heidemann, M. Schneider, D. Herein, U. Bentrup, M. Kant, J. Catal. 245 (2007) 369–380.
- [8] J. He, Y. Liu, W. Chu, W. Yang, Appl. Catal. A Gen. 556 (2018) 104–112.
- [9] R.C.R. Santos, D.M.V. Braga, A.N. Pinheiro, E.R. Leite, V.N. Freire, E. Longhinotti, A. Valentini, Catal. Sci. Technol. 6 (2016) 4986–5002.
- [10] M. Sultan, S. Paul, D. Vanhove, Stud. Surf. Sci. Catal. 122 (1999) 283–290.
- [11] S. Paul, V. Le Courtois, D. Vanhove, Ind. Eng. Chem. Res. 36 (1997) 3391–3399.
- [12] G. Busca, F. Cavani, E. Etienne, E. Finocchio, A. Galli, G. Selleri, F. Trifirò, J. Mol. Catal. A Chem. 114 (1996) 343–359.
- [13] S. Liu, L. Chen, G. Wang, J. Liu, Y. Gao, C. Li, H. Shan, J. Energy Chem. 25 (2016) 85–92.
- [14] M.H. Haider, N.F. Dummer, D. Zhang, P. Miedziak, T.E. Davies, S.H. Taylor, D.J. Willock, D.W. Knight, D. Chadwick, G.J. Hutchings, J. Catal. 286 (2012) 206–213.
- [15] H. Shou, L. Li, D. Ferrari, D.S. Sholl, R.J. Davis, J. Catal. 299 (2013) 150–161.
- [16] M.J. Darabi Mahboub, J.L. Dubois, F. Cavani, M. Rostamizadeh, G.S. Patience, Chem. Soc. Rev. 47 (2018) 7703–7738.
- [17] N. Mizuno, H. Yahiro, J. Phys. Chem. B 102 (1998) 437–443.

- [18] S. Wu, Q. Kan, W. Ding, F. Shang, H. Liu, J. Guan, *React. Kinet. Mech. Catal.* 106 (2012) 157–164.
- [19] A. Aboukaïs, D. Ghossoub, E. Blouet-Crusson, M. Rigole, M. Guelton, *Appl. Catal. A, Gen.* 111 (1994) 109–118.
- [20] R. Bayer, C. Marchal-Roch, F.X. Liu, A. Tézé, G. Hervé, *J. Mol. Catal. A Chem.* 114 (1996) 277–286.

**Chapter 4**  
**Catalytic selective oxidation of IBAN to MAA**  
**and MAC in a periodic reactor**

## Chapter 4 Catalytic selective oxidation of IBAN to MAA and MAC in a periodic reactor

### 4.1 Introduction

It has been shown in the previous section that heteropolycompounds with a Keggin structure, especially Cs-based catalysts, were active and selective for the selective oxidation of *isobutane* in a classical fixed-bed reactor where oxygen and *isobutane* are co-fed [1–7]. It is proposed for the first time to the best of our knowledge to implement the concept of a periodic reactor to the selective oxidation of *isobutane*.

The main principle of a periodic reactor applied to an oxidation reaction is to use an oxygen-carrying materials, as in the chemical looping concept, rather than a catalyst [8,9]. In general, periodic reactors have been considered for hydrocarbon conversion, and one application is of course selective oxidation [10]. It consists of a two-step process in which the reduction of the oxygen carrier by the hydrocarbon takes place in the first step and the reduced carrier is re-oxidized and regenerated by oxygen in the second step. Hence, this process separates the catalyst regeneration from the reaction through a time gap. Thus, the main difference in principle between the co-feeding process and this process is the decoupling of the reaction in two steps so that the operation conditions can be optimized independently. The concept of periodic reactor opens up new areas for the optimization of a variety of oxidation processes. The key to this development is the oxygen carrier. In a periodic reactor, the oxygen carrier does not act as a catalyst but as a reactant. This oxygen carrier needs to meet specific requirements [11]: 1) high reactivity in both oxidation and reduction reactions, 2) good selectivity to the required oxidation, 3) good stability after many redox cycles.

Based on the above, the Cs-based Keggin type HPA catalysts were selected to evaluate their catalytic activity in a periodic reactor. The catalysts before and after reaction were characterized by BET, XRD, Raman and XPS to better understand the structural and chemical changes during the periodic operation. Only the catalyst based on cesium-vanado-molybdcic acid supported on silica ( $x\text{CsV}_1/\text{SiO}_2$  samples) was used in the present study. During the testing process, on-line detection of the chemical species present in the reactor effluent was performed by a mass spectrometer. The sampling speed of the mass spectrometer was about 5 ~ 6 seconds

for each analysis. Therefore, the data processing of the test results allows us to obtain complete information during the test, including the instantaneous changes within each cycle.

## 4.2 Catalytic evaluation in selective oxidation of isobutane in a periodic reactor

### 4.2.1 Effect of reaction temperature

A temperature range of 320-360 °C was selected to evaluate its effect on the catalytic activity at a constant cycling time of 2 minutes for the reaction and 3 minutes for the re-oxidation (labelled in the followings as 2R-3O). 40CsV<sub>1</sub> was chosen as a catalyst with 25 cycles of looping reaction, as depicted in Figure 4.1. As one can see *isobutane* conversion and the product selectivity are fluctuating between each cycle over the whole test, irrespective of the reaction temperature. This fluctuation is due to the fact that the conversion and selectivity of each cycle are calculated by integrating the partial pressures of the components in that cycle. However, due to the low conversion of *isobutane*, the integration of the MS signal of IBAN is submitted to important errors, whereby the accuracy in the conversion value of IBAN is around  $\pm 0.5$  % (absolute) and in the selectivity of  $\pm 2$  % (absolute). However, the main tendency in the conversion remains unchanged and one can see that the catalyst shows stable conversion throughout the test, without any deactivation, as also confirmed by the XRD and Raman results presented in the following section.

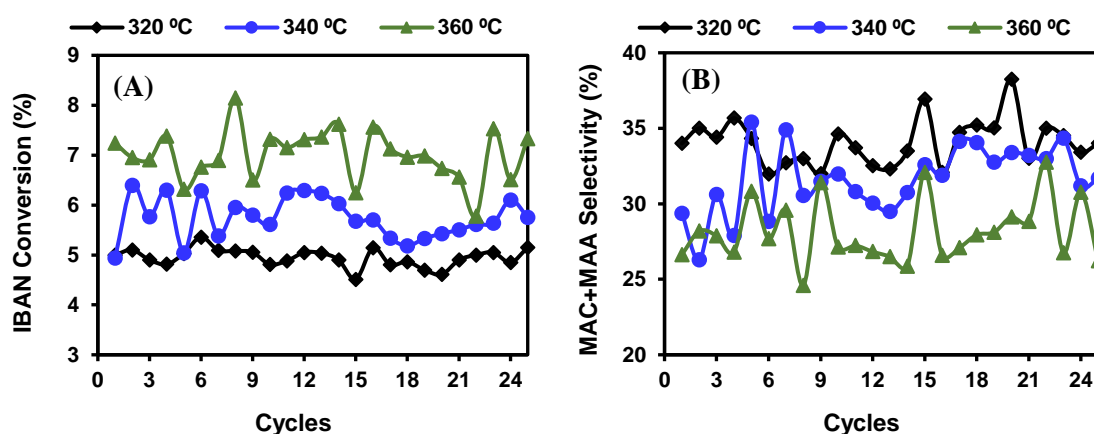


**Figure 4.1** Performances of 40CsV<sub>1</sub> catalyst under different reaction temperatures in a periodic reactor. (A) IBAN conversion, (B) Selectivity to MAA and MAC. (Test: 2 min reduction vs. 3 min re-oxidation, molar ratio of O<sub>2</sub>/IBAN = 2.14)

In order to make comparison easier, linear tendencies of catalytic performances in terms of IBAN conversion and products selectivity on 40CsV<sub>1</sub> catalyst with variable reaction temperatures are presented in Figure 4.2. As one can see, the IBAN conversion on 40CsV<sub>1</sub> sample increases with the temperature, with the highest selectivity to MAA and MAC at 320 °C and the highest conversion of IBAN at 360 °C. In addition, the CO<sub>x</sub> selectivity increases with temperature and leads to an increase in oxygen consumption (Table 4.1). The higher oxygen consumption at high temperatures is due either to the increased mobility of oxygen in the network at high temperatures during the reduction process or to the increased introduction of oxygen at high temperatures during the reoxidation process [12]. Another phenomenon noticed is similar to our previous results obtained under the condition of co-feed in a fixed-bed: the generation of C<sub>2</sub> by-products such as acetic acid presents the same trend as that for CO<sub>x</sub>. On the other hand, the trend of C<sub>3</sub> compounds such as acetone shows a trend similar to that of the main product C<sub>4</sub> compound: a lower temperature is more favorable for the formation of acetone.

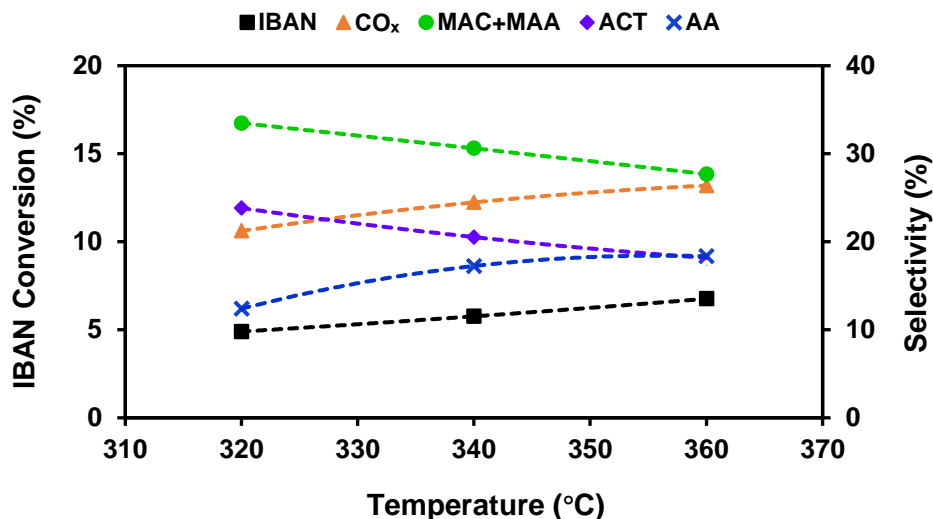


**Figure 4.2** Effect of the reaction temperature on the catalytic performances of 40CsV<sub>1</sub> catalyst. (IBAN = *isobutane*, MAC = *methacrolein*, MAA = *methacrylic acid*, AA = *acetic acid*, ACT = *acetone*)

Afterwards, the catalytic performance of another two CsV<sub>1</sub> catalysts with 30 and 50 wt.% loadings were evaluated, detailed results were summarized in Table 4.1. The 10CsV<sub>1</sub> and 20CsV<sub>1</sub> catalysts have not been selected to evaluate their catalytic activity on a periodic reactor

due to their particularly low conversions of *isobutane* in previous tests (co-feed condition in fixed-bed reactor). As can be seen, IBAN conversion decreases and selectivity to MAC and MAA increase with decreasing the active phase loading at a given reaction temperature. Moreover, the catalytic activity in terms of IBAN conversion and products selectivity on each catalyst present the same trend when varying the reaction temperature. Considering the conversion and main products selectivity, 340 °C has been fixed as a temperature for further study. To depict more clearly the relationship between the active phase loadings and the catalytic activity, the performances of obtained at 340 °C over the three catalysts are presented in Figure 4.3. With increasing the active phase loading from 30 to 40 wt.%, the conversion of *isobutane* increased, while the selectivity to the main products MAC+MAA decreased. The increase in IBAN conversion and the decrease in MAC+MAA selectivity were minor when further increasing the active phase loading up to 50 wt.%, implying that the active phase loading at 40 wt.% is the optimal. This may be due to the fact that the sample with 40 wt.% active phase exhibits monolayer coverage on the SiO<sub>2</sub> surface.

**Table 4.1** Catalytic performance in IBAN oxidation of  $x\text{CsV}_1/\text{SiO}_2$  catalysts with different loadings at various reaction temperatures.

Catalysts	Temperature, °C	Conversion <sup>a</sup> , %				Selectivity, %					Carbon balance, %
		O <sub>2</sub>	IBAN	MAA	MAC	CO	CO <sub>2</sub>	ATH	ACT	AA	
50CsV <sub>1</sub>	360	4.4	6.1	10.0	16.6	17.3	11.3	8.9	17.9	16.6	99.7
	340	4.1	6.0	13.0	16.7	14.4	10.3	8.4	18.9	16.6	99.4
	320	3.4	5.2	15.8	16.3	11.1	9.5	9.0	22.1	14.4	99.8
40CsV <sub>1</sub>	360	4.8	6.8	9.7	18.0	16.1	10.3	8.0	18.2	18.4	99.8
	340	4.0	5.8	12.1	18.5	13.1	11.4	5.9	20.5	17.2	99.9
	320	3.2	4.9	15.9	17.6	10.7	10.6	7.7	23.8	12.4	99.9
30CsV <sub>1</sub>	360	3.1	4.9	12.3	20.3	9.3	10.9	8.8	26.2	10.8	99.8
	340	2.8	4.6	13.4	20.5	8.1	10.5	8.8	27.9	9.9	99.9
	320	2.4	4.0	13.0	21.4	5.9	10.9	8.4	32.1	7.3	99.9

<sup>a</sup> Reaction conditions: Atmospheric pressure, Contact time: 3 s;

Test: 2 min reduction vs 3 min re-oxidation (2R-3O), molar ratio of O<sub>2</sub>/IBAN = 2.14;

IBAN = *isobutane*, MAA = methacrylic acid, MAC = methacrolein, AA = acetic acid, ACT = acetone and ATH = acetaldehyde.

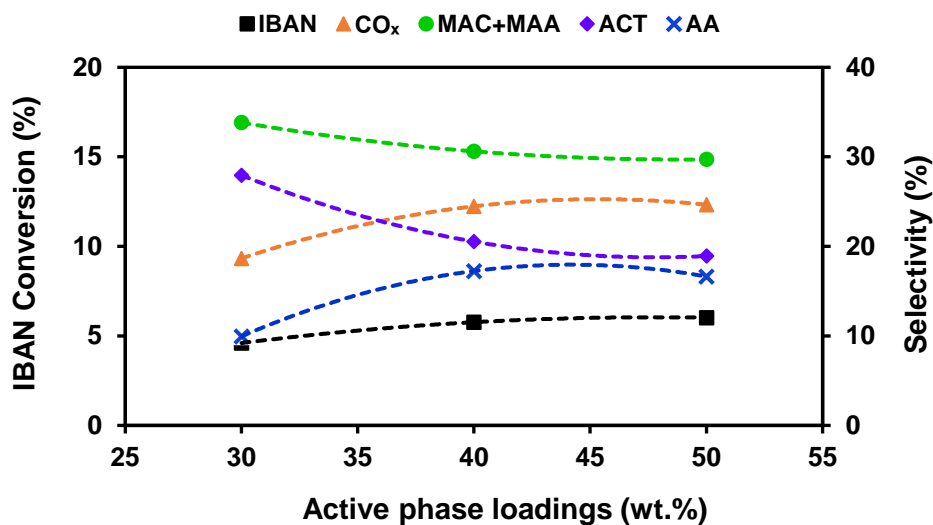


**Figure 4.3** Relationship between active phase loadings with IBAN conversion and selectivity  $x\text{CsV}_1/\text{SiO}_2$  catalysts at 340 °C.

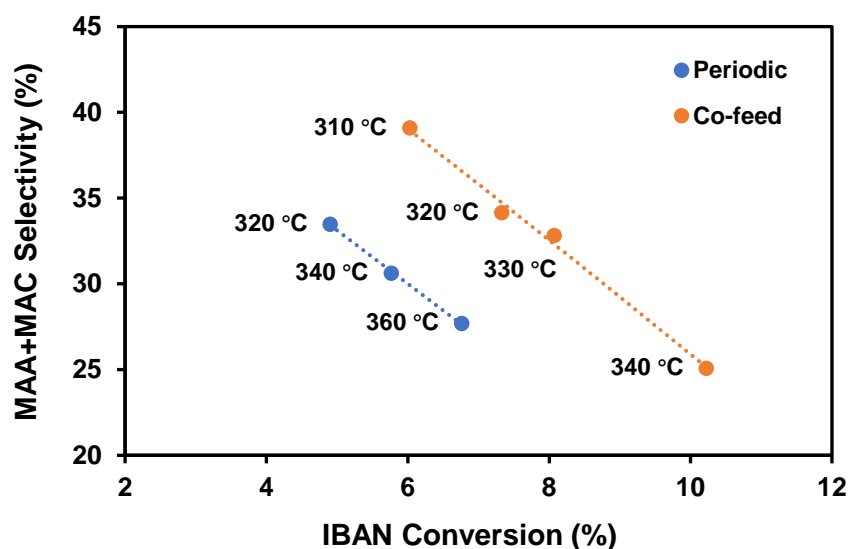


**Figure 4.4** Relationship between selectivity to MAC+MAA and IBAN conversion obtained on  $40\text{CsV}_1$  catalyst in a periodic reactor (cycling time: 2R-3O) and in a classical co-fed fixed-bed reactor at different reaction temperatures.

In addition, Figure 4.4 shows the relationship between IBAN conversion and desired products (MAA+MAC) selectivity of  $40\text{CV}_1$  sample at different reaction temperatures in periodic and co-fed reactors. It is worth mentioning here that when the cycling time of the oxygen for looping tests was 3 min (2R-3O), the selectivity to MAA and MAC was close at 320 °C for both conditions (33.5 % for the periodic reactor and 34.2 % for the co-feed,

respectively), while at 340 °C, the selectivity of the desired products was 30.6 % (5.8 % IBAN conversion) for the periodic test and 25.0 % (10.2 % IBAN conversion) for the co-feed condition. This indicates that high temperature will lead to more by-products under co-feed condition. The cycling tests separate the reduction process from the oxidation process, reducing the conversion of *isobutane* and reducing the production of oxygen-intensive products. Correspondingly, in the periodic reactor, the amount of oxygen injection also has a significant effect on the production of products, which is therefore investigated in more detail in the following tests.

#### **4.2.2 Effect of the cycling time**

First of all, the catalytic performances of 40CsV<sub>1</sub> sample during the reduction step of a 2R-3O cycle was monitored at 340 °C to understand its instantaneous performance, as shown in Figure 4.5. *Isobutane* was injected for 2 min, and instantaneous conversion of *isobutane* and produced products selectivities are shown. The behavior is similar with the other 24 cycles (25 cycles were done in total for this test). The converted *isobutane* gradually decreased after 20 s as the available oxygen (lattice or surface oxygen) in the oxygen carrier (40CsV<sub>1</sub>) is consumed. At the same time, CO and CO<sub>2</sub> formation decreases rapidly in the first 20 seconds. Methacrolein is formed at the beginning of the reaction, before it gradually decreases. However, in the first 40 seconds of the reaction, methacrylic acid increased as conversion of *isobutane* and the intermediate MAC decreased. In the following, the amount of both decreases as the available oxygen is consumed. As for other by-products, acetone and acetaldehyde are formed steadily during the reaction cycle, while the formation of acetic acid follows the same trend as the consumption of *isobutane*.

As seen before, the *isobutane* and oxygen signals change during a cycle, meaning that the catalyst is never in a stationary regime. Correspondingly, the length of the cycling time is of evident impact in periodic reactor, whereby it was studied in more detail.

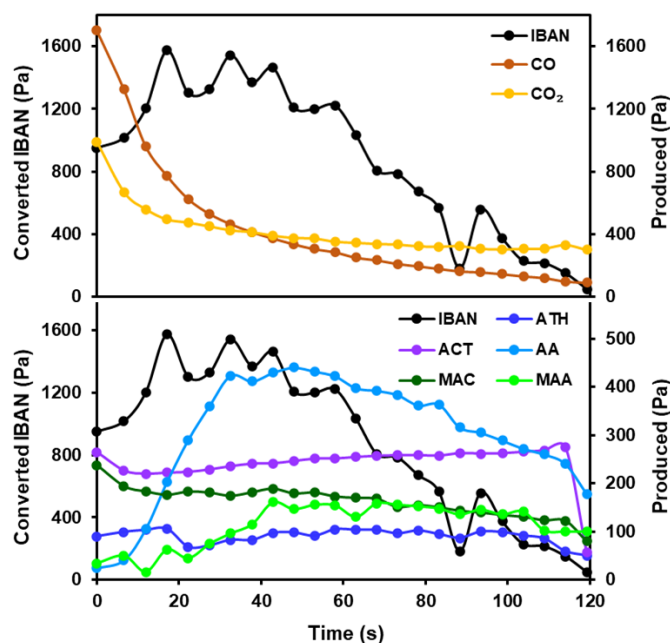


**Figure 4.5** Concentration profiles evolution during the reduction step (2 minutes) over 40CsV<sub>1</sub> at 340 °C with a cycling time 2R-3O (IBAN = *isobutane*, MAA = methacrylic acid, MAC = methacrolein, AA = acetic acid, ACT = acetone and ATH = acetaldehyde)

In the previous test, the cycling time was 2 min of *isobutane* and 3 min of oxygen (2R-3O) and the corresponding theoretical molar ratio of oxygen/*isobutane* was 2.14. In the following tests, the duration of the cycle time is changed by shortening the oxidation time of oxygen. As shown in Table 4.2, when the reduction time was maintained at 2 min and the injection of O<sub>2</sub> ranges from 3 min to 0.2 min (theoretical molar ratio of oxygen/*isobutane* ranging from 2.14 to 0.14), the conversion of oxygen increased dramatically, while the conversion of *isobutane* decreased. The increasing conversion indicates that oxygen is in excess.

**Table 4.2** Catalytic performance in IBAN oxidation of 40CsV<sub>1</sub> sample with different cycling times.

Molar ratio O <sub>2</sub> /IBAN	Cycling time	Conversion <sup>a</sup> , %		Selectivity, %							Carbon balance, %
		O <sub>2</sub>	IBAN	MAA	MAC	CO	CO <sub>2</sub>	ATH	ACT	AA	
2.14	2R-3O	4.0	5.8	12.1	18.5	13.1	11.4	5.9	20.5	17.2	99.9
1.43	2R-2O	5.8	5.7	13.7	18.2	11.1	12.0	6.4	22.9	14.5	99.6
0.71	2R-1O	8.8	4.7	13.7	21.7	6.1	12.6	5.6	29.1	10.0	99.7
0.36	2R-0.5O	15.3	4.3	20.3	22.4	5.5	10.9	4.2	25.9	9.5	99.9
0.14	2R-0.2O	30.8	3.2	11.8	22.3	6.9	13.1	5.5	30.8	7.8	99.4

<sup>a</sup> Reaction conditions: Atmospheric pressure, Contact time: 3 s; Reaction temperature: 340 °C;

IBAN = *isobutane*, MAA = methacrylic acid, MAC = methacrolein, AA = acetic acid, ACT = acetone and ATH = acetaldehyde.

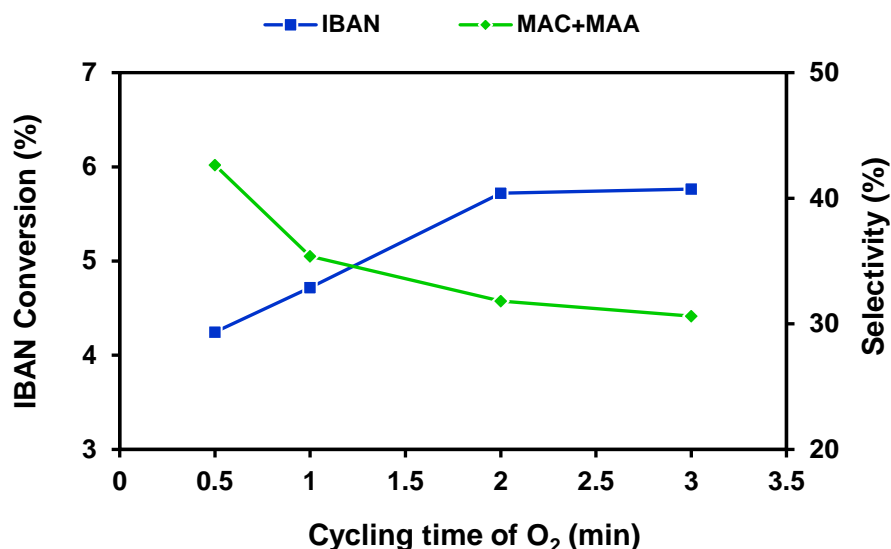


**Figure 4.6** IBAN conversion and MAA+MAC selectivity on 40CsV<sub>1</sub> sample at 340 °C with a cycling time of 2 min for the reduction and from 3 to 0.5 min for reoxidation.

However, when the cycling time of O<sub>2</sub> decreased from 3 min to 2 min (O<sub>2</sub>/IBAN from 2.14 to 1.43), the conversion of IBAN and the selectivity to the main products (MAA and MAC) changed and maintain a plateau, as can be observed in Figure 4.6. Since plateau is maintained, it can be concluded that even at oxygen/*isobutane* 1.43, the oxygen injected during the reoxidation cycle was still not the limiting factor. This is in good agreement with the XPS results (Table 4.5). The proportion of V<sup>5+</sup> in spent catalyst was increased compared to the fresh catalyst, meaning that more V<sup>4+</sup> was oxidized by the excess of oxygen. Furthermore, the selectivity to the main products increases with decreasing the oxygen cycle time and reached maximum (42.7 %) for a molar ratio of oxygen/*isobutane* of 0.36. At the same time, the selectivity to CO<sub>x</sub> decreased to its minimum (16.4 %). The catalytic performance of the same catalyst was also evaluated under co-feed conditions at the same temperature as shown in Figure 4.7. Whereas the selectivity to MAC and MAA was 25 % and to CO<sub>x</sub> was 33.6 % (10.2 % *isobutane* conversion). Of course, the periodic reaction separates the reduction from the oxidation process and reduces the conversion of *isobutane*, thus reducing the production of oxygen-intensive products.

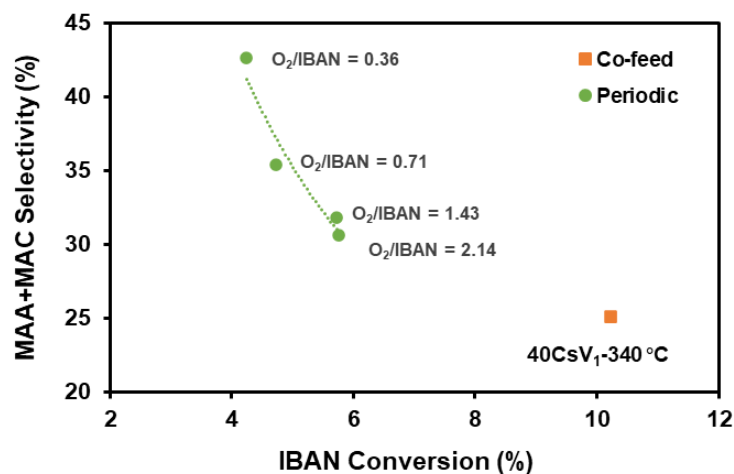


**Figure 4.7** Relationship between IBAN conversion and selectivity to (MAC+MAA) obtained on 40CsV<sub>1</sub> catalyst under periodic and co-feed conditions at 340 °C.

A more detailed information about the reaction process is shown in Figure 4.8. It can be clearly observed that the *isobutane* conversion decreased more rapidly during a cycle when the reoxidation duration was shorter (Figure 4.8A). The selectivities to the main products MAA and MAC are also shown in Figure 4.8B. In a single cycle, the amount of produced MAA and MAC increases during the first 40 s, and then logically decreases as the available oxygen in the oxygen carrier (40CsV<sub>1</sub>) is consumed.

For the comparison of all the cycles of an experiment (Figure 4.8C) one can see that the use of higher quantities of oxygen was favorable for the IBAN conversion. With an O<sub>2</sub>/IBAN molar ratio of 2.14, a mean conversion of 5.8 % was observed during the periodic test. On the other hand, high O<sub>2</sub>/IBAN molar ratio led to a decrease in MAA and MAC selectivity (Figure 4.8D). This decrease in MAA and MAC selectivity can be explained by the decomposition of the as-formed by-products because of the presence of oxygen in excess [13]. One can further conclude from Figure 4.8C and D that the catalyst maintains a good oxygen uptake and release capacity throughout the 20 cycles during the reactions, thus maintaining a stable performance. Moreover, the catalyst does not constantly over-reduce according to the XPS of the spent catalysts (*cf. section 4.2.3*), irrespective of the conditions. It is noteworthy that there are two other phenomena that can be seen from Figure 4.8D: first, the selectivity to the desired products seems to increase in the initial few cycles ( $\leq 10$  cycles), and then tends to stabilize, especially

when the molar ratio of oxygen/*isobutane* is less than 0.71. This can be explained by the large specific surface area of the catalyst and its pore structure, where some oxygen will be present on the catalyst as physisorbed species, and as the adsorbed oxygen are consumed, the selectivity of the desired products also increases and later remains stable. Another phenomenon is that when the  $O_2/IBAN$  molar ratio is further reduced from 0.36 to 0.14, the decrease in *isobutane* conversion is accompanied by a slight decrease in the selectivity of MAA and MAC. There is a possible hypothesis that can explain this phenomenon: That is the low oxygen injection was not sufficient to completely re-oxidized the catalyst or not able to completely entered the bulk of the catalyst to form lattice oxygen during the regeneration step. Thus, unregenerated catalyst leads to a decrease of *isobutane* conversion and selectivity to the main products in restarted the reduction process. All in all, the reaction is more favorable when the molar ratio of  $O_2/IBAN$  is 0.36.

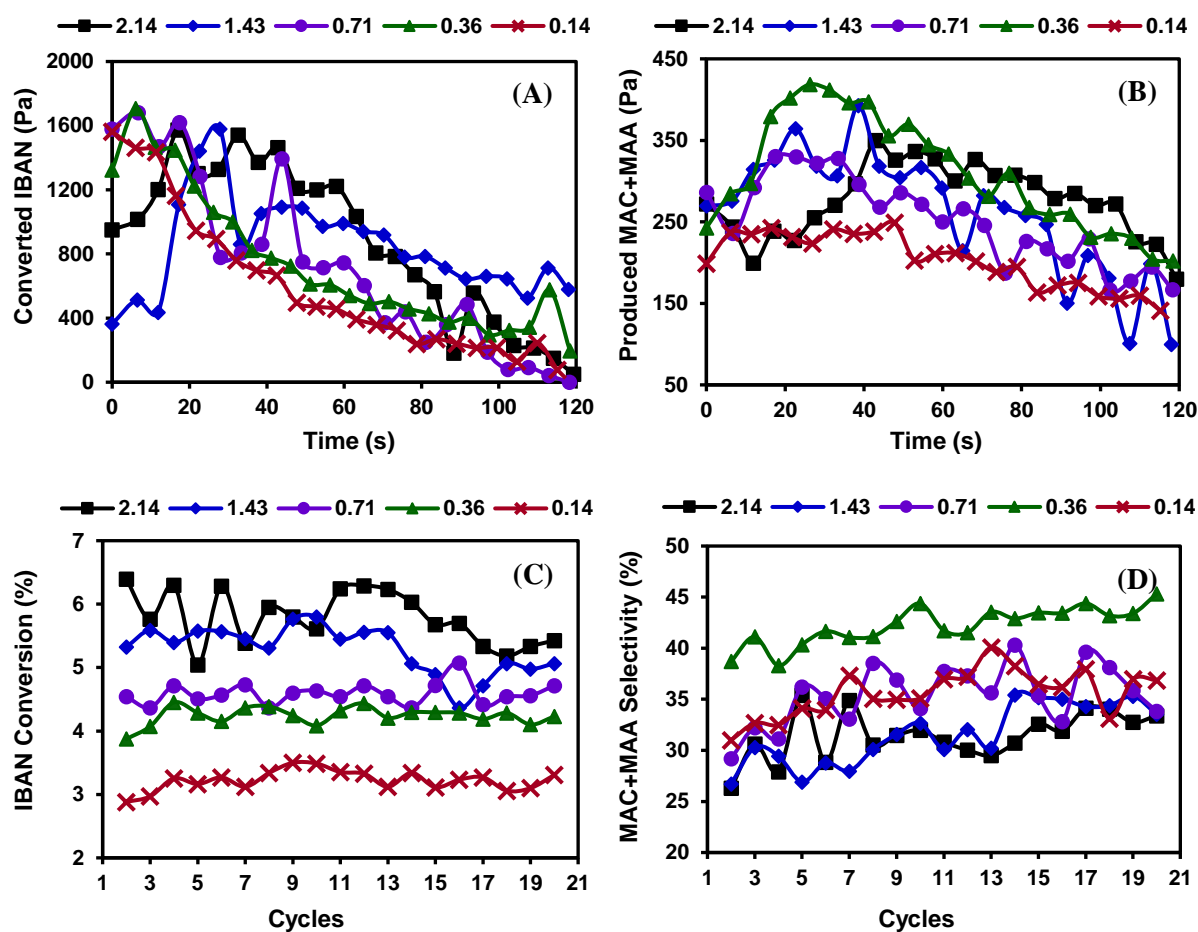


**Figure 4.8** Conversion and selectivity on 40CsV<sub>1</sub> sample with different molar ratios of  $O_2/IBAN$  at the reaction temperature of 340 °C. The molar ratios of  $O_2/IBAN$  were: 2.14, 1.43, 0.71, 0.36 and 0.14. (A) and (B) show the reduction part of a cycle, while (C) and (D) show the changes during the periodic tests.

### 4.3 Physicochemical properties of the catalysts used in periodic conditions

#### 4.3.1 Crystal phases and structural features analysis by XRD and Raman

The physical and structural properties of fresh and spent catalysts were determined and summarized following the catalytic tests in a periodic reactor under atmospheric pressure. The XRD patterns of fresh and spent 40CsV<sub>1</sub> catalysts are shown in Figure 4.9A. It can be seen that, the diffractograms are similar before and after reaction, implying that there is no significant decomposition of the Keggin structure during the test under periodic conditions. This further indicates that the active phase impregnated on the SiO<sub>2</sub> support exhibits excellent thermal stability. It should also be noted that the diffraction peaks of the spent catalyst become narrower compared to those of the fresh one, implying an increase in crystallinity of the catalyst after reaction, probably due to sintering. The Raman spectra of supported 40CsV<sub>1</sub> catalyst is shown in Figure 4.9B. The existence of the Keggin structure is characterized by the appearance of the following well-known vibration bands [5,14]:  $\nu_s$  (Mo=O<sub>d</sub>) at 983 cm<sup>-1</sup>,  $\nu_{as}$  (Mo-O<sub>b</sub>-Mo) at 871 cm<sup>-1</sup>,  $\nu_{as}$  (Mo-O<sub>c</sub>-Mo) at 600 cm<sup>-1</sup> and  $\delta$  (Mo-O-Mo) at 255 and 235 cm<sup>-1</sup>, respectively. The absence of vibration bands at 818 cm<sup>-1</sup> and 660 cm<sup>-1</sup>, which can be attributed to crystalline MoO<sub>3</sub>, further confirms that the active phase is well stabilized on the support [1].

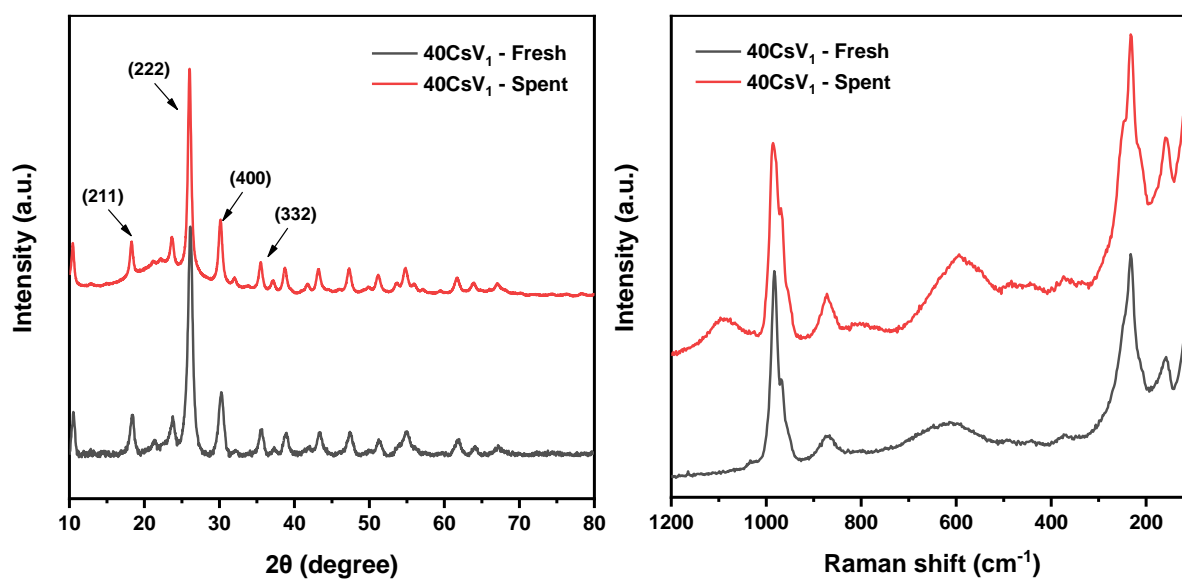


**Figure 4.9** XRD patterns (A) and Raman spectra (B) of the fresh and spent 40CsV<sub>1</sub> catalysts (The spent catalyst was tested at a cycling time of 2R-3O and a reaction temperature ranging from 320 to 360 °C).

### 4.3.2 BET specific surface area and pore volume of the catalysts

Table 4.3 shows the specific surface area and pore volume of the catalysts before and after the reaction, which was tested under the following conditions: cycling time 2R-3O and reaction temperature from 320 to 360 °C. After the catalytic test, the specific surface areas of 30CsV<sub>1</sub>, 40CsV<sub>1</sub> and 50CsV<sub>1</sub> catalysts decreased slightly from 219.8 to 206.5, 179.4 to 160.4, and 150.9 to 146 m<sup>2</sup>/g, respectively. This may be due to the increase in crystallinity of the catalyst after reaction, which is consistent with the results obtained from XRD diffraction peaks on 40CsV<sub>1</sub> catalyst. Meanwhile, the pore volume of the catalyst after the reaction did not change significantly, meaning that no deposition of carbonaceous species in the pores took place, which could also be confirmed by XPS analysis.

**Table 4.3** Textural properties of the fresh and spent catalysts.

Fresh-Catalysts	30CsV <sub>1</sub>	40CsV <sub>1</sub>	50CsV <sub>1</sub>
$S_{BET}$ , m <sup>2</sup> /g	219.8	179.4	150.9
$V_{pore}$ , cm <sup>3</sup> /g	0.69	0.49	0.40
Spent-Catalysts	30CsV <sub>1</sub>	40CsV <sub>1</sub>	50CsV <sub>1</sub>
$S_{BET}$ , m <sup>2</sup> /g	206.5	160.4	146.0
$V_{pore}$ , cm <sup>3</sup> /g	0.72	0.52	0.49

### 4.3.3 Surface analysis by XPS

X-ray photoemission spectroscopy measurements were carried out on the fresh and spent CsV<sub>1</sub>/SiO<sub>2</sub> samples in order to investigate the oxidation states of the vanadium and to estimate the surface compositions. All spectra were analyzed by a peak-fitting procedure. The wide peaks that assign to vanadium (V2p<sub>3/2</sub>) of 40CsV<sub>1</sub> and 50CsV<sub>1</sub> catalysts are reported in Figure 4.10. The BE values of the vanadium (V2p<sub>3/2</sub>) are gathered in Table 4.4. The peak of V2p<sub>3/2</sub> was deconvoluted to V<sup>5+</sup> and V<sup>4+</sup> at 518 and 517 eV, respectively [15,16]. In the Keggin unit, V atoms replace Mo atoms to change the redox properties, making the initial extraction of H-species of tertiary C atoms easier at the V=O site [16]. The V<sup>5+</sup>/V<sup>4+</sup> ratio was calculated according to the area of the corresponding peaks.

**Table 4.4** Surface analysis results for the samples before and after reaction

Catalysts		Binding energy (BE), eV		$V^{5+}/V^{4+}$ ratio
		$V2p_{3/2}, V^{5+}/V^{4+}$		
40CsV <sub>1</sub>	Fresh	518.0/516.9		35 / 65
	Spent <sup>a</sup>	518.1/516.9		41 / 59
50CsV <sub>1</sub>	Fresh	518.0/516.9		30 / 70
	Spent <sup>a</sup>	518.1/516.9		37 / 63

<sup>a</sup> Test conditions: Cycling time of 2R-3O and a reaction temperature ranging from 320 to 360 °C.

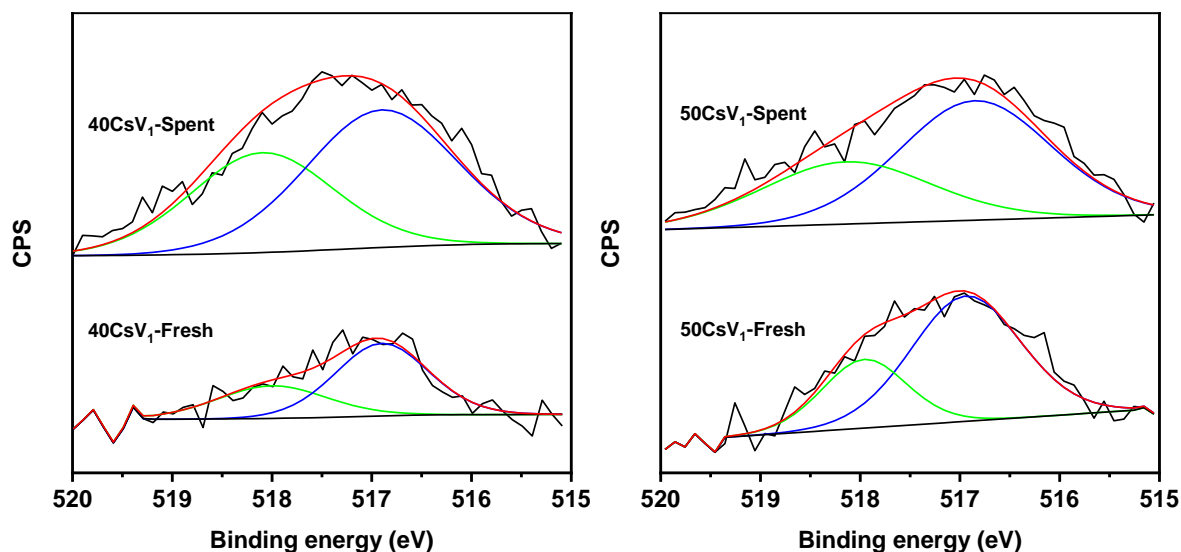


**Figure 4.10**  $V2p_{3/2}$  spectra of the samples before and after reaction: (A) 40CsV<sub>1</sub> catalysts and (B) 50CsV<sub>2</sub> catalysts. The spent catalyst was tested at a cycling time of 2R-3O and a reaction temperature ranging from 320 to 360 °C.

From the results one can see that the  $V^{5+}/V^{4+}$  ratio for spent catalysts increased slightly compared to that for the fresh ones, as shown in Figure 4.10 and Table 4.4. It can be assumed that this change is caused by the oxidation of the regenerated catalyst during the cyclic test. It should be noted that all tests started with the reduction of the catalyst (*i.e.*, the catalytic reaction) and ended with the reoxidation of the catalyst. In fresh samples,  $V^{4+}$  was dominating, a mixture of  $V^{4+}$  and  $V^{5+}$  can be observed on the surface, which indicates that there was not enough oxygen to react with the vanadium atoms during the synthesis process. This is caused by the drying of the samples under vacuum conditions after the synthesis by the impregnation method. The reduction of the transition metal centers (V, Mo) may be explained by the oxidation of  $O^{2-}$  ligands (lattice oxygen) to molecular  $O_2$ , which is lost to the environment (also called autoreduction). [17]. During the catalytic reaction, the catalyst was re-oxidized at reaction

temperature (from 320 to 360 °C) and in the presence of oxygen.

In order to study the influence of the reduction time and re-oxidation time on the oxidation state, four more samples were analyzed by XPS. Figure 4.11 and Table 4.5 show the influence of the cycling time on the vanadium oxidation state. The amount of oxygen injected in the cycling test for the 40CsV<sub>1</sub> sample at 340 °C gradually decreased with each cycle as the oxidation time varied. The V2p peak was again deconvoluted in order to distinguish between V<sup>5+</sup> and V<sup>4+</sup> species, thus determining the V<sup>5+</sup>/V<sup>4+</sup> ratio. As one can see, the V<sup>5+</sup>/V<sup>4+</sup> ratio decreased with decreasing O<sub>2</sub>/IBAN ratio, from 42/58 for an oxygen/IBAN ratio of 2.14, to 31/69 for an oxygen/IBAN ratio of 0.14.

This phenomenon can be explained by the redox mechanism of the reaction: vanadium V<sup>5+</sup> is consumed when *isobutane* is oxidized (reaction step) and re-oxidized in the reoxidation step. It is well known for the PMoV HPA catalysts, that vanadium reduces before molybdenum [5], although the presence of both V<sup>4+</sup> and Mo<sup>5+</sup> is a requirement to activate IBAN as well as O<sub>2</sub> to O<sup>2-</sup> [18,19]. Correspondingly, contrary to Mo-based oxides, mixed V<sup>5+</sup>/V<sup>4+</sup> valences compounds can be present at the steady state, whereby the effective amount of oxygen injected during the oxidation cycle allowed to the vanadium on the surface of sample to have more time to react with the oxygen and thus being reoxidized in the oxidation cycle. However, the observed performance in the previous section (*cf. section 4.2*) showed that when the oxygen injection time is too long, more highly oxidized products are formed, which also indicates the presence of unselective forms of oxygen.

**Table 4.5** Surface analysis results for the 40CsV<sub>1</sub> samples before and after reaction

Catalysts	Cycling time	Molar ratio O <sub>2</sub> /IBAN	Binding energy (BE), eV	V <sup>5+</sup> /V <sup>4+</sup> ratio
			V2p <sub>3/2</sub> , V <sup>5+</sup> /V <sup>4+</sup>	
40CsV <sub>1</sub> -Fresh	-	-	518.0/516.9	35 / 65
	2R-3O	2.14	518.1/516.8	42 / 58
	2R-2O	1.43	518.1/516.9	39 / 61
40CsV <sub>1</sub> -Spent <sup>a</sup>	2R-1O	0.71	518.1/516.8	34 / 66
	2R-0.5O	0.36	518.1/516.9	32 / 68
	2R-0.2O	0.14	518.1/516.9	31 / 69

<sup>a</sup> Reaction temperature: 340 °C.

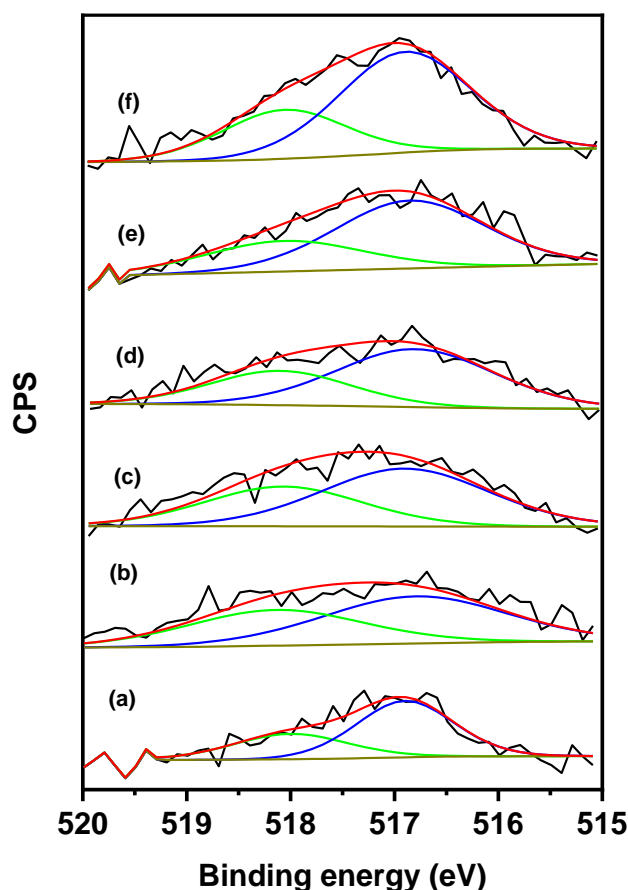


**Figure 4.11**  $V2p_{3/2}$  spectra of the 40 wt.%  $Cs_2H_2PMo_{11}VO_{40}/SiO_2$  catalysts: Fresh catalyst (a) and spent catalysts at 340 °C with different  $O_2/IBAN$  molar ratios: (b) 2.14, (c) 1.43, (d) 0.71, (e) 0.36, (f) 0.14.

#### 4.4 Conclusions

The periodic reactor concept was applied for the first time to the selective oxidation of *isobutane* to methacrolein and methacrylic acid using  $xCsV_1$  catalysts. In contrast to co-feed conditions in a classical fixed-bed reactor, the reactant and oxidant are separated by a time gap under periodic conditions. In addition, periodic reactor tests have the advantage of providing more information during the reaction period than continuous feed fixed-bed reactors, because one can track the consumption and formation of reactants and products in each single cycle. The effects of the reaction temperature, the amount of active phase, and the duration of the reoxidation step (and hence of the molar ratio of oxygen/*isobutane* injected in each cycle) were studied. Over a selected temperature range (320 to 360 °C), the results indicated that high temperature may be beneficial to the re-oxidation of the catalyst, also called oxygen carrier, to regenerate the active phase thus leading to improved conversion of IBAN. On the other hand,

under these conditions, IBAN was mainly converted to highly oxidized products, in detriment to the selectivity to the main desired products MAA and MAC. Therefore, 340 °C was chosen for further investigation. At the same time, increasing the active phase loading from 30 to 40 wt.% led to an increase in IBAN conversion, but resulted in a decrease in main products selectivity. Further increasing the active phase loading up to 50 wt.%, the change of IBAN conversion and main products selectivity were minor. Thus, 40CsV<sub>1</sub> catalyst should be optimal. With respect to the O<sub>2</sub>/IBAN ratio, increasing the O<sub>2</sub>/IBAN ratio led to a higher conversion, but at the expense of the selectivity to MAA and MAC. 40CsV<sub>1</sub> catalyst presented the high MAC+MAA selectivity of 42.7 % (4.3 % IBAN conversion) and a high yield of 1.8 % with the molar ratio of O<sub>2</sub>/IBAN = 0.36 at 340 °C reaction temperature.

The catalysts before and after the reaction were characterized showing that the catalysts exhibited a high stability during the periodic reaction process, as can be seen from XRD and Raman. The crystal structure of the catalyst did not decompose, and the active phase was still present on the surface of the catalyst. The presence of V<sup>4+</sup>/V<sup>5+</sup> species in the catalysts before and after the reaction indicates that vanadium was constantly reduced and re-oxidized under reaction conditions (Mars and Van Krevelen mechanism), underlining the good redox properties of the catalyst.

## References

- [1] X. Cai, Y. Ma, Q. Zhou, Z. Zhang, W. Chu, W. Yang, *React. Kinet. Mech. Catal.* (2021).
- [2] J. He, Y. Liu, W. Chu, W. Yang, *Appl. Catal. A Gen.* 556 (2018) 104–112.
- [3] Y.L. Cao, L. Wang, L.L. Zhou, G.J. Zhang, B.H. Xu, S.J. Zhang, *Ind. Eng. Chem. Res.* 56 (2017) 653–664.
- [4] D. Weber, P. Weidler, B. Kraushaar-Czarnetzki, *Top. Catal.* 60 (2017) 1401–1407.
- [5] F. Jing, B. Katryniok, F. Dumeignil, E. Bordes-Richard, S. Paul, *J. Catal.* 309 (2014) 121–135.
- [6] Q. Deng, S. Jiang, T. Cai, Z. Peng, Z. Fang, *J. Mol. Catal. A Chem.* 229 (2005) 165–170.
- [7] F. Jing, B. Katryniok, E. Bordes-richard, S. Paul, *Catal. Today* 203 (2013) 32–39.
- [8] J. Adánez, C. Dueso, L.F. de Diego, F. García-Labiano, P. Gayán, A. Abad, *Energy & Fuels* 23 (2009) 130–142.
- [9] P. Peltola, J. Saari, T. Tynjälä, T. Hyppänen, *Energy* 210 (2020).
- [10] R.M. Contractor, H.E. Bergna, H.S. Horowitz, C.M. Blackstone, B. Malone, C.C. Torardi, B. Griffiths, U. Chowdhry, A.W. Sleight, *Catal. Today* 1 (1987) 49–58.
- [11] T. Kane, Thesis, Université de Lille (2018).
- [12] J. Tête, Thesis, Ecole Centrale de Lille (2003).
- [13] B. Katryniok, R. Meléndez, V. Bellière-Baca, P. Rey, F. Dumeignil, N. Fatah, S. Paul, *Front. Chem.* 7 (2019).
- [14] A. Brückner, G. Scholz, D. Heidemann, M. Schneider, D. Herein, U. Bentrup, M. Kant, *J. Catal.* 245 (2007) 369–380.
- [15] Y. Suchorski, L. Rihko-Struckmann, F. Klose, Y. Ye, M. Alandjiyska, K. Sundmacher, H. Weiss, *Appl. Surf. Sci.* 249 (2005) 231–237.
- [16] F.L. Jing, Thesis, Université de Lille (2012).
- [17] J.K. Lee, V. Russo, J. Melsheimer, K. Köhler, R. Schlögl, *Phys. Chem. Chem. Phys.* 2 (2000) 2977–2983.

[18] E. Bordes-Richard, *Catal. Today* (2019) 1–12.

[19] E. Bordes, R.M. Contractor, *Top. Catal.* 3 (1996) 365–375.

**Chapter 5**  
**Catalytic selective oxidation of IBAN to MAA**  
**and MAC in a TZFBR**

## Chapter 5 Catalytic selective oxidation of IBAN to MAA and MAC in a TZFBR

### 5.1 Introduction

A two-zone fluidized-bed reactor (TZFBR) was employed to selectively oxidize *isobutane* to methacrylic acid and methacrolein and to evaluate the catalytic performance of heteropolycompounds catalysts in such a reactor. Unlike in a fixed-bed reactor, in a TZFBR the reduction and re-oxidation occur in different zones even if they are actually both located in the same reactor vessel. Obviously, the ideal case is to be able to internally reoxidize the catalyst in the same reactor where the reaction takes place, avoiding oxygen contact with IBAN or MAA and MAC. 40CsV<sub>1</sub> catalyst, which presented the best catalytic activity under both co-feed and periodic conditions, was selected for this purpose. First, to verify the correct fluidization of the catalyst, the hydrodynamic properties (minimum fluidization velocity, pressure drop) were determined. Then, to check the mechanical stability of the solid catalyst during the fluidization and reaction in TZFBR, attrition tests were carried out on 100 g of diluted catalyst (20 g of 40CsV<sub>1</sub> mixed with 80 g of CARiACT SiO<sub>2</sub>) under nitrogen for 24 h (named '*fluidized catalyst*' in the following) and after 15 days of reaction at 325 °C (named '*spent catalyst*'). Afterwards, the effects of the oxygen/*isobutane* molar ratio and of the reaction temperature on the catalytic performance during reaction were studied in the TZFBR.

### 5.2 Physicochemical properties of the catalysts

#### 5.2.1 Microstructure of the catalysts

Figure 5.1 shows the typical optical microscope images of diluted catalyst 40CsV<sub>1</sub> spheres before and after fluidization. In (B) and (C), the pale white spheres are SiO<sub>2</sub> and the yellow-green spheres are catalysts. As shown in the figures, part of the catalyst turned blue after fluidization by N<sub>2</sub> and after reaction, which indicates that some of the active phase on the SiO<sub>2</sub> surface is reduced during these processes. However, the observed morphology did not change and no obvious damage and active phase shedding were detected, which indicates that the catalyst maintains good mechanical stability during fluidization.

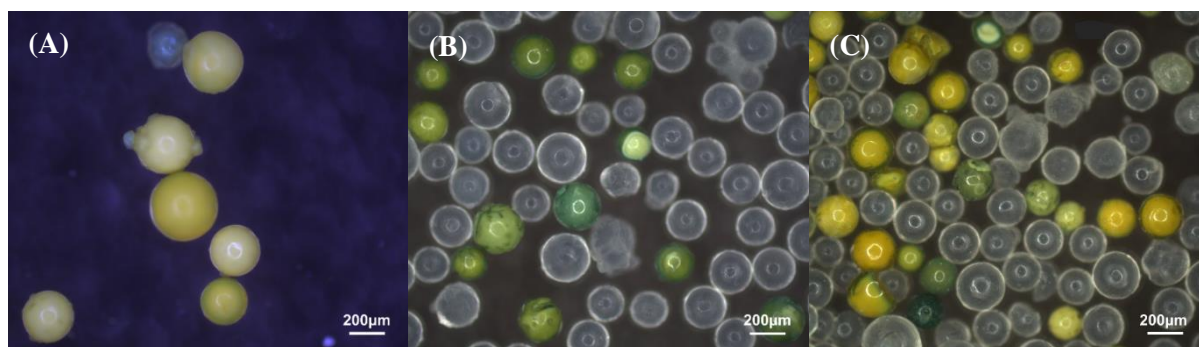


**Figure 5.1** Typical optical microscope images of 40CsV<sub>1</sub>/SiO<sub>2</sub> spheres: (A) fresh, (B) fluidized, (C) spent.

### 5.2.2 Crystal phases analysis of the samples by XRD

Figure 5.2 shows the XRD patterns of the diluted catalysts (20 wt.% 40CsV<sub>1</sub> and 80 wt.% SiO<sub>2</sub>) before and after the fluidization by N<sub>2</sub> and after reaction. The patterns exhibit diffraction peaks at  $2\theta = 26.2^\circ$  and  $30.4^\circ$  assigned to the lattice planes of (222) and (400) belonging to the Keggin-type CsV<sub>1</sub> (*cf. section 3.2.3*), showing that the catalysts did not decompose into metal oxides during these processes, underlining the good stability of the catalyst under the fluidized reaction conditions.

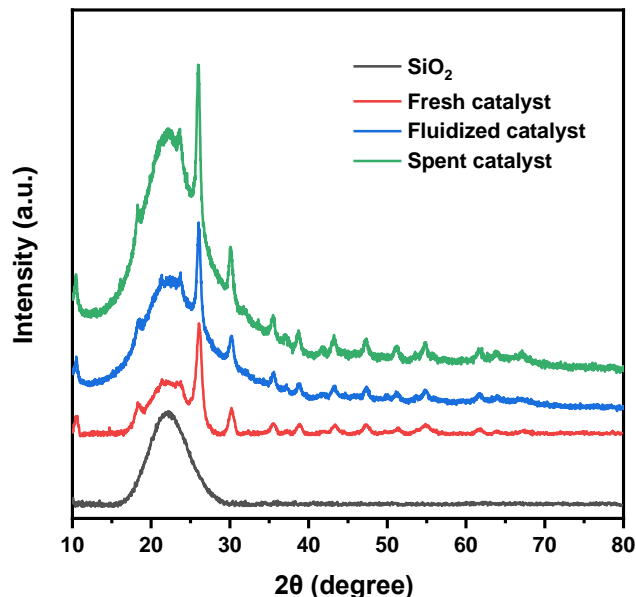


**Figure 5.2** XRD patterns of fresh, fluidized and spent catalysts.

### 5.2.3 Structural features of the catalysts observed by IR-Raman spectroscopy

IR-Raman spectroscopy was used to verify the presence of HPA active phase in fresh, N<sub>2</sub>-fluidized and spent catalysts. As shown in Figure 5.3, the typical Raman spectra bands of

$\text{Cs}_2\text{H}_2\text{PMo}_{11}\text{VO}_{40}$  at  $983\text{ cm}^{-1}$ ,  $871\text{ cm}^{-1}$ ,  $600\text{ cm}^{-1}$ ,  $255$  and  $235\text{ cm}^{-1}$ , which can be ascribed to the vibrations of the  $\nu_s \text{ Mo}=\text{O}_d$  bond,  $\nu_{as} \text{ Mo}-\text{O}_b-\text{Mo}$ ,  $\nu_{as} \text{ Mo}-\text{O}_c-\text{Mo}$ ,  $\delta$  (Mo-O-Mo), respectively, are still present [1,2]. These results confirm that the catalyst has good mechanical stability, and the friction of catalyst particles during the fluidization did not lead to abrasion of the active phase from the surface of the catalyst.

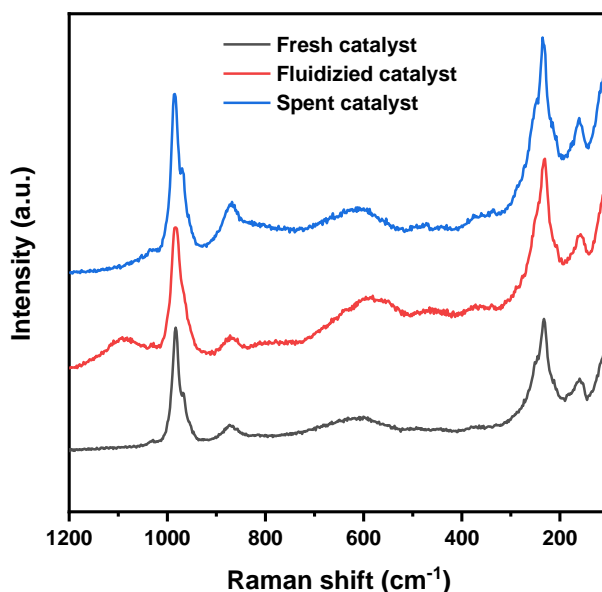


**Figure 5.3** Raman spectra of fresh, fluidized and spent catalysts.

#### 5.2.4 Surface analysis by XPS

The surface elements of the catalyst were analyzed by X-ray photoemission spectroscopy of fresh and spent 40CsV<sub>1</sub> samples. All spectra were analyzed by peak-fitting procedure. Figure 5.4 presents the peaks of vanadium ( $\text{V}2_{\text{P}_{3/2}}$ ) in catalysts. The BE values of vanadium ( $\text{V}2_{\text{P}_{3/2}}$ ) are collected in Table 5.1. As can be seen from the results, the  $\text{V}^{5+}/\text{V}^{4+}$  ratio of the spent catalyst was elevated from 35/65 to 42/58 compared to the fresh catalyst. This phenomenon was caused by the regeneration of the catalyst by oxygen during the fluidization test, which is consistent with the conclusion in the previous chapter (*cf. section 4.3.3*). The elemental analysis of the catalyst surface also confirms that the active phase on the catalyst surface did not suffer significant abrasion during fluidization reaction.

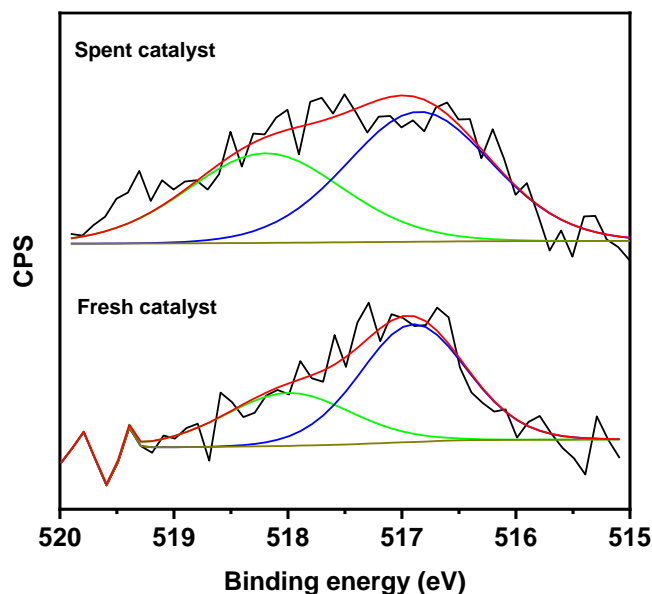


Figure 5.4 V2p<sub>3/2</sub> spectra of the samples before and after reaction.

Table 5.1 Surface analysis results for the samples before and after reaction

Catalysts	Binding energy (BE), eV		V <sup>5+</sup> /V <sup>4+</sup> ratio
	V2p <sub>3/2</sub> , V <sup>5+</sup> /V <sup>4+</sup>		
40CsV <sub>1</sub>	Fresh	518.0/516.9	35 / 65
	Spent <sup>a</sup>	518.0/516.9	42 / 58

<sup>a</sup> Test conditions: Temperature = 340 °C, atmospheric pressure.

### 5.2.5 Size distribution of the catalysts

The comparison of the physical and textural properties, such as particle diameter of the catalysts before and after 24 h of fluidization and after 15 days of reaction did not show any significant change. Correspondingly, for final verification of the mechanical stability of the catalyst particles, the granulometry was measured. In Figure 5.5 is shown the size distribution curve of the fresh, fluidized and spent catalysts. As one can see, for the spent catalyst (after 15 days of fluidization at 325 °C) there is no significant change in the mean size of the particles, while the distribution of the fluidized catalyst was similar to the fresh one. This indicates that no decrease in particle diameter was observed after a long reaction time and therefore no significant abrasion phenomenon occurred.

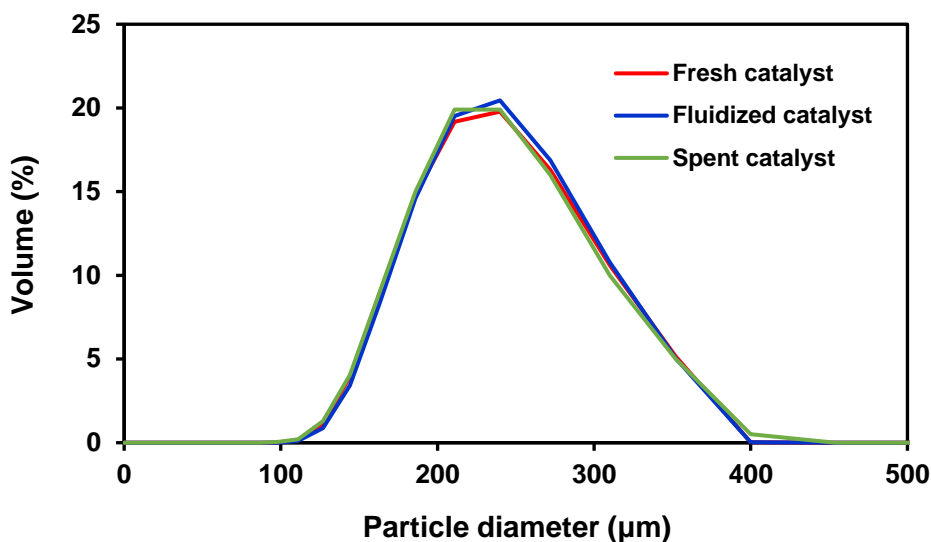


Figure 5.5 Size distribution of fresh, fluidized and spent catalysts.

### 5.3 Catalytic performance evaluation for the selective oxidation of *isobutane* in a TZFBR

#### 5.3.1 Hydrodynamic study and catalytic tests

Before studying any catalytic reaction in our experimental set-up, it is important to understand the hydrodynamic of the fluidized-bed reactor, which has obviously a direct impact on the catalytic performance. To study the hydrodynamic behavior of the TZFBR, the support CARiACT Q-10 SiO<sub>2</sub> mixed with the 40CsV<sub>1</sub> catalyst (80 g of SiO<sub>2</sub> support and 20 g of catalyst) was used, which corresponds to a bed height of 12.5 cm. This height was chosen in order to avoid a too shallow bed where the gas can short-circuit, resulting in poor conversion [3]. Considering that the fluidized-bed total height was 14 cm (measured in a glass fluidization column with identical diameter, Figure 5.6), the regeneration zone and reaction zone heights were chosen equal with a value of 7 cm ( $V_{reaction} / V_{regeneration} = 1$ ). The height was chosen to avoid a too small reoxidation zone, which would not enable continuous reoxidation of reduced catalyst, and also for total oxygen consumption, to avoid oxygen contact with IBAN, MAC and MAA [3]. A system of U tube manometers was installed to measure the pressure drop  $\Delta P$  of the catalytic bed (Figure 5.7).

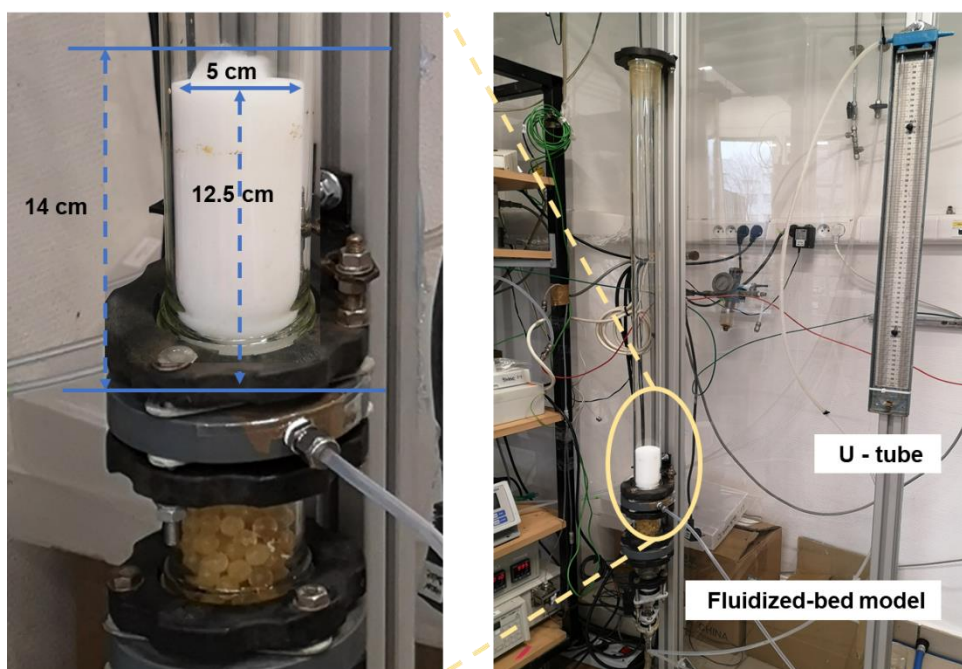


Figure 5.6 Model of glass fluidized column.

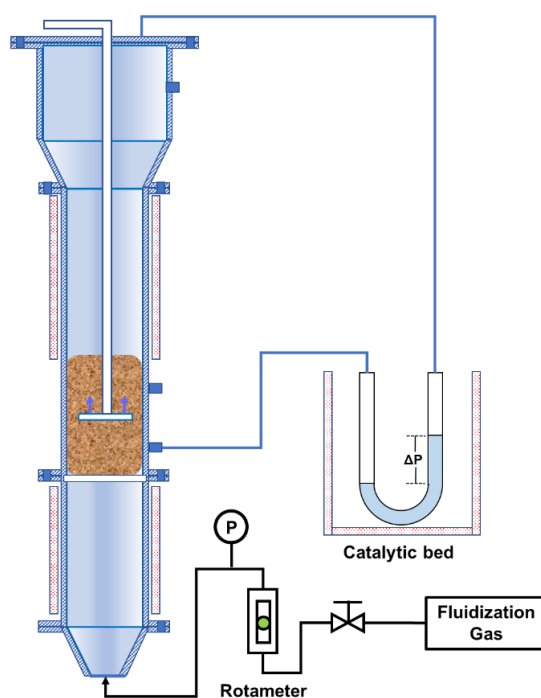
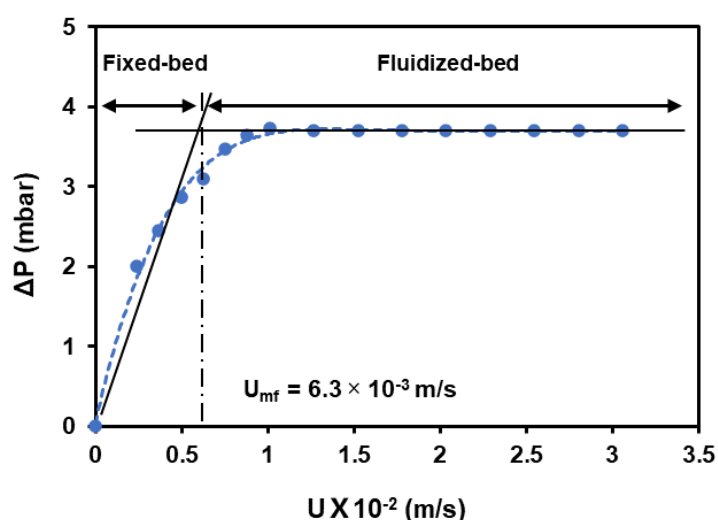


Figure 5.7 Measurement of the  $\Delta P$  pressure drop in the fluidized catalytic bed.

The minimum fluidization velocity ( $U_{mf}$ ) was determined by measuring the pressure drop through the catalytic bed ( $\Delta P$ ) as a function of the gas velocity ( $U$ ), as shown in Figure 5.8 and Figure 5.9. As can be seen from these figures, the minimum fluidization velocity occurs at the intersection of the pressurized and constant pressure lines, which is the transition point from

the fixed-bed to the fluidized-bed. Here, the minimum fluidization velocity ( $U_{mf}$ ) was found at  $6.3 \times 10^{-3}$  m/s at room temperature and  $5.0 \times 10^{-3}$  m/s at reaction temperature of 325 °C ( $U_{mf}$  does not change during the reaction). Since the density of the gas decreases with the temperature, the velocity required to achieve a fluidization state at 325 °C is lower than that at room temperature. From the results of this measurement, it was decided to employ a velocity during the catalytic tests of  $1.0 \times 10^{-2}$  m/s, which is twice the minimum experimental fluidization velocity ( $U/U_{mf} = 2$ ), so as to ensure the optimal fluidization and avoid the back-mixing of gas when the flow velocity is too high ( $U \geq 2.6 U_{mf}$ ) [4].



**Figure 5.8** Pressure drop as function of the gas velocity (measured in decreasing order) for the diluted catalyst at room temperature.

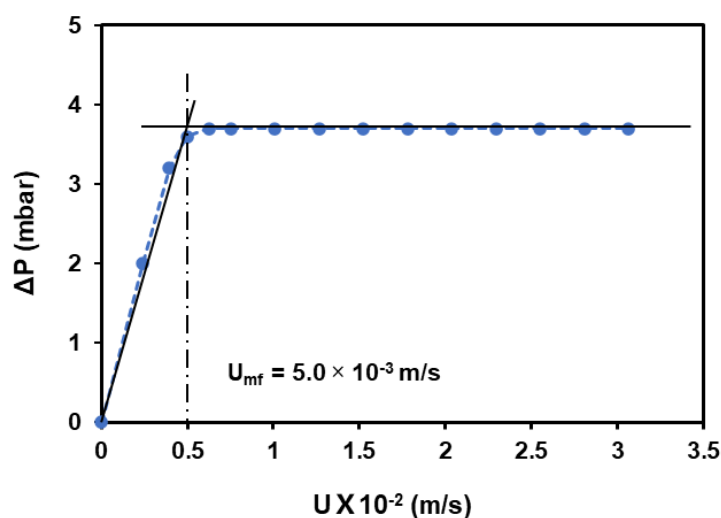


**Figure 5.9** Pressure drop as function of the gas velocity (measured in decreasing order) for the diluted catalyst at reaction temperature of 325 °C.

According to the pressure drop, it is possible to evaluate the quantity of solid participating to the fluidization in a fluidized bed, calculated by the relation between the theoretical and experimental drop pressure [5]:

$$\alpha = \frac{\Delta P_{\text{experimental}}}{(m \cdot g / A)}$$

The value  $\alpha$  is referred as “fluidization quality”,  $\Delta P$  is the pressure drop measured experimentally,  $m$  is the mass of diluted catalyst (100 g),  $g$  is standard gravity (9.81 m/s<sup>2</sup>), and  $A$  is the surface area of the catalyst bed (cross section of  $1.96 \times 10^{-3}$  m<sup>2</sup>). According to the above equation, the fluidization quality during the experiment was calculated to 75 % at room and reaction temperature. In a lab-scale fluidized-bed, this fluidization quality (the effect of the column walls) is suitable for catalytic reactions in TZFBR.

### 5.3.2 Effect of oxygen/*isobutane* molar ratio

The TZFBR is a reactor enabling continuous reaction, in which the concentration of oxygen is of utmost importance. Too high oxygen concentration will reduce the selectivity to the desired product, and too low oxygen concentration will not enable the complete reoxidation of the catalyst leading to progressive catalyst deactivation. Therefore, a long-term catalytic experiment was conducted with different oxygen concentrations in the fluidization gas in order to study the influence of the molar ratio of oxygen to *isobutane* on the catalytic reaction. The molar ratios of oxygen/*isobutane* in TZFBR were 6, 3, 2 and 0.6 respectively, corresponding to air flowrates of 1.3, 4.0, 6.0 and 12.0 L/h STP, respectively. Therein, the molar ratio of 2 is the theoretical molar ratio for the selective oxidation of *isobutane* to methacrylic acid, and the molar ratio of 3 is based on the optimum molar ratio of oxygen/*isobutane* observed in the fixed-bed reactor. The other operating conditions employed were: reaction temperature of 340 °C (same  $\Delta P$  pressure drop as that at 325 °C), the flowrate of fluidized gas was 70 L/h STP corresponding to a gas velocity ( $U$ ) of  $1.0 \times 10^{-2}$  m/s. The catalytic results obtained are depicted in Figure 5.10 and Table 5.2.

**Table 5.2** Catalytic performance in IBAN oxidation for 40CsV<sub>1</sub> with different oxygen/*isobutane* molar ratios.

O <sub>2</sub> /IBAN molar ratio	Conversion <sup>a</sup> , %		Selectivity, %				Carbon balance, %
	O <sub>2</sub>	IBAN	CO <sub>x</sub>	AA	ACT	Others	
6	10.9	15.4	92.3	2.5	-	5.2	98.9
3	16.9	13.4	90.2	1.8	-	8.0	98.7
2	19.1	10.5	87.9	2.2	-	9.9	98.8
0.6	18.6	3.3	75.4	6.6	1.8	16.2	98.2

<sup>a</sup> Reaction conditions: Temperature = 340 °C, atmospheric pressure, contact time 6.8 s.

IBAN = *isobutane*, AA = acetic acid, ACT = acetone and MAA = methacrylic acid.

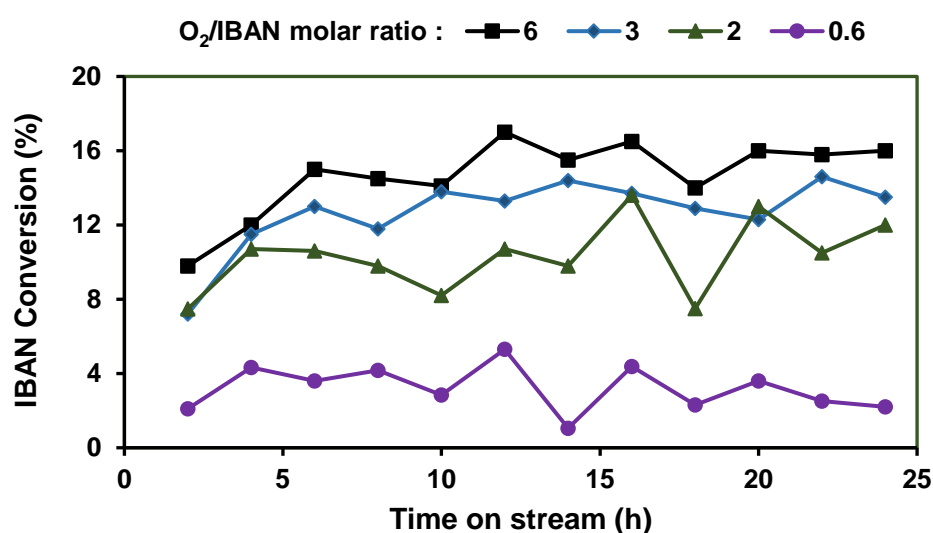


**Figure 5.10** Influence of the O<sub>2</sub>/IBAN molar ratio on the IBAN conversion (T = 340 °C).

From the catalytic results, it can be seen that the use of a high molar O<sub>2</sub>/*isobutane* ratio led to an increase in the IBAN conversion. When a flow of 12.0 L/h STP (corresponding to a molar ratio of oxygen/*isobutane* = 6) of air was injected with the fluidizing gas, a IBAN conversion of 15.4 % was observed. The latter remained rather stable after the 5 first hours of reaction and during the 24 h of the experiment (Figure 5.10). However, at this molar ratio, 92.3 % of CO<sub>x</sub> was formed as product, and a small amount of acetic acid was also detected (2.5 %), as shown in Table 5.2. This indicates that *isobutane* was oxidized non-selectively under these conditions. Subsequently, the air flow rate was then decreased to 6.0 and 4.0 L/h STP (*i.e.*, molar ratios of oxygen/*isobutane* = 3 and 2, respectively) to verify whether the decrease of oxygen in the fluidized gas was beneficial for the selective oxidation to MAC and MAA. The results showed

that the selectivity of  $\text{CO}_x$  was still about 90 %, again with a small amount of acetic acid (1.8 – 2.2 %). With regard to the IBAN conversion a decrease from 15.4 to 13.4 % and 10.5 % was observed, respectively, whereby the oxygen conversion increased to gradually to 19.1 % (10.9 % for oxygen/*isobutane* = 6). A further decrease of the molar ratio of oxygen/*isobutane* to 0.6 resulted in a decreased IBAN conversion of no more than 3.3 %. In addition to acetic acid (6.6 %), a small amount of acetone (1.8 %) was also detected under these conditions. A further decrease of the oxygen/*isobutane* ratio was technically not feasible since the lower limit of the flowmeter for air was reached.

As a conclusion, the molar ratio of oxygen/*isobutane* significantly influenced the conversions of IBAN and  $\text{O}_2$ . However, the main products observed were  $\text{CO}_x$  and C2 compounds, which indicates that either MAC and MAA are probably decomposed in the TZFBR.

### 5.3.3 Effect of the reaction temperature

In order to study the influence of the reaction temperature on the catalytic performance of 40CsV<sub>1</sub> in the TZFBR, the latter was lowered to 325 °C, notably with the idea to limit the decomposition of MAA and MAC to  $\text{CO}_x$ .

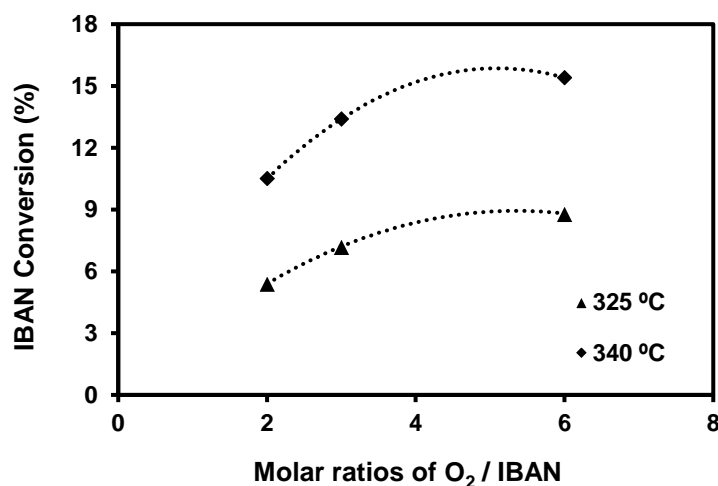


**Figure 5.11** Influence of the reaction temperature on IBAN conversion using different  $\text{O}_2$ /IBAN molar ratios at the reaction temperature of 325 and 340 °C.

Figure 5.11 describes the effect of the reaction temperature (325 and 340 °C) on the IBAN conversion when the molar ratios of O<sub>2</sub>/*isobutane* were 2, 3 and 6. The results showed that, as expected, the IBAN conversion was higher at 340 °C than at 325 °C in all experiments. At 325 °C, the conversion of IBAN decreased from 15.4 %, 13.4 %, 10.5 % to 8.8 %, 7.2 % 5.4 % compared to 340 °C, at O<sub>2</sub>/IBAN molar ratios of 6, 3 and 2 respectively. As aforementioned, the reduced temperature of 325 °C was selected in order to limit the formation of non-selective oxidized carbon. However, the low conversion at 325°C resulted in low amounts of products, which were finally under the detection limit of the TCD detector of the online GC, whereby no quantitative results are shown here. As indication, the main product at this temperature was still CO<sub>x</sub> at 325 °C.

Our hypotheses for the observed high selectivity to carbon oxide are: 1) The IBAN conversion decreased with the decrease in the molar ratio of oxygen/*isobutane*, which resulted in an excess of oxygen in the reaction system. Thus, oxygen was not entirely consumed in the reoxidation zone (lower area) and finally reached the reaction zone (upper area), where it subsequently reacts with *isobutane* to yield CO<sub>x</sub>; 2) The movement of bubbles in fluidized systems generates an influence on the mixing of particles and gas contact with the solids. The rising gas bubbles from the bottom of the reactor carry solids and associated gases, which are released by bursting at the bed surface. The released solids then flow downwards against the rising bubbles. In this case, the downward flowing solid carries the interstitial gas is carried downwards, resulting in backflow mixing [4]. Therefore, the undesired gas mixing can lead to overoxidation of desirable product to CO<sub>x</sub>, main product selectivity reduces significantly.

## 5.4 Conclusions

In this chapter, the mechanical stability of the catalyst was verified by performing fluidization tests of the catalyst particles in the TZFBR without IBAN feeding during 24 h or with IBAN feeding during 15 days at 325 °C. It was found that the minimum experimental fluidization velocity ( $U_{mf} = 5.0 \times 10^{-3}$  m/s) did not change during the fluidization or the reaction. Therefore, it can be concluded that the hydrodynamic properties remain unchanged during the reaction, which also indicates that the particle are not altered significantly during the

fluidization. This was also confirmed by several characterization techniques: optical microscope images showed that the morphology of the catalyst did not undergo any change after fluidization and reaction, except that a part of the catalyst was slightly reduced. Furthermore, the size distribution of the catalysts determined by granulometry indicated that the catalyst particles do not undergo significant mechanical abrasion. However, Raman spectroscopy and XRD showed that the active phase on the surface of the catalyst was well preserved, and no serious shedding occurred during the fluidization process.

In order to evaluate the catalytic performance of the catalyst in the TZFBR, a series of long-term catalytic tests was carried out. First, the molar ratio of oxygen/*isobutane* in the selective catalytic oxidation of *isobutane* was investigated. From the results, it was observed that the conversion of *isobutane* is significantly impacted by the oxygen/*isobutane* molar ratio as increasing the molar ratio was favorable to the *isobutane* conversion. However, the selectivity to carbon oxide was higher than 90 %. Hence, the influence of temperature on the conversion was very favorable, however once again accompanied by a large increase in the formation of CO<sub>x</sub>.

As a conclusion, the results of these tests of selective catalytic oxidation of *isobutane* in a TZFBR indicate that this type of reactor did not achieve the expected results in our initial attempts at selective oxidation of IBAN to MAC and MAA. The possible reasons are as follows: in the catalytic oxidation of *isobutane* to methacrolein and methacrylic acid by heteropolyacid, the conversion of *isobutane* is low (usually less than 10 %) whereby oxygen is not becoming the limiting factor and is not entirely consumed in the reoxidation zone (the oxygen conversion was never above 20 %). Correspondingly, this excess of oxygen reaches the reaction zone and can lead to MAC and MAA which are generated on the catalytic bed, with subsequent degradation in the huge dead volume after the fluidized-bed, form non-selective CO<sub>x</sub>.

## References

- [1] F. Jing, B. Katryniok, F. Dumeignil, E. Bordes-Richard, S. Paul, *J. Catal.* 309 (2014) 121–135.
- [2] A. Brückner, G. Scholz, D. Heidemann, M. Schneider, D. Herein, U. Bentrup, M. Kant, *J. Catal.* 245 (2007) 369–380.
- [3] B. Katryniok, R. Meléndez, V. Bellière-Baca, P. Rey, F. Dumeignil, N. Fatah, S. Paul, *Front. Chem.* 7 (2019).
- [4] H. V. Nguyen, A.B. Whitehead, O.E. Potter, *AIChE J.* 23 (1977) 913–922.
- [5] R. Meléndez, Thesis, L'Université des Sciences et Technologies de Lille. (2015).

# **Chapter 6**

## **General conclusions and perspectives**

## Chapter 6 General conclusions and perspectives

### 6.1 General conclusions

In the first part of this thesis, Cs and Rb-based HPAs were prepared by impregnation using silica as a support, in order to obtain Keggin-type supported catalysts of high specific surface area for the selective oxidation of *isobutane* to MAC and MAA, which belongs to the so-called surface-reaction type. Three series of catalysts with 10 wt.%-50 wt.% loadings of Keggin-type catalysts ( $x\text{CsV}_1/\text{SiO}_2$ ,  $x\text{CsV}_2/\text{SiO}_2$  and  $x\text{RbV}_2/\text{SiO}_2$  catalysts) were prepared. The textural properties of the catalysts were evaluated showing that the actual specific surface area was larger than the calculated theoretical ones, suggesting that the active phase itself was contributing to specific surface area by developing its own porosity. However, catalysts containing high loadings (50 wt.%) resulted in a detachment of the active phase from the support. The catalyst with 40 wt.% loading of active phase exhibited optimal reducibility and the high amount of acid sites. According to calculation, 30 - 40 wt.% of HPA over the silica support we used is close to a monolayer, meaning that the active phase is more homogeneous on the  $\text{SiO}_2$  support.

Subsequently, the catalytic performances in selective oxidation of *isobutane* to MAA and MAC were evaluated in a fixed-bed reactor under co-feed conditions. The catalysts loaded with 30 wt.% of active phase (30CsV<sub>1</sub>, 30CsV<sub>2</sub>, 30RbV<sub>1</sub>, and 30RbV<sub>2</sub> catalysts) were firstly selected to assess the effect of temperature on the catalytic performances. We found that the counter cation and the degree of vanadium substitution had a significant impact on the catalytic performance.  $\text{Cs}^+$  as a counter-ion in the presence of one V in the HPA structure achieved the highest MAA and MAC selectivities at a given level of *isobutane* conversion. In fact, it has been reported that compounds with a stoichiometry in vanadium  $> 1$  are not obtained under a pure state, but as a mixture of polyanions, thus unfavorable to catalytic activity. In addition, another postulate is that the decrease in catalyst activity at stoichiometric vanadium content of 2 is also associated with  $\text{VO}_2$  speciation. Rubidium-containing catalysts required higher reaction temperatures to convert *isobutane*, which did not favor the selectivity to the desired product. The difference in the catalytic performance between CsV and RbV can be explained

by looking at their respective acidities. The trend observed for the performance followed the order:  $30\text{CsV}_1 > 30\text{RbV}_1 > 30\text{CsV}_2 > 30\text{RbV}_2$ . However, as known from the literature, the acidic sites are indispensable for the activation of a C-H bond, which is the rate determining step in the studied reaction. As a conclusion, an active catalyst must present a well-balanced combination of appropriate textural and acidic properties, which are well represented by the notion of surface acid site density. Thus, a direct correlation between the acidity and the catalytic activity was established (*i.e.*, the tendency of *isobutane* to transform).

In the following part of the study, the performance of the  $\text{CsV}_1/\text{SiO}_2$ ,  $\text{CsV}_2/\text{SiO}_2$  and  $\text{RbV}_2/\text{SiO}_2$  catalysts with active phase contents ranging from 10 to 50 wt.% were studied. It was shown that using higher contents of active phase led to an increase in IBAN conversion (*e.g.*,  $\text{CsV}_1/\text{SiO}_2$  catalysts, from 0.4 % to 10.1 %). This could be explained by the fact that with the increase in the active phase loading, the surface acid sites density increased, which led to an increase in catalytic activity. The highest selectivity to MAA and MAC was observed on the 40 wt.% loaded samples, which not only had high acidity, but also a highly homogeneous dispersion of the active phase on the support. Within all the catalysts tested, through the above test comparison,  $40\text{CsV}_1$  showed the best catalytic performance.

In view of the results obtained in the first part of the thesis, the work was then focused on  $\text{CsV}_1/\text{SiO}_2$  catalysts to investigate the catalytic performance in different types of catalytic reactors. Since the reaction follows the Mars and Van Krevelen mechanism, the reduction and reoxidation steps of the catalyst can be decoupled. First, it was carried out in a periodic reactor, which is based on alternating injection of *isobutane* and oxygen in an inert gas stream and water vapor. The aim of this work was to explore the possibility of performing selective oxidation of IBAN to MAA and MAC in a periodic mode. The main strategies followed in this part include the study of the effect of the reaction temperature and of the oxygen concentration during the reaction. Increasing the reaction temperature showed a positive impact on the conversion of the reactant *isobutane*, while it presented negative effect on the selectivity to the desired products (MAA and MAC). This tendency was consistent with that observed in the co-feed fixed-bed reactor. However, the periodic reactor tests also provide more information during the reaction,

since one can follow the consumption and formation of reactants and products in each single cycle (*i.e.*, the partial pressure of each component). The results showed that the conversion of *isobutane* and the formation of products decreased with the consumption of available oxygen species in the catalyst for a duration of 120 s per cycle. For the whole periodic tests, low concentration of oxygen injected into the reoxidation part of the cycles led to a high selectivity to the desired products (MAC+MAA). The selectivity to these products reached the highest value (42.7 %) when the molar ratio of oxygen to *isobutane* was 0.36, and the selectivity of CO<sub>x</sub> decreased to the lowest (16.4 %) at the same time. In addition, the XPS results show the presence of V<sup>4+</sup>/V<sup>5+</sup> species in the catalysts before and after the reaction. This indicates that vanadium is constantly reduced and re-oxidized under reaction conditions. Meanwhile, the V<sup>5+</sup>/V<sup>4+</sup> ratio decreased with decreasing the O<sub>2</sub>/IBAN ratio, from 42/58 for an oxygen/IBAN ratio of 2.14, to 31/69 for an oxygen/IBAN ratio of 0.14.

Following the use of the periodic reactor, the partial oxidation of *isobutane* to MAA and MAC was attempted in a two-zone fluidized-bed reactor (TZFBR). Compared to the periodic reactor where the catalyst was reduced and re-oxidized by time gaps, the TZFBR provided a spatial separation that allowed the reaction to proceed continuously. First, the hydrodynamic behavior of the TZFBR reactor was studied showing that good mixing and fluidization were obtained under the reaction conditions. This was illustrated by the fluidization quality, which was 75 %, a very satisfying value for a lab-scale fluidized-bed, which must be considered as much more sensitive to wall effects than an industrial reactor. The attrition of the catalyst particles and the mechanical stability of the catalyst was verified by performing attrition tests of the catalyst particles in the TZFBR with and without IBAN feeding at 325 °C. The results evidenced that the particles properties did not evolve significantly under operation, which indicated that the catalyst supported on the SiO<sub>2</sub> surface exhibited a high mechanical stability. Then, a series of long-term catalytic tests on selective catalytic oxidation of *isobutane* were carried out, whereby the molar ratio of O<sub>2</sub>/IBAN and the reaction temperature were varied. The results evidenced that the conversion of IBAN increased with increasing the O<sub>2</sub>/IBAN molar ratio and also upon increasing the temperature. Unfortunately, the TZFBR was not selective at

all for the partial catalytic oxidation of *isobutane* to desired products. It may be because the oxygen injection was still very high compared to the oxygen consumed for conversion of *isobutane*, whereby the oxygen was not entirely consumed and entered the reaction zone, thus causing the over oxidation of *isobutane* or intermediately formed MAC and MAA in the reaction zone.

The aim of these studies was to explore the possibility of employing reactors that can separate the reduction and regeneration processes. Although the catalytic results obtained are not sufficiently convincing, it is important to emphasize that, since the reaction has never been studied nor in periodic mode, nor in a TZFBR, more experimental and methodological considerations would be required in order to boost the performances.

## 6.2 Perspectives

Future work is still necessary to pursue the development of the selective oxidation of IBAN to MAA and MAC. Studies need to be performed on different aspects. On the one hand, to improve the catalyst itself to find an excellent oxygen carrier. On the other hand, to investigate different reactor concepts to provide the better operating conditions for this reaction.

As for the composition of the catalyst, cesium and rubidium were used as counter-cations and V was used to substitute Mo in Keggin anions in this thesis. Besides, our group also focused in previous studies on cesium and/or ammonium salts of *I*-vanado-*II*-molybdenum phosphoric acid [1–3]. In addition, various parameters could be the subject of more detailed studies: further modification of Keggin anion can be achieved by replacing Mo with other metal elements such as Fe, Sb, As and Nb, or even as counter-cations. Despite some reports on them [4–6], optimization attempts can still be made by adjusting the introduced amount.

From the above conclusions, it can be stated that silica-based materials are quite stable to be used as support for dispersing heteropolycompounds and then for preparing catalysts for the selective oxidation of *isobutane* to MAA and MAC. So, one can try to develop or modify the support. Therefore, for example, the surface modified silica like  $\text{NH}_3\text{-SiO}_2$  could be explored to prepare bi-functional samples. These properties as well as their oxidizing ability are controllable over a wide range, which is of use in catalyst design. The dispersion of HPA on

the support and the formation of the crystalline  $\text{NH}_4^+$  salt may lead to high catalytic performance of the catalyst [7]. In addition, another possibility would be the treatment of inert  $\text{SiO}_2$  with basic or slightly acidic aqueous solutions of ammonium compounds in order to impact acidic properties of its surface. The obtained modified silica samples could then be used as supports for HPA [8].

In this work, the concept of the reactors separating the reduction and reoxidation processes was attempted for the partial oxidation of *isobutane*. In addition to the influent factors such as reaction temperature and oxygen concentration that we have already studied, many other parameters remain to be considered. For example, in the periodic reaction, the amount of reactant to which the oxygen carrier is exposed plays an important role in this process. The amount can be changed by the concentration of the reactants, or by changing the exposure time of a certain concentration (or the contact time).

However, in addition to some fundamental parameters, what can be also done and what is more meaningful are technical improvements. The selective oxidation of *isobutane* to MAC and MAA in a periodic reactor requires more accurate detection technique for the products due to the low reactant conversion. But, the detection by mass spectrometry tracks the fragments of the products, and the current one requires manual removal background and calculation of partial pressures, it has many interference factors and cumbersome data processing. Thus, a modern, highly sensitive mass spectrometer is essential for the detection of periodic reactions. Alternatively a fast, short detection interval micro-GC system, which could reduce the detection time to less than 1 minute for C1-C6 alkanes and only 0.24 minutes for *isobutane* [9], may not be fast enough at present to provide information on instantaneous conversion, but can provide the data on periodic changes.

Optimization of the catalytic performance in terms of reactant conversion, yield, productivity, and selectivity to the desired product is related not only to a thorough knowledge of the nature of the catalyst and interactions between reacting components and surface-active phases, but also to the development and use of a suitable reactor configuration, where all these features can be successfully exploited. Obviously, there is a long way to go in improving and

developing the selective oxidation of isobutane to methacrylic acid and methacrolein.

## References

- [1] F. Jing, B. Katryniok, E. Bordes-Richard, S. Paul, *Catal. Today* 203 (2013) 32–39.
- [2] F. Jing, B. Katryniok, F. Dumeignil, E. Bordes-Richard, S. Paul, *J. Catal.* 309 (2014) 121–135.
- [3] F. Jing, B. Katryniok, F. Dumeignil, E. Bordes-Richard, S. Paul, *Catal. Sci. Technol.* 4 (2014) 2938–2945.
- [4] F. Cavani, R. Mezzogori, A. Pigamo, F. Trifirò, *Chem. Eng. J.* 82 (2001) 33–42.
- [5] T. Mazari, C.R. Marchal, S. Hocine, N. Salhi, C. Rabia, *J. Nat. Gas Chem.* 19 (2010) 54–60.
- [6] X. Guo, C. Huang, Y. Li, *Korean J. Chem. Eng.* 25 (2008) 697–702.
- [7] M. Kanno, Y.K. Miura, T. Yasukawa, T. Hasegawa, W. Ninomiya, K. Ooyachi, H. Imai, T. Tatsumi, Y. Kamiya, *Catal. Commun.* 13 (2011) 59–62.
- [8] E. Janiszewska, M. Kot, M. Zieliński, *Microporous Mesoporous Mater.* 255 (2018) 94–102.
- [9] R. Van Loon, *Agilent Technologies.* (2012).

Titre : Valorisation d'alcane légers par voie catalytique

L'oxydation sélective de l'*isobutane* (IBAN) en méthacroléine (MAC) et en acide méthacrylique (MAA) est d'un grand intérêt pour l'industrie chimique ainsi que pour la recherche fondamentale. Les avantages de cette réaction proviennent non seulement de son faible coût en matière première et de la simplicité du procédé, mais aussi de l'absence de réactifs toxiques et de la réduction des déchets. Des études ont montré que les hétéropolycomposés à structure Keggin (sous forme d'acide partiellement neutralisé pour en augmenter la stabilité) présentent les meilleures performances catalytiques pour l'activation de l'*isobutane*. Cela est dû à leurs propriétés d'acidité et d'oxydoréduction fortes et modifiables. Dans ce travail, des hétéropolyacides de type Keggin (HPA) contenant du rubidium ou du césium comme contre-cations, ont été préparés et supportés sur silice commerciale. Plus précisément, les phases actives  $\text{Cs}_2\text{H}_2\text{PMo}_{11}\text{VO}_{40}$  ( $\text{CsV}_1$ ),  $\text{Cs}_{2.5}\text{H}_{2.5}\text{PMo}_{10}\text{V}_2\text{O}_{40}$  ( $\text{CsV}_2$ ),  $\text{Rb}_2\text{H}_2\text{PMo}_{11}\text{VO}_{40}$  ( $\text{RbV}_1$ ) et  $\text{Rb}_{2.5}\text{H}_{2.5}\text{PMo}_{10}\text{V}_2\text{O}_{40}$  ( $\text{RbV}_2$ ) ont été supportées sur CARIACT  $\text{SiO}_2$ , avec différentes teneurs en poids (10-50 Pds%). Il a été démontré que la stabilité thermique et la réductibilité des HPA ont été améliorées grâce au support. Les propriétés texturales, les caractéristiques structurales, les propriétés d'acidité et d'oxydoréduction et la stabilité des catalyseurs ont été étudiées à l'aide de diverses techniques afin d'établir des corrélations entre les propriétés physico-chimiques des échantillons et leurs performances catalytiques. Les résultats de la performance catalytique de l'*isobutane* en MAA et MAC ont montré qu'une densité de sites acides équilibrée est nécessaire pour catalyser efficacement la conversion de l'*isobutane* en MAA + MAC. En plus du développement du catalyseur, l'utilisation de nouvelles configurations de réacteurs a été étudiée pour diminuer la formation de produits de suroxydation. En plus du réacteur à lit fixe, l'oxydation de l'*isobutane* en MAC et MAA a également été appliquée dans deux autres types de réacteurs : le réacteur de type pulsé et le lit fluidisé à deux zones. Ces réacteurs découplent les étapes d'oxydation du réactif et de ré-oxydation du catalyseur selon le mécanisme redox de Mars et Van Krevelen. L'influence de divers paramètres de réaction, tels que le rapport molaire oxygène/*isobutane*, la température de réaction et le temps de cycle, a été étudiée. De manière surprenante, dans aucun de ces réacteurs, une performance comparable à celle du réacteur à lit fixe n'a été atteinte.

Mots-clefs : *isobutane*, catalyse, hétéropolyacide

Title : Catalytic selective oxidation of light alkanes

Over the past few decades, selective oxidation of *isobutane* (IBAN) to methacrolein (MAC) and methacrylic acid (MAA) has received great interests both in the chemical industry and in fundamental research. The advantages of this reaction originate only from its low raw-materials' cost and reduced process complexity, but also from limiting the use of toxic reactants and the reduction of wastes. Successive studies and reports have shown that heteropolycompounds with Keggin structures (under the form of a partially neutralized acid to increase their stability) present the best catalytic behavior for *isobutane* conversion. This is due to their strong and tunable acidity and redox properties. In this work, Keggin-type heteropolyacids (HPAs) containing rubidium or cesium as counter cations have been prepared. Keggin-type polyoxometalates (POMs) as heterogeneous catalyst perform surface-type reaction, however the low surface area and low thermal stability of the bulk heteropolycompounds (HPCs) limit their applications. Therefore, supported Keggin-type HPCs were investigated as catalysts. More precisely the active phase  $\text{Cs}_2\text{H}_2\text{PMo}_{11}\text{VO}_{40}$  ( $\text{CsV}_1$ ),  $\text{Cs}_{2.5}\text{H}_{2.5}\text{PMo}_{10}\text{V}_2\text{O}_{40}$  ( $\text{CsV}_2$ ),  $\text{Rb}_2\text{H}_2\text{PMo}_{11}\text{VO}_{40}$  ( $\text{RbV}_1$ ) and  $\text{Rb}_{2.5}\text{H}_{2.5}\text{PMo}_{10}\text{V}_2\text{O}_{40}$  ( $\text{RbV}_2$ ) were supported on a commercial CARIACT  $\text{SiO}_2$  carrier, with various loadings of 10-50 wt.% to obtain high specific surface area. It was evidenced that the thermal stability and reducibility of the Keggin type HPAs were improved by supporting the active phase on  $\text{SiO}_2$ . The textural properties, structural features, acidity and redox properties and the stability of the catalysts were studied using various techniques to establish correlations between the key properties of the samples and their catalytic performances. The results in catalytic performance of *isobutane* to MAA and MAC showed that a well-balanced surface acid site density is necessary to get an efficient catalyst for *isobutane* conversion and MAA + MAC selectivity. Furthermore, the investigation of the catalytic performances not only focused on the improvement of catalyst properties, but also on using novel reactor configurations that can continuously provide uniform and controllable oxygen concentration to decrease the generation of overoxidation products. In addition to the fixed-bed reactor oxidation of *isobutane* to MAC and MAA was therefore also applied in two other reactor types: periodic reactor and two zone fluidized-bed. Such reactors decouple the reaction and oxidation steps of the HPC-based catalysts, which follow the Mars and Van Krevelen redox mechanism. The influence of various reaction parameters, such as oxygen/*isobutane* molar ratio, reaction temperature and cycling time were studied. Surprisingly, in none of these reactors, a performance comparable to that of the fixed-bed reactor could be reached.

Keywords : *isobutane*, catalysis, heteropolyacid